

DECLARATION

-----

I Declare that this thesis is the result of my own investigations only, and has not been submitted either in full or in part for the award of any other degree. During the research programme I was not a registered candidate or enrolled student for another award of the C.N.A.A. or any other academic or professional institution.

Mark Wilson

## ADVANCED STUDIES

---

During the research program I undertook a course of advanced studies. These included the extensive reading of literature relevant to the research project; the attending of several one day, and one week long, conferences related to my studies; and undergoing a course of tuition on the use of both transmission and scattering electron microscopy for use in micrography and film analysis.

## ABSTRACT

-----

### A MULTIPLE-FILM MAGNETORESISTIVE REPLAY HEAD, FOR AUDIO APPLICATIONS "

by

MARK LEE WATSON BSc.

Sensors have been fabricated, which are able to read the information stored on magnetic tape using the anisotropic magnetoresistance effect. These have major advantages over conventional replay heads in that they are multi-track devices, with very small trackwidths. To overcome the signal limitation imposed by the reduced trackwidth the sensor consists of two long magnetoresistive elements which are folded together. By differentially sensing the magnetoresistive signal in each of the elements second harmonic distortion can be removed. To improve the linearity of the magnetoresistive response, the sensors are arranged in such a way that the sensor signal current in each of the elements provides the field necessary to correctly bias the head. A theoretical evaluation of the bias field for all configurations of element has been performed, and was found to fit experimental data.

Sixteen tracks are provided across the width of a compact cassette tape, and the design specifically allows the finished sensors to be packaged using standard components. Several performance related features have been considered, and various other fabrication aids included on the photomasks used to build the sensors. These photomasks are provided by the S.E.R.C. from an original computer program written in a graphics language, which defines the size and shape of the various elements making up the device. The heads are fabricated using photolithographic methods, from thin films of several materials all of which are R.F. sputtered. To improve the performance of the sensors, various electro-magnetic properties of the magnetoresistive layers have been measured using apparatus built especially for the purpose. These properties have been optimised by varying the bias potential used in the sputtering process. The finished heads have been tested, and have been found to compare well with the theory derived to describe their performance.

## ACKNOWLEDGEMENTS

-----

I would like very much indeed to thank the following people for their help and support during the course of the research for, and preparation of this thesis :-

Prof. D.J. Mapps, to whom I am deeply indebted for instigating the project, and then supplying me with a constant stream of support and encouragement; and without whom this thesis would literally not have been possible.

All of the technical staff within the department. Particularly Mr. R.C. Cox, Mr C. Ward, Mr. S. Warner, Mr. R. Howes and Mr. N. Fry, all of whose experience and expertise has been of enormous benefit to me during the course of my research.

The staff at the S.E.R.C Rutherford and Appleton Laboratories E.B.L.F facility, particularly Mrs. J. Bryant and Mr. J. Ayers, for their help in typing and editing the Gaelic program to define the masks.

Mr. B. Lakey, and Miss C. Jocelyn of the Polytechnics Electron Microscopy Unit, for helping me with the preparation of the samples used to measure the films grain structure.

Dr. M. Akhter of the Electrical engineering department, for the many useful discussions regarding the device fabrication, and Dr. D. Wilton of the Mathematics department for his help in the analysis of the average bias field problem.

The thesis is dedicated to Mrs. B.H. Watson (nee' Allan), who during the course of the project metamorphosed from girlfriend, to fiancée, and finally made the mistake of marrying me! No-one could have asked for, or received more support and encouragement than I have been given by her, for which I am extremely grateful.

CONTENTS -----	PAGE NUMBER -----
DECLARATION . . . . .	(i)
ADVANCED STUDIES . . . . .	(ii)
ABSTRACT . . . . .	(iii)
ACKNOWLEDGEMENTS . . . . .	(iv)
CONTENTS . . . . .	(v)
LIST OF FIGURES . . . . .	(viii)
LIST OF PLATES . . . . .	(ix)
 CHAPTER ONE . . . . .	 1
1.0 Introduction . . . . .	2
1.1 Historical background to research in Magnetoresistance. . . . .	2
1.2 Use of the transverse magnetoresistive effect to sense magnetic fields . . . . .	16
1.3 Transverse Anisotropic Magnetoresistance in Magnetic Recording . . . . .	19
1.3(i) Increased short wavelength resolution . . . . .	21
1.3(ii) Optimisation of the bias field . . . . .	23
1.4 The multiple film approach to improve sensor performance . . . . .	30
References Part One . . . . .	32
 CHAPTER TWO . . . . .	 35
2.0 Preparation and characterisation of sputtered NiFe thin films . . . . .	36
2.1 Film preparation . . . . .	36
2.2 Characterisation of ferromagnetic magnetoresistive films . . . . .	43
2.3 Coercivity and anisotropy field measurements . . . . .	45

2.4	Resistivity and magnetoresistivity measurements . . . . .	51
2.5	Grain size measurements . . . . .	60
2.6	Other physical dimension measurements. . . . .	64
	References Part Two . . . . .	65
CHAPTER THREE . . . . .		66
3.0	Design and fabrication of multiple-film heads. . . . .	67
3.1	The use of multiple-film elements in magnetoresistive replay heads. . . . .	67
3.2	Design of the multiple-film magnetoresistive head. . . . .	71
3.2(i)	The head element assembly. . . . .	72
3.2(ii)	The conductor pattern. . . . .	76
3.2(iii)	Fabrication aids included in the design . . . . .	81
3.3	Micro-Fabrication of the sensor array. . . . .	91
3.4	Optimisation of the anisotropic magnetoresistance effect . . . . .	97
	References Part Three. . . . .	103
CHAPTER FOUR . . . . .		104
4.0	Theoretical analysis of multiple-film magnetoresistive head. . . . .	105
4.1	Origins of the anisotropic magnetoresistive effect . . . . .	105
4.2	Device calculations applied to single sensors . . . . .	119
4.3	Theory for two-element devices . . . . .	124
4.4	Analysis of the bias field produced by the sense current. . . . .	128
4.5	Theory for the six-element multi-layer head . . . . .	139

References Part Four . . . . .	151
CHAPTER FIVE . . . . .	153
5.0 Experimental Results . . . . .	154
5.1 Experimental methods used to evaluate the heads performance. . . . .	154
5.2 Results from two-element device . . . . .	156
5.3 Results of six-element device. . . . .	159
CHAPTER SIX . . . . .	171
6.0 Discussion . . . . .	172
APPENDIX (I) . . . . .	A1.0
APPENDIX (II) . . . . .	A2.0
APPENDIX (III). . . . .	A3.0
APPENDIX (IV) . . . . .	A4.0
APPENDIX (V) . . . . .	A5.0

LIST OF FIGURES

PAGE NUMBER

-----	-----
1. Various Results of Resistivity and Magnetoresistivity Vs. Thickness . . . .	7
2. Magnetoresistive Response of NiFe Element .	17
3. The "Barber-Pole" Sensor . . . . .	26
4. Schematic Diagram of Multiple-Film Head .	29
5. Plasma Production for R.F. Sputtering . .	37
6. Schematic Diagram of Vacuum System . .	41
7. Optical Configuration of Transverse, Longitudinal and Polar Kerr Effects . .	44
8. Schematic Diagram of Field Coil, and Optics of Kerr-Effect Apparatus . . . . .	47
9. Potentiometric Circuit for Resistivity and Magnetoresistivity Measurement. . . . .	54
10. A Typical R.H Plot. . . . .	58
11. Two Widths of Magnetoresistive Sensor Connectors. . . . .	73
12. Bias/Sense Currents for Multiple-Film Head.	75
13. Diagram of the Configuration used to Optimise Lead-out Resistances . . . . .	77
14. Graph of L and C Measurements Taken Using Conductive Paper . . . . .	79
15. Coding Scheme for Chips on the Whole Substrate . . . . .	82
16. Graph of Sputtering Bias Vs. Film Coercivity and Anisotropy Field . . . .	98
17. Graph of Sputtering Bias Vs. Film Magnetoresistance . . . . .	100
18. Diagram Showing Generation of Fermi-Surface in K-Space. . . . .	108
19. Diagram Showing Modified Potential Well for Crystals . . . . .	111
20. Schematic Diagram of Band Structure of Ni .	116



21.	Single Sensor Configuration . . . . .	120
22.	Diagram Showing Element Separations Used in the Calculation of the Bias-Field . . . . .	129
23.	Graph of Average Field Measured Using Large-Scale Model . . . . .	134
24.	. . . . .	136
25.	Various configurations of sensor and bias stripe, predicted using the . . . . .	137
26.	. . . . .	138
27.	Sensor arrangement for differential sensing scheme. . . . .	141
28.	Predicted losses due to sensor signal cancellation . . . . .	144
29.	Variation in waveform asymmetry for different sense currents . . . . .	157
30.	Results of uniform field experiments from six-element device . . . . .	161
31.	Six-element sensor output as a function of applied field . . . . .	163
32.	Outputs from various sensor widths using the standard tape test . . . . .	165
33.	Theoretical outputs, and experimental results, from six-element device . . . . .	169

## LIST OF PLATES

PAGE NUMBER

-----	-----
1. The Nordico Sputtering Plant. . . . .	39
2. The Kerr-Effect Measurement Apparatus . . . . .	48
3. The Kerr-Effect Measurement Apparatus . . . . .	50
4. Close-Up of 4-Contact Pad for Magnetoresistance Measurement . . . . .	52
5. The magnetoresistance Measurement Apparatus . . . . .	55
6. The magnetoresistance Measurement Apparatus . . . . .	56
7. A Typical Electron Micrograph . . . . .	62
8. Coding Scheme as placed Between Conductors . . . . .	83
9. Coding Scheme as used on the Whole Substrate. . . . .	85
10. Fabrication of Magnetoresistive Multiple-Film Heads . . . . .	87
11. Completed Head . . . . .	89
12. Sacraficial Elements between Magnetoresistive Sensors . . . . .	91

CHAPTER ONE

-----

" The anisotropic magnetoresistance effect observed in thin ferromagnetic films, and its use in magnetic recording "

## 1.0 Introduction.

### 1.1 Historical background to Research in Magnetoresistance.

In 1856 Professor W. Thompson [1] began a series of experiments on "the electro-dynamic qualities of metals" which was to lay the foundations for a vast area of research and development that continues to this day. Following his initial results in which he described the variation in electrical resistance of several different metals, a second paper was published the following year [2] giving the first description of Anisotropic Magnetoresistance. In this paper it was shown that the electrical resistivities of Iron and Nickel are increased when these materials are magnetised.

Between 1857 and 1930 research into the phenomena continued, although interpretation of the data given is often difficult due to the longitudinal resistivity being a more favoured area of investigation than transverse measurements. Additionally the initial condition of the materials magnetisation is not known in many cases, making conclusions about the actual magnetoresistance indeterminate. In 1930 McKeehan [3] placed the study of the longitudinal resistivity on a more rational footing. In this paper he listed over 40 references on work done prior to his study; and gave results showing that the longitudinal resistivity of Nickel and Permalloy are approximately functions of magnetic moment

orientation only, and do not necessarily depend on whether a given orientation is produced by the application of a magnetic field or by elastic stress.

Building on this investigation Bozorth in 1946 [4] extended the domain theory of Doring [5] with measurements of the longitudinal and transverse resistivities of several Nickel-Iron alloys of varying composition. In addition to which the first use of the difference between the longitudinal and perpendicular resistivities of the specimen was given in order to overcome irregularities introduced by the initial magnetic state. The variation in the percentage change in resistivity as a function of the amount of Nickel in the alloy was also described, although this dependence had already been shown for Nickel-Cobalt alloys by Shirikawa in 1936 [6]. For the NiFe system the maximum magneto-resistive change occurred at 90%Ni/10%Fe, and for the NiCo alloys at 80%Ni/20%Co. It was also shown that the effect of stress was more complicated than had previously been reported, with the result depending on the particular alloy, its magneto-strictive coefficients, and crystalline grain structure. Only in favourable cases would the application of an external applied magnetic field restore the samples resistivity to the unstressed value.

With the growth in research during the late 1940's a clearer picture of the electronic and magnetic behaviour of ferro-magnetic materials began to emerge. In 1949 Snoek [7]

pointed out that the mean saturation-magnetostriction of NiFe and NiCo alloys vanish when the number of Bohr magnetons per atom becomes equal to one. Another coincidence noted was the occurrence of a maximum in the magnetoresistance at about the same compositions. These observations stimulated Smit in 1951 [8] and Van Elst in 1959 [9] to conduct comprehensive investigations of the magnetoresistance of Nickel and Iron, NiFe, NiCo, and NiCu alloys.

In Smit's paper it was shown that the behaviour of pure metals was essentially different from that of the alloys investigated. At low temperatures the predicted maximum in the magnetoresistance of the alloys having one Bohr magneton per atom was observed. An explanation of the difference between the longitudinal and transverse resistance was also given involving spin-orbit interaction. The later paper of Van Elst gave data on some 40 different nickel alloys, and discussed the results in the light of several theoretical suggestions. His conclusion being that the essential factor in the anisotropy of the magnetoresistance was the density of energy states at the surface of the fermi distribution of the electrons.

There have been several studies published since these papers in which the variation in the percentage magnetoresistance change as a function of the thickness of NiFe thin films has been examined. The first of these was by Mitchell et. al. in 1964 [10]. For this investigation glass

substrates were used heated to 300 degrees, and the vacuum held at  $10^{-6}$  Torr during evaporation. The evaporation rate was given as 2000 Angstroms/min. To align the easy axis a constant 20 Oe magnetic field was applied oriented in the plane of the film. The main conclusions drawn were that the thickness dependence of the resistivity could be explained by the scattering of the conduction electrons by the films surfaces as predicted by Fuchs [11]. However a correction was made to the thickness measurements, in which 85 Angstroms was deducted from each value taken, supposedly to allow for a 100 Angstrom non-conducting layer. In all other respects the data from thin films of NiFe was found to be comparable to the bulk values, once allowance had been made for the anomalously high resistivity of the films due to their dimension constraints, and strain interaction between the film and substrate.

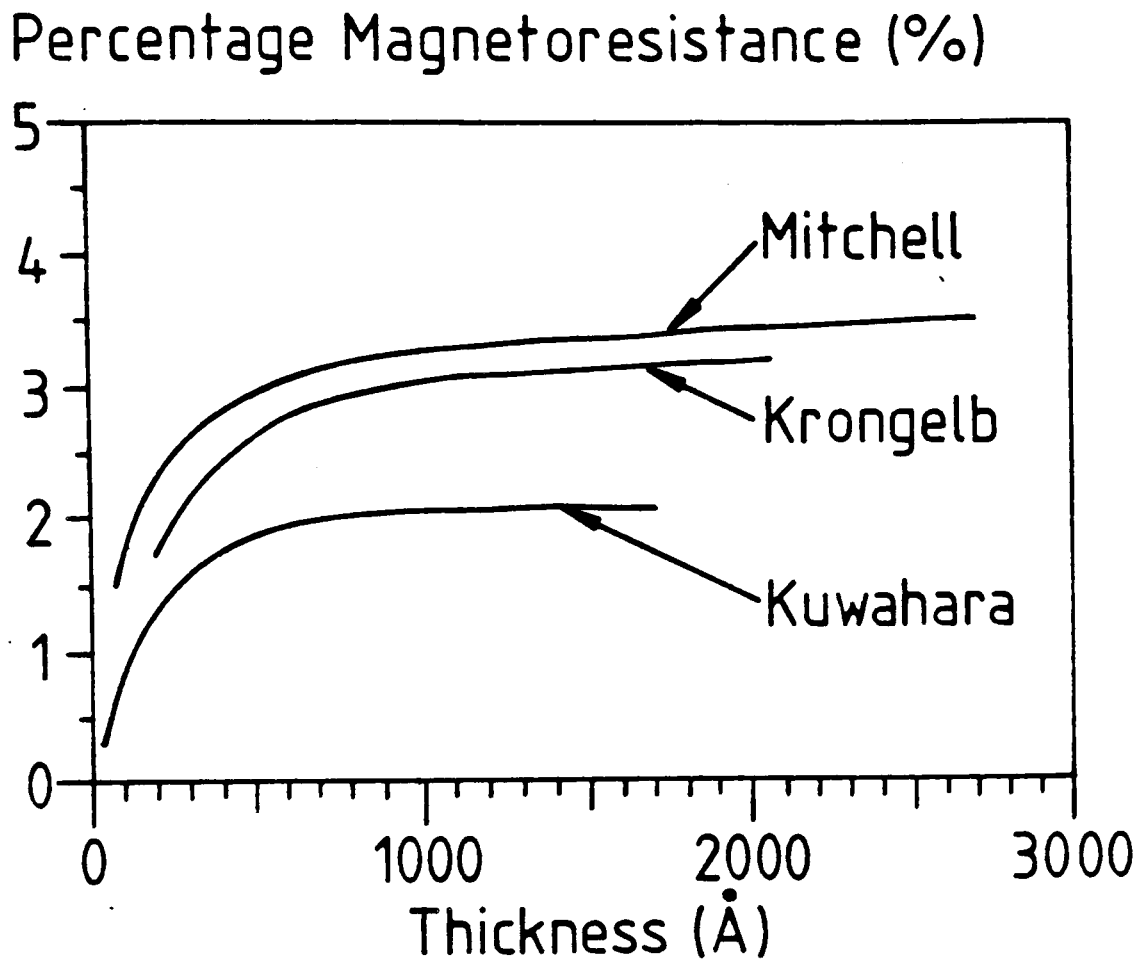
In 1965 Kuwahara [12] published similar experimental results to Mitchells, with the exception that the thickness of the films was given as a "magnetic thickness", taken from the vertical opening of the hysteresis loop for each specimen, compared with that taken from a standard film. A decrease in the saturation magnetisation of the 80%/20% NiFe films was found with decreasing thickness, with a rapid decrease for films thinner than 100 Angstroms. However no intrinsic relationship between the magnetoresistance and the saturation magnetisation was found, although an  $M^2$  variation was postulated. Additional results were published

in 1968 by Williams [13] which followed closely the earlier work of Mitchell, with a near linear variation in magnetoresistance over the thickness range 100-1000 Angstroms reported.

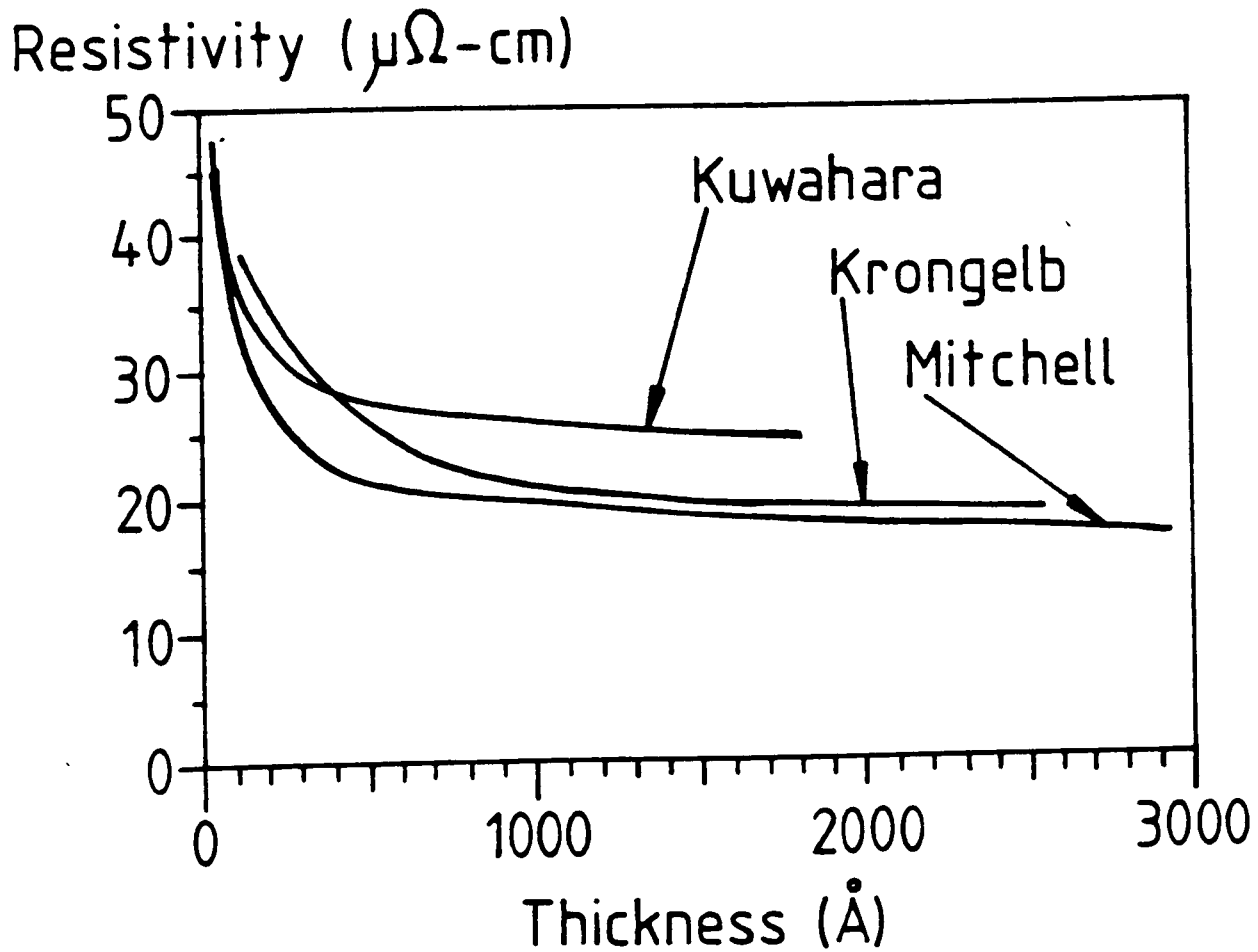
The effect of deposition conditions and composition of the NiFe alloy on the magnetoresistive and magnetic properties of evaporated films was further studied by Krongelb [14], and reported in 1973. The object of this work was to investigate the variation of the coercivity as the magnetoresistance was improved by varying the deposition parameters. It was found that the optimum fractional change in the resistivity for the NiFe films, could be produced by using a high substrate temperature ( 300 degrees ) and an alloy with 14-15% Iron. However these conditions led to a high coercivity and dispersion making such films undesirable for use in device fabrication due to unpredictable switching. The deposition parameters required to produce acceptable films were reported as being:- a) a substrate temperature of 250 degrees centigrade; b) an alloy composition of 18-19% Iron; c) a vacuum of better than  $2 \times 10^{-6}$  Torr and d) the application of a constant 60 Oe magnetic field in the plane of the film to define the easy axis. Additional work on the annealing of the films was reported by Krongelb and others [15] later that year. In this it was shown that films could be deposited at the lower substrate temperature, in order to reduce the high coercivity problem; and then annealed under a vacuum of  $5 \times 10^{-8}$  Torr in an orienting field of 500 Oe, thus



Figure 1



Experimental results obtained from evaporated films



substantially improving their performance. This increase in performance was attributed to a growth in particle size, and grain size within the film.

Prior to this work Chen et. al. had in 1971 [16] studied the geometrical size effect in single crystal and polycrystalline Nickel films, by measuring their transverse magnetoresistivity anisotropy at room, liquid nitrogen, and liquid helium temperatures. They concluded that the distortions in the transverse magnetoresistivity anisotropy observed were primarily due to the demagnetisation field and a geometric size effect introduced by the thickness of the films being less than the electron mean free path. From the transverse measurements taken, this size effect was determined, but was found to differ from that calculated from the free electron model. It was postulated that the materials electronic structure played a greater part than allowed for in the theory. The results of the early investigations on vacuum evaporated NiFe films are given graphically in Figure (1).

Although the size effect introduced by the thickness limitation in thin films had been postulated for many years, no consideration had been given to the effect of geometry or scale of the other film dimensions on the magnetic performance of thin films until practical devices became possible. In 1961 Middelhoek [17] had made a study in his PhD. thesis of the effect of the structure of ferromagnetic

films on their magnetic properties and domain formation. One conclusion reached in this work was that the theoretical calculation for the direction of magnetisation in the film from the simple domain model did not coincide with experimental observations. In fact, reversal of the magnetisation was found to occur at critical values of the external field determined by the formation of domains, a characteristic which was found to be film dependent.

Using this study as a starting point, Fluitman described in 1973 [18] an examination he had made of the variation in magnetoresistance and coercivity of NiFe elements, as a function of their thickness to width ratio. The thickness was varied from 200-10,000 Å, and the width from 2-1000 microns. The films were produced by a method similar to Krongelbs, using glass substrates heated to 250 degrees, and an aligning field of 40 Oe. From measurements of the transverse magnetoresistance and coercivity, it was found that the geometry of the elements had a marked effect on both of these properties. If the demagnetising field of the film was small the magnetoresistive response was governed by the films dispersion; requiring the application of a small transverse field in the reverse field direction to restore the magnetisation direction to its original state, once the film had been saturated by an applied transverse field. However, it was recognised that other processes were involved to do with the propagation of domain walls; resulting in domains

being formed having opposite directions of  $M$ . For films having a large demagnetising field the anisotropy of the strip was governed by an anisotropy constant associated with the elements geometry. Thus for films with a small dispersion, the magnetoresistive response was similar to that of films having a small anisotropy field; but for films having a large dispersion ( $>10$  degrees) the magnetisation vector relaxed back to its undisturbed position without the application of a reverse field. Additionally the higher values of coercivity resulting from decreased element width were ascribed to the fact that small strips behave increasingly like single domain systems.

The examination of the magnetisation dynamics of magnetoresistive elements having small dimensions continued with more work on the coercivity variation as a function of element width by Kryder et.al. in 1979 [19]. It had already been noted by Herd and Ahn in 1979 [20] that the high coercivities associated with small element widths could be reduced by a factor of 10 using multi-layered NiFe films with an insulating spacer. In the same year they published the results of an investigation into this reduction, using Lorentz electron microscopy to examine the switching behaviour of single and bi-layer strips of varying thicknesses [21]. The electron micrographs given in this paper showed the formation and growth of the domain patterns formed in both types of element at remnance, and with an increasing reverse field. It was postulated that for the

single layers having a low coercivity, the formation of charged walls retarded switching under application of a reverse field; whilst in films having a high coercivity, reversal takes place by the sweeping of the closure domains from the ends, through the strip. The reduction in coercivity by the use of an insulating separation layer was explained by the closely coupled layers enhancing the rotation of blocks; and the movement across the strip of the reverse domains from along the edge.

This use of an inter-layer between two NiFe elements to reduce domain related effects in their magnetoresistive response was modified by Van Ooyen et. al., in work reported in 1982 [22], in which a conducting non-magnetic inter-layer of Molybdenum was used. The thickness of the inter-layer was varied from 40-4000 Angstroms, whilst the NiFe layers were kept at a constant thickness of 750 Angstroms. Various combinations of easy-axis orientation and applied field direction were also examined. It was found that the laminated elements magnetoresistive behaviour deviated from that of a single layer element, and a qualitative interpretation of the result was given. Additionally, calculations were made to predict the resistance response to an external applied field. The model used assumed a homogeneous magnetisation in each NiFe film, but in differing directions. The magnetic energy was then minimised with respect to the direction of magnetisation in each film, and the resistance calculated. In order to calculate the total magnetic energy, the anisotropy,

field, and demagnetising energies were considered. The calculated results were found to be in good agreement with the measured behaviour. This configuration was further analysed by Pohm et. al. [23] using a one dimensional model to predict the magnetisation distribution in the magnetoresistive elements. This model showed that for very small elements both demagnetising and exchange effects had to be allowed for; and provides a convenient method for calculating the average demagnetising effects and magnetoresistive response for such elements.

In addition to reduced sensitivity due to the higher coercivities associated with small width elements, it had been noted that the magnetoresistive response became characterised by numerous irreversible jumps. These jumps are magnetic in origin, and are related to "Barkhausen Noise". They were studied by Tsang and Decker [24] who observed separately the magnetoresistive response and the domain behaviour of small elements using a bitter solution technique. It was found that the hard-axis response was governed by the nucleation and expansion of reversed polarity Neel walls. Although detailed correlation between these effects and the elements magnetoresistance was not possible, in this work published in 1980; the following year the simultaneous observation of the domain structure in the film, and its magnetoresistive response was described by the same authors [25]. Detailed discussion of their observations was given with the conclusion that domain wall

state transitions constituted the major source of noise. To understand the nature of the positive to negative polarity Neel wall transitions, the energetics of the formation of such reverse polarity segments, and the elementary properties of such segments in different applied fields were considered. It was established that the transverse magnetic reversal of the elements typically involved the systematic creation and intensification of buckling domain patterns. The easy-axis dispersion effect and the longitudinal demagnetisation energy effect were identified as being the causes of these domain patterns, and the observed jumps in the magnetoresistive response were attributed to wall state transitions caused by instabilities in the domain patterns thus formed.

This research continued, and in 1982 a systematic study of wall populations in a variety of film geometries and film properties was made. The effect of an applied transverse magnetic field on the domain response of elements having different orientations of uniaxial anisotropy easy-axis was also observed [26]. It was revealed that the geometry dependent longitudinal demagnetising energy constitutes the primary factor in the creation of domains in typical transverse reversals. For elements having a length to width ratio close to unity, dispersion effects in the uni-axial anisotropy combined with this effect to produce high wall populations which were postulated to be both geometry and material dependent. Edge effects were also found to be important in the elements magnetoresistive response, in that

they determined the resultant buckling pattern geometries; and any fluctuations in these edge states could produce long term fluctuations in the geometry of the domain patterns. Other orientations of the anisotropy axis were found to produce new reversal behaviour, especially in the case where the axis was oriented transversely, but these orientations did not reduce domain activity.

Work still continues on the domain nucleation and propagation of small magnetoresistive elements in an attempt to understand their micromagnetic behaviour, and improve their performance for use in practical devices. In a paper published in 1984 Tsang [27] discussed outstanding problems in the use of the phenomena in small field sensors with the conclusion that much work would be required to utilise all of the possibilities of such devices without compromising their advantages. The following year Ozimek and Paul [28] presented the results of an investigation they had made of the magnetisation dynamics of micron size thin NiFe films both with and without an under layer of Titanium. They postulated that the lack of motion of domain walls minimised the Barkhausen noise and this minimisation could be achieved by decreasing the length to width ratio, or increasing the film thickness. In elements in which there was a high aspect ratio and a reduced thickness it was found that edge domain walls were nucleation centres for domain reversal. Further it was considered that a higher aspect ratio had a greater effect on the domain properties of the elements than did the



thickness. The use of a Titanium under layer was found to increase the asymmetry of the B-H cycle, and decrease the reproducibility of the results.

From this brief outline it can be seen that a great deal of fundamental research has been done to improve the understanding of the transverse magnetoresistive effect in the 100 years since it was first discovered. In particular it can be seen how extensive research into the magnetic and electrical properties of small elements of magnetoresistive material has made the fabrication of practical devices for use in wide range of applications possible. It must be pointed out however that this is only one small part of the much larger subject of Galvanomagnetism. Much work has also been done to investigate the wider topics of thin film resistivity and ferromagnetism. Although it is not intended to expand on them here, attention must be brought to the work of Mayadas and Shatzkes published in 1970 [29] and 1974 [30], in which a theoretical model for the resistivity of thin NiFe single crystal and polycrystalline films was given, based on the much earlier work of Fuchs [31]. In the field of the ferromagnetism of thin films the work of Prutton [32], who described the film dependence of various magnetic properties other than the anisotropic magnetoresistance, and Hoffman [33] who gave the first mathematical descriptions of phenomena such as the observed magnetisation ripple, has improved the understanding of the magnetic behaviour of such

films considerably. Thus although this thesis describes the design, fabrication, testing, and theoretical description of a device utilising the transverse anisotropic magnetoresistance effect, it must be seen in the context of the much wider subject.

## 1.2 Use of transverse magnetoresistive effect to sense magnetic fields.

In the previous section outline has been given to the research into the anisotropic transverse magnetoresistive effect with respect to its optimisation for use in practical devices. Although the effect is now thought to be well understood as a phenomenological concept, detailed calculations still prove difficult. In their paper published in 1975, McGuire and Potter [34] treated the theoretical problem both from symmetry considerations, and microscopic theory. In the first case the experimentally observed  $\cos^2$  dependance of the materials resistivity as a function of applied field is derived. This treatment follows that of Birss for magnetostriction, in that a resistivity tensor is derived relative to the crystallographic axes of a single crystal sample. This can be divided into symmetric and antisymmetric parts of which the associated electric fields are attributed to generalised magnetoresistance and Hall effects respectively. This is then extended to the more practical case for device fabrication, using polycrystalline

Graph showing the variation in resistance of Nife element as a function of applied field

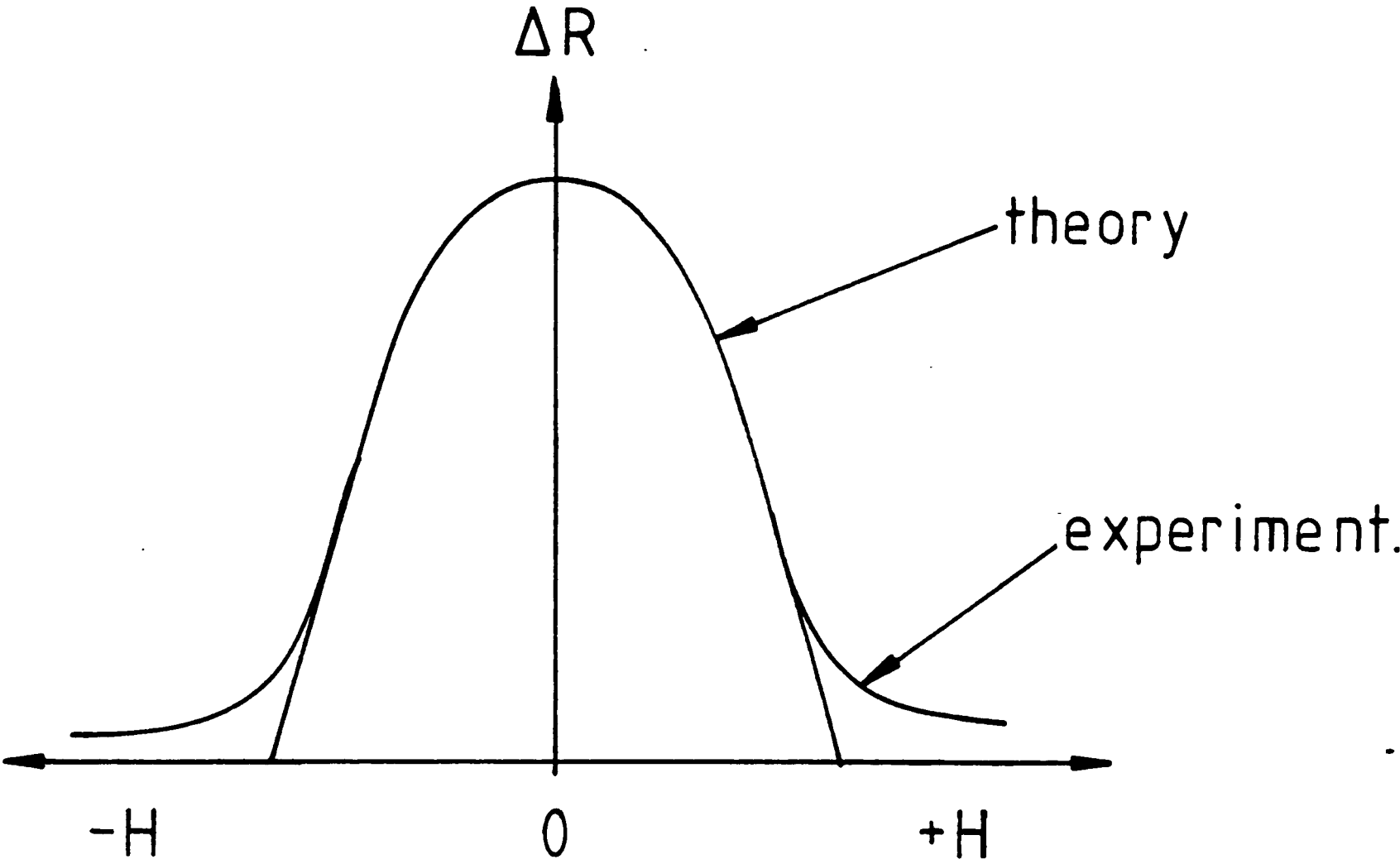


Figure 2

samples, by integrating the resistivity tensor over the volume of a cone pointing in an arbitrary current vector direction within the sample. The result is given in equation (1).

$$r_{(poly)} = r_{(0)} + r_{(1)} \cos^2(\Theta) \dots\dots\dots(1)$$

This expression gives the variation of the resistivity of a polycrystalline sample as a function of the transverse resistivity  $r(0)$ , the anisotropic magnetoresistance  $r(1)$ , and  $(\Theta)$ , the angle between the current density vector and the magnetisation vector. It has been observed experimentally for various alloys and sample geometries.

For many field sensing applications a linear response of the detection elements to applied field is required. In order to obtain such a response from the field dependence given in equation (1), it can be seen that the detection element must be biased in such a way that it operates on the linear part of the response curve. In figure (2) it is shown how the theoretical response is modified by the demagnetising effect introduced by the width limitation of practical magnetoresistive elements. This demagnetisation field manifests itself by distorting the direction of  $M$  across the width of the strip. Thus for elements having a large demagnetising field, which is the usual case for very narrow elements; the operating point has to be carefully selected.

The first commercial applications were described in the 1960's [35, 36] in which thin film memories were created using uni-axial permalloy films. The information was then stored using linear arrays of elements strung along a conductor, and determining in which of the two possible easy axis directions the film element was magnetised. However, despite the advantages of such an information retrieval system, the increase in the number of elements on a given address line made the signal to noise ratio for magnetoresistive readout unacceptable. Despite this setback interest in the use of the effect in practical devices has not waned, and today it is used in many applications, including Magnetometry, Bubble-sensing in magnetic bubble memories, and large and small scale magnetic field sensing of both constant and oscillating fields.

### 1.3 Transverse Anisotropic Magnetoresistance in magnetic recording.

The first use of the transverse anisotropic magnetoresistive effect to read information stored on magnetic tape was proposed in 1971 by R.P. Hunt [37]. Two configurations were considered, one in which the detection element was placed parallel to the tape, and the second in which it was transverse. Due to considerations of wear, and ease of fabrication only the second configuration has been widely developed. By using the principle of the minimisation of free energy, together with the expression given in

equation (1) an expression was developed for the signal voltage. The equations derived by Wallace [38] for the horizontal and vertical components of the magnetic field above a uniformly magnetised tape then allowed the wavelength response of this single Magnetoresistive element to be calculated. Results were given for the theoretical and experimental output of the vertical configuration heads, showing a very good agreement between them. Indeed it is a measure of the success of Hunts equations that even though more rigorous expressions for the head response have been developed, the bulk of descriptions of working devices published since 1971, still refer to his original description.

Despite the good agreement between the predicted and actual head response, and the improved head output over conventional ring heads for certain recorded wavelengths; there are still problems associated with this method of information retrieval. These comprise the need to increase the short recorded wavelength response, particularly for high density digital storage applications; and the requirement that the output is linearised to avoid distortion introduced by the non-linear dependence of the magnetoresistance on applied field. Much work has been done to overcome these difficulties, although a satisfactory production device has yet to be realised. A brief outline of the research into these problems that has been reported is given in the next two sections.

### 1.3(i) Improved short wavelength resolution.

In order that the response of the magnetoresistive elements should not have an unrealistic short wavelength sensitivity, a method has to be found to improve this aspect of the performance. In his review of digital magnetic recording theory R.I. Potter proposed placing the element between two magnetic shields [39]. These acted to shield the element from the approaching transition until the last possible moment. A detailed analysis of the theoretical response was given in this paper, and improved upon by R.W. Cole et. al. the same year [40]. The first practical device was described by Shelledy and Brock [41] the following year and the theoretical analysis extended to include the case in which the element is not placed symmetrically between the shields. An improvement was also made to the mathematical description that year by Davies and Middleton [42], in which the output from elements recessed from the front face of the shields was predicted.

Since then work has been reported on the investigation of shield length on the magnetoresistive elements response [43]; comparisons between the calculated and actual short wavelength response [44], and other modelling experiments using resistive paper [45, 46]. An improved mathematical model, describing the design proposed by Shelledy and Brock was recently published [47] in which the complexity of the

design parameters for such a head was examined analytically, and compared with experiment. In recent years however the emphasis has tended to shift away from shielded elements due to the complexity of the design parameters, the extra difficulties in the fabrication due to the introduction of the added process steps for each shield, and the discovery of other simpler methods of providing the required resolution.

It has been recently pointed out that the reduced sensitivity to short wavelength transitions is to some extent caused by the height of the element and the introduction of an insensitive dead zone at the elements edge [48]. This is caused by the high demagnetising fields found there and introduces a separation loss diminishing dramatically the element response at higher recording densities. One method of overcoming this problem is to include Flux Guides in the design either with or without an associated shield structure in order that the tape flux is shunted up to the most sensitive region of the element. W. F. Druyvesteyn et. al. have reported such a head with the magnetoresistive element positioned in the gap of a magnetic circuit comprising of a ferrite substrate and a magnetic yoke [49]. A second more drastic but easily fabricated method is to use an extremely narrow element with the front edge flush with the tape surface. F. Jeffers and H. Karsh have reported results from such a sensor that was only 4.6 microns in height, which gave an excellent output and signal to noise ratio [48]. One major drawback with this configuration is the fact that even using



extremely hard wear resistant substrates such as sapphire the possibility of damage to the sensor is ever present.

### 1.3 (ii) Optimisation of Bias Field.

As has been shown in section 1.2 the quadratic dependence of the magnetoresistive response on external applied field requires the linearisation of the output. This is particularly important in the use of the effect in Audio Replay applications to avoid the introduction of large second harmonic distortion. To achieve this, several different biasing schemes have been proposed ranging in sophistication from the relatively simple to the very complex. In order that the biasing scheme used in this research can be seen in the context of other methods, the main forms shall be described, and their merits (or otherwise), discussed.

The various schemes proposed to linearise the response of magnetoresistive replay heads can be grouped into two main areas a) Those in which the elements magnetisation vector is rotated relative to the current density by the application of an external applied field; and b) those in which the current vector has been rotated relative to the magnetisation by the use of a conducting overlay deposited on the stripe, or the magnetisation vector rotated relative to the current direction by displacing the element easy-axis direction during fabrication.

To achieve the first, the earliest attempts were made using permanent magnetic chips placed behind the array of sensing elements at sufficient distance to linearise the output, without risking information erasure. Although effective in experimental devices this method has several severe drawbacks for production heads, in that careful positioning of the permanent magnet is required to provide the optimum bias for each head produced. Additionally this bias scheme is unsuitable for heads having shields as the magnet-chips cannot be made small enough to fit within the shield structure, and are obviously ineffective if placed outside it.

In 1975 Bajorek and Thompson reported experiments using permanent magnet films to bias the elements [50]. Several materials were considered to overcome the surface roughness problems associated with the thick layers required to provide sufficient field, and such a method was proved to be technically feasible; although the problem of providing the necessary insulation limited the useful separation available for its utilisation in shielded heads. The problem of the thickness limitation imposed by the shield separation was tackled by H. Uchida et. al. [51] who simply ignored the shield concept, and constructed a head having a Rare-Earth Cobalt permanent magnet bias; but one in which only the very edge of the element was biased, thus increasing the short wavelength resolution by reducing the separation loss. This does however lower the signal to noise ratio, in that with

only the edge of the sensor operating linearly the voltage drop across the under-biased part acts to lower the overall percentage magnetoresistive change available.

The idea of using a coupled magnet film adjacent to the magnetoresistive element has recently been extended to the use of a soft magnetic film [52] as reported by F. Jeffers et. al. In this design a high permeability film is located close to, but electrically insulated from the detection element. The sense current in the stripe produces a field which magnetises the soft adjacent layer, which in turn generates a magnetostatic field large enough to correctly bias the element. This design like that of Uchida requires no shield structure to obtain its short wavelength resolution.

Due to the requirement that any form of permanent magnet film or chip bias be individually tailored to suit each particular element, and the degree of difficulty faced in altering the bias once fabricated; a second form of linearisation was proposed by Shelledy and Brock [41]. In this design a non-magnetic electrically conducting layer was deposited next to the magnetoresistive stripe and in intimate electrical contact with it. In this configuration the sense current passing through the adjacent conductor provided a bias field which could be easily altered to suit the particular characteristics of the individual stripe. The bias conductor material chosen was Ti, due to the similarity in the resistivities of NiFe and Ti. Although there is an

Diagram showing the Conductor/NiFe element arrangement,  
as used in the "Barber Pole" type sensor

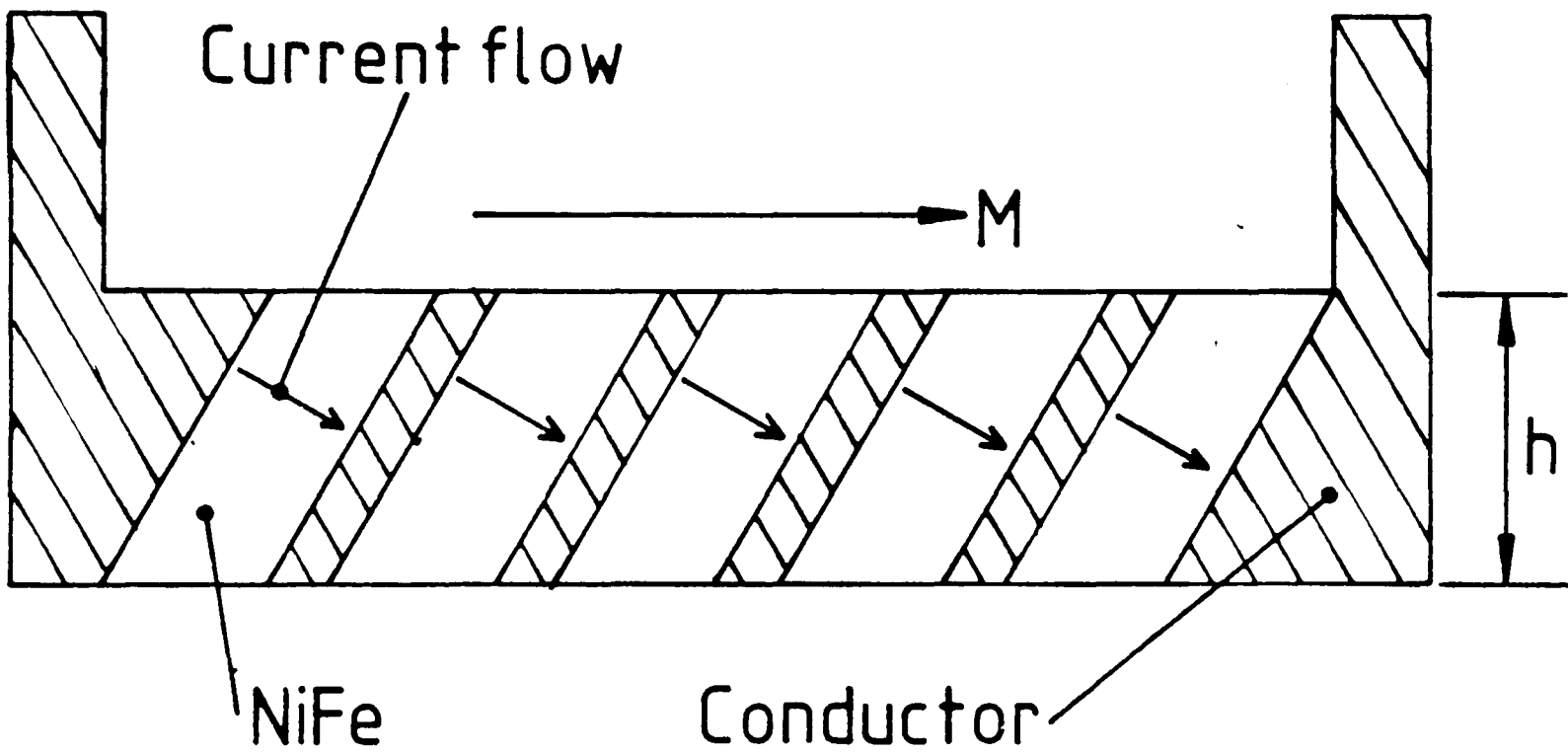


Figure 3

obvious loss in sensitivity due to the reduced magnetoresistive change as a proportion of the total element resistance, the fabrication is very simple, and does not impose a width limitation for shielded structures.

The introduction of an insulating layer between the Ti and NiFe elements restores the response of the Magnetoresistive element, but adds another step in the fabrication of the device. This method of bias was proposed by O. Voegeli [53] and extended by G. V. Kelley et. al. to include the case in which the bias element is also a magnetoresistive sense element [54]; the sense current in each stripe thus providing the field necessary to bias its neighbour. Various other methods along these lines have been proposed in which the bias conductor is non-magnetic [55]; a single bias conductor placed between two magnetoresistive elements is used [56]; and a combination of magnetostatic coupling and internally generated bias field linearises the response [57].

Despite the ease of control the use of an active element to supply the bias allows, its application to devices having a large number of small-trackwidth elements (e.g. for parallel digital storage), creates the problem of limiting the space in which to place the extra conductors. In order that the magnetoresistive response is linearised, without reducing the feature size to unacceptable limits, a passive biasing scheme was proposed by K.E. Kujik et. al. in 1975

[58]. The pre-determined angle between the current vector and the magnetisation direction being obtained by applying an angled conductor pattern of very low resistivity compared to the stripe. Due to the equipotential areas formed within this pattern the current flowing between them is rotated by an angle that can be controlled by the geometry of the overlay (Fig 3 ). Several other advantages are obvious for this method: the reduced danger of information erasure, the accuracy of the bias being dependent only on the accuracy of the fabrication and lasting the lifetime of the head, and the ability to use this form of construction in shielded heads.

Extensive use of this configuration has been made in replay heads, with it being incorporated with an inductive write head [59], and used in 32 track parallel digital compact cassette storage [60]. However there are several disadvantages with the design, not the least being the loss of useful response due to a percentage of the element being covered by the conducting overlay. In cases where the trackwidth is very small the noise caused by domain wall movement can be very large, which limits the minimum trackwidth possible before the signal to noise ratio becomes unrealistic. Additionally once fabricated the bias is fixed, reducing the flexibility of the head, and removing the capacity to adjust the operating point to suit individual applications. The possibility of obtaining a linear response by patterning the stripes such that there is an angle of 45

Schematic diagram showing the arrangement of the six-elements in the multiple film array, and the direction of the current flow through the array

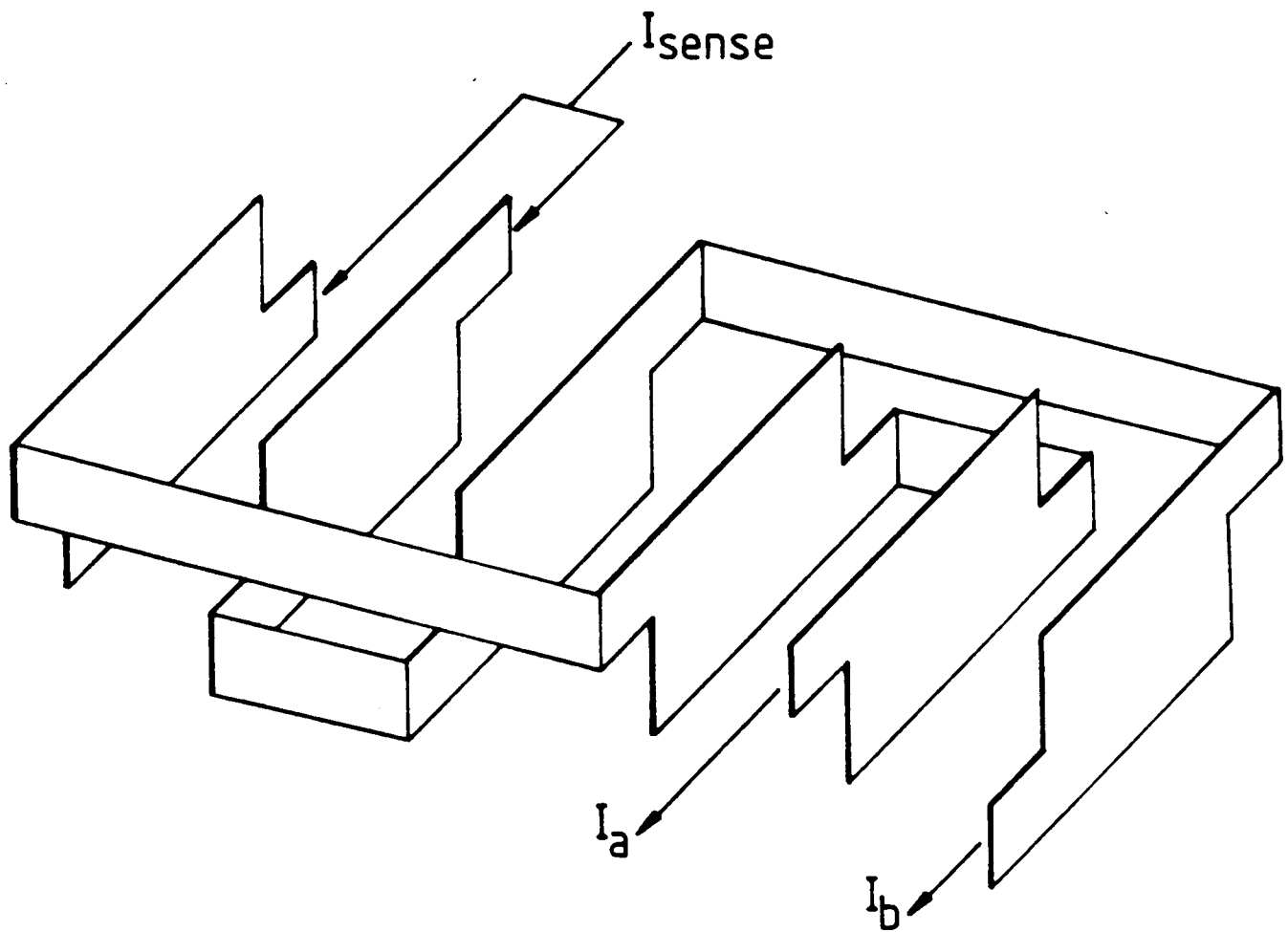


Figure 4

degrees between the easy axis and the current direction has also been investigated and a head using this configuration reported [61]. This would appear at first sight to be an extremely simple method of linearising the output, but for small element heights the demagnetising fields are large decreasing the rotation of the magnetisation available by limiting the the magnitude of the anisotropy fields obtainable.

In addition to the methods described, several other schemes have been proposed which fit neither of the categories outlined at the beginning of this section. One of these is the case described by F.J. Jeffers [62] in which the elements are patterned such that the films easy axis is canted at an angle to the length of the stripe. To control the magnetisation orientation and cancel current generated fields, a non-magnetic bias conductor is placed between the elements making the device response independent of sense current. Another hybrid is the use of a barber pole structure in conjunction with an exchange induced uniaxial anisotropy from NiFe/FeMn exchange coupled films as reported by C.Tsang and R.E. Fontana [63].

#### 1.4 The multiple-film approach to improve sensor performance.

As has been shown in the previous sections magnetoresistive replay heads have several advantages over



conventional ring heads. Due to the photolithographic techniques used in their manufacture very small trackwidths are possible, and as they are field sensing rather than rate-of-change of field sensing devices; they are eminently suitable to slow speed tape drives particularly in the audio recording cassette industry. Additionally for digital applications the reduced trackwidth enables the data-rate to be increased without increasing the tape speed. However one problem remains, if the trackwidth is reduced the overall length of the element is reduced also, decreasing the signal to noise ratio unacceptably.

To overcome this problem a head has been developed in which the sensor is folded over several times increasing the signal available considerably whilst maintaining the reduction in trackwidth. Another advantage of this design is that it has proved possible to construct a structure in which two magnetoresistive elements are folded together. This results in the field produced by the sensing current flowing in one element providing the bias field required by the sensor adjacent to it, in order to linearise its output. A schematic diagram of the head configuration is shown in figure (4). In this fashion a high degree of signal linearity and amplitude are possible without the need to include any additional fabrication steps complicating the heads design and manufacture.

## REFERENCES CHAPTER ONE

-----

- 1) W.Thompson. Proc. Roy. Soc. Pt 4 pp146 (1856)
- 2) W.Thompson. Proc. Roy. Soc. vol.8 pp546 (1857)
- 3) L.W. McKeehan. Phys. Rev. vol.36 pp948 (1930)
- 4) R.M. Bozorth. Phys. Rev. vol.70 pp923 (1946)
- 5) W. Doring. Ann. d. Physik vol.32 pp259 (1938)
- 6) S. Shirikawa. Sci. Rept. Tokohu Univ. Honda vol. pp.1 (1936)
- 7) J.L.Snoek Nature vol.163 pp837 (1949)
- 8) J. Smit Physica vol. XVI pp 612 (1951)
- 9) H.C. Van Elst Physica vol.25 pp708 (1959)
- 10) E.N. Mitchell, H.B. Haukaas, H.D. Bale, J.B. Streeper. J.Appl. Phys.vol.35 pp2604 (1964).
- 11) K. Fuchs. Proc. Cambridge Phil. Soc. vol.34 pp100 (1938)
- 12) K. Kuwahara. Trans Jap. Inst. Metals. vol.6 pp192 (1965)
- 13) F.C. Williams, E.N. Mitchell. Jap. Jnl. Appl. Phys. vol.7 pp739 (1968)
- 14) S. Krongelb. Jour. Electronic Mat. vol.2 pp228 (1973)
- 15) S. Krongelb, A. Gangulee, G. Das. IEEE Trans. Mag. vol. MAG-9 pp568 (1973)
- 16) T.T. Chen, V.A. Marsocci. J. Appl. Phys. vol.43 pp 1554 (1972)
- 17) S. Middlehoek Phd. Thesis Amsterdam University (1961)
- 18) J.H.J. Fluitman. Thin Solid Films vol.16 pp269 (1973)
- 19) M.H. Kryder, K.Y. Ahn, N.J. Mazzeo, S. Schwartz, S.M. Kane IEEE Trans.Mag. vol MAG-15 pp99 (1980)
- 20) S.R. Herd, K.Y. Ahn. J. Appl. Phys. vol50 pp2384 (1979)
- 21) S.R. Herd, K.Y. Ahn, S.M. Kane. IEEE Trans. Mag. vol MAG-15 PP1824 (1979)
- 22) J.A.C. Van Ooyen, W.F. Druyvesteyn, L.Postma. J. Appl. Phys. vol53 pp2596 (1982)

- 23) A.V. Pohm, C.S. Comstock, L. Peary. IEEE Trans. Mag. vol MAG-20 pp863 (1984)
- 24) S. Decker, C. Tsang. IEEE Trans. Mag. vol MAG-16 pp643 (1980)
- 25) C. Tsang, S. Decker. J. Appl. Physics. vol.52 pp2465 (1981)
- 26) C. Tsang, S. Decker. J. Appl. Physics. vol.53 pp2602 (1982)
- 27) C. Tsang. J. Appl. Physics. vol.55 pp2226 (1984)
- 28) E.J. Ozimek, D.I. Paul. J. Appl. Physics. vol.55 pp2232 (1984)
- 29) A.F. Mayadas, M. Shatzkes. Phys. Rev. B. vol.1 pp1382 (1970)
- 30) A.F. Mayadas, M. Shatzkes. J. Appl. Phys. vol.45 pp2780 (1974)
- 31) K. Fuchs. Proc. Cambridge Phil. Soc. vol.34 pp100 (1938)
- 32) M. Prutton. Brit. Jnl. Appl. Phys. vol.15 pp815 (1964)
- 33) H. Hoffman. Thin Solid Films. vol.58 pp223 (1979)
- 34) T.R. McGuire, R.I. Potter. IEEE Trans. Mag. vol.MAG-11 pp1018 (1975)
- 35) C.P. Battaral, M. Galinier. IEEE Trans. Mag. vol.MAG-5 pp 18 (1969)
- 36) P. Huijer. Proc. Int. Sol. States Conf. pp36 (1962)
- 37) R.P. Hunt IEEE Trans. Mag. vol.MAG-7 pp150 (1971)
- 38) R.L. Wallace. Bell Systems Tech. Jnl. vol 30 pp1146 (1951)
- 39) R.I. Potter. IEEE Trans. Mag. vol.MAG-10 pp 502 (1974)
- 40) R.W. Cole et. al. IBM Jnl. Res. Dev. vol.18 pp 551 (1974)
- 41) F.B. Shelledy, G.W. Brock. IEEE Trans. Mag. vol.MAG-11 pp1206 (1975)
- 42) A.V. Davies, B.K. Middleton. IEEE Trans. Mag. vol.MAG-11 pp1689 (1975)
- 43) G.V. Kelley, R.A. Ketcham. IEEE Trans. Mag. vol.MAG-14 pp 515 (1978)

- 44) T.A. Schwarz, S.K. Decker IEEE Trans. Mag. vol.MAG-15  
pp1622 (1979)
- 45) B.K. Middleton, A.V. Davies, D.J. Sansom. IERE Conf.  
Proc. No.43 pp353 (1979)
- 46) B.K. Middleton IERE Jnl. vol.50 pp419 (1980)
- 47) D.J. O'Conner, F.B. Shelledy, D.E. Heim. IEEE Trans.  
Mag. vol.MAG-21 pp1560 (1985)
- 48) F. Jeffers, H. Karsh. IEEE Trans. Mag. vol.MAG-20 pp703  
(1984)
- 49) W.F. Druyvesteyn et. al. IEEE Trans. Mag. vol.MAG-19  
pp1748 (1983)
- 50) C.H. Bajorek, D.A. Thompson. IEEE Trans. Mag. vol.MAG-11  
pp1209 (1975)
- 51) H. Uchida. IEEE Trans. Mag. vol.MAG-18 pp1152 (1982)
- 52) F. Jeffers et. al. IEEE Trans. Mag. vol.MAG-21 pp1563  
(1985)
- 53) O. Voegeli. U.S. Patent 3,860,965.
- 54) G.V. Kelley et. al. IEEE Trans. Mag. vol.MAG-17 pp2890  
(1981)
- 55) W.F. Druyvesteyn et. al. IEEE Trans. Mag. vol.MAG-17  
pp2884 (1981)
- 56) R.L. O'Day IBM Tech. Disc. Bulletin. vol.15 pp2680  
(1973)
- 57) R.L. Comstock et.al. IEEE Trans. Mag. vol. MAG-17 pp2739  
(1981)
- 58) K.E. Kuijk et. al. IEEE Trans Mag vol.MAG-11 pp1215  
(1975)
- 59) J.C. van Lier et. al. IEEE Trans. Mag. vol.MAG-12 pp716  
(1976)
- 60) W. Metzdorf, M. Boehner, H. Haudek. IEEE Trans. Mag.  
vol.MAG-18 pp763 (1982)
- 61) C.H. Bajorek et. al. IBM J. Res. & Dev. vol.18 pp541  
(1974)
- 62) F. Jeffers. IEEE Trans. Mag. vol.MAG-15 pp1628 (1979)
- 63) C. Tsang, R.E. Fontana. IEEE Trans. Mag. vol.MAG-13  
pp1149 (1982)

## CHAPTER TWO

-----

" The preparation methods and characterisation measurements required to optimise the electro-magnetic performance of thin NiFe films for use in magnetoresistive replay heads "

## 2.0) Preparation and characterisation of Sputtered NiFe Thin Films.

### 2.1) Film preparation.

All of the thin films used in the production of the device described in this thesis were R.F. sputtered using commercial sputtering systems. The object of sputtering is to remove material from the target and deposit it on the surface of a substrate thus forming a thin film of the target material. To this end a plasma is formed in the chamber consisting of high energy ions and electrons which then bombard the target, agitating the surface atoms to such an extent that some are knocked free. These are then able to condense onto other surfaces within the vacuum chamber one of which is the substrate. Unlike D.C. sputtering, in which a steady voltage is applied to the electrodes, and the current flow through the plasma is controlled by the emission of secondary electrons from ions in the plasma, and by ionisation due to electron impact; R.F. sputtering can be used to produce thin-films of insulating as well as conducting materials. If an attempt was made to sputter material from an insulating target in a D.C. sputtering system, in which the plasma is self-sustained; the charge build up on the surface of the target would soon extinguish the plasma, once the target surface voltage had dropped below

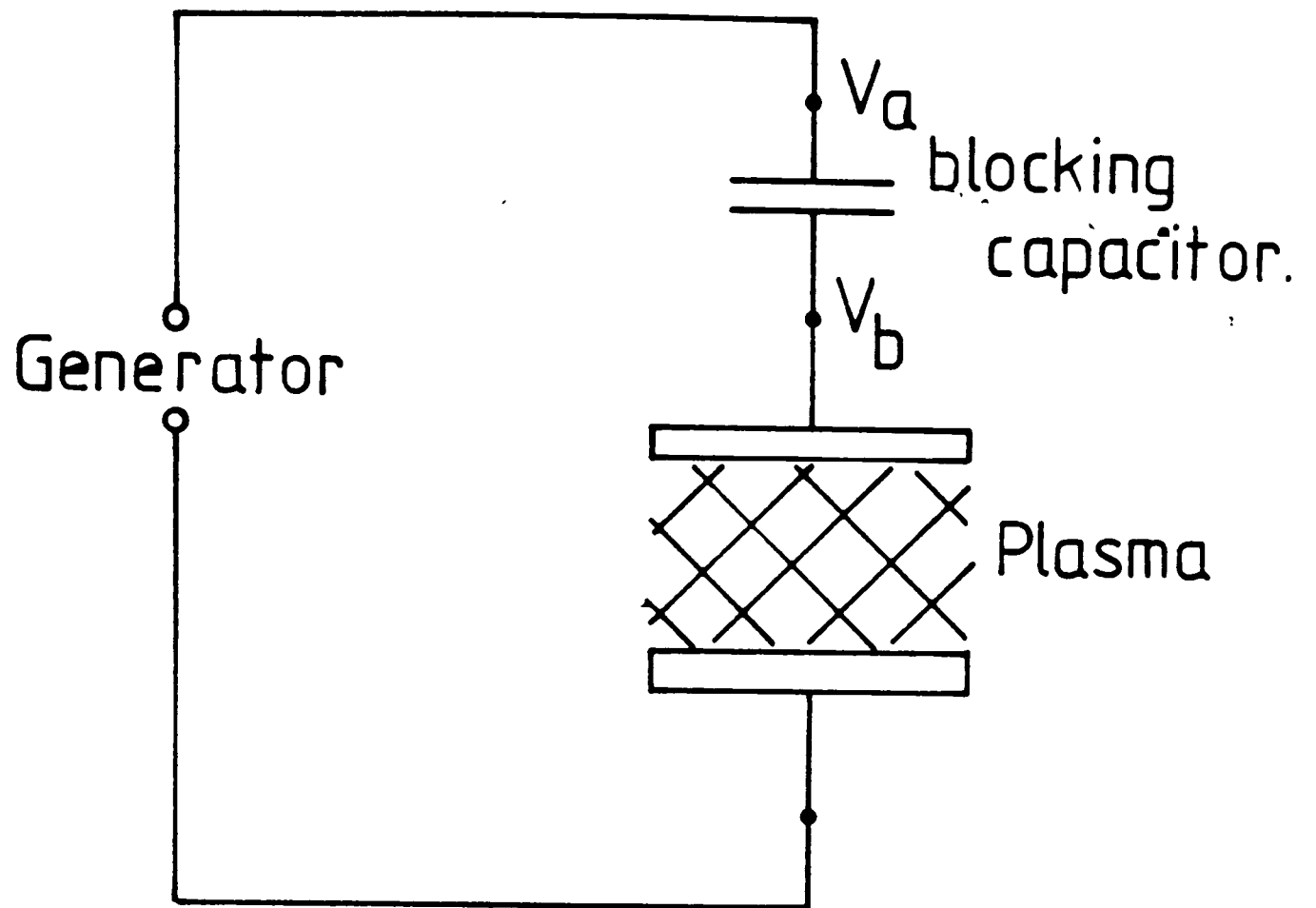
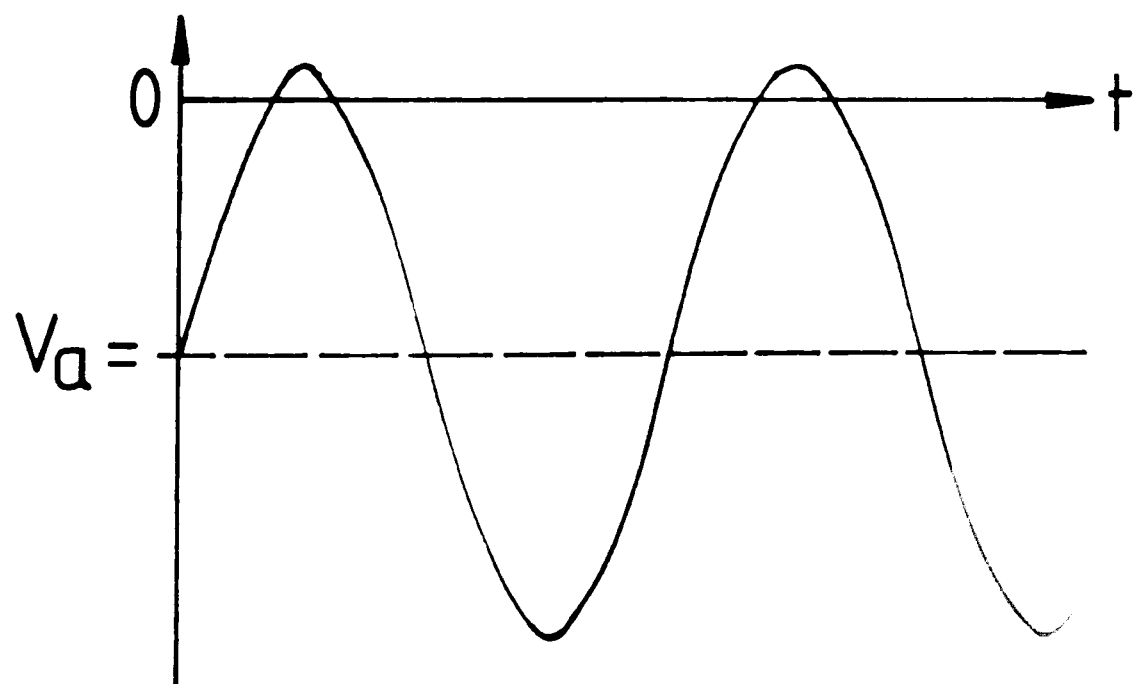
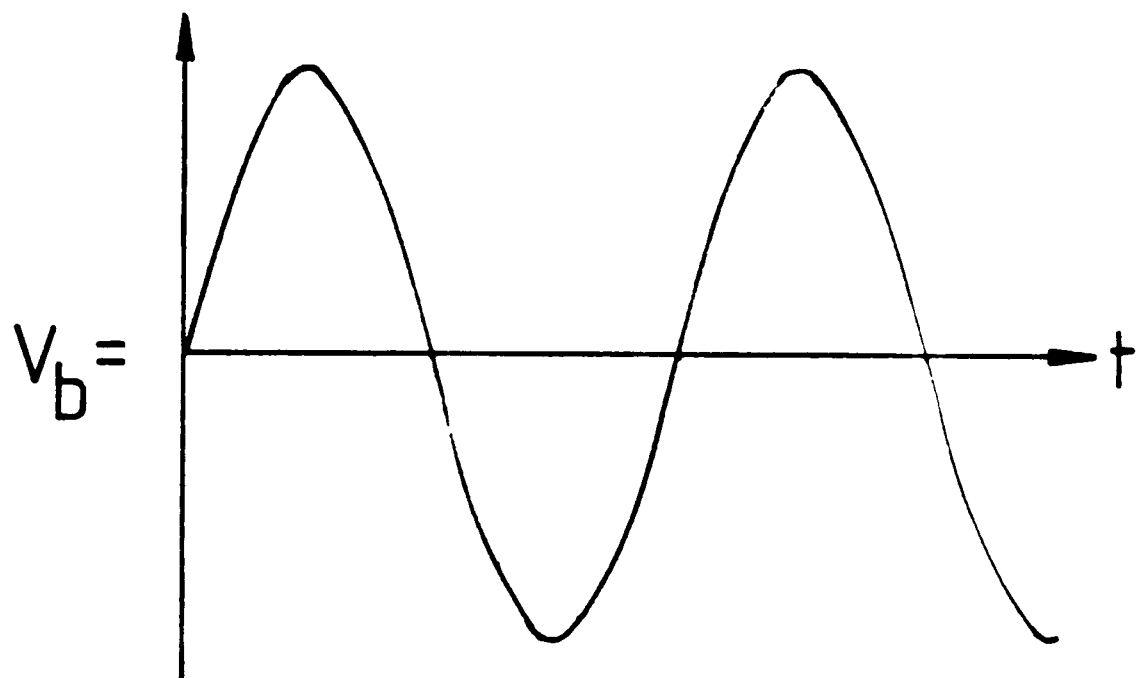


Figure 5



the voltage required to sustain the discharge. This advantage together with the increased efficiency over D.C. sputtering makes R.F. sputtering the more widely used method of thin film deposition. This is despite the fact that this form of sputtering requires the use of an impedance matching network between the power supply and the discharge chamber, which allows the impedance of the plasma and associated potentials to be matched to the generator impedance, increasing the power dissipation in the plasma and protecting the generator.

To understand the asymmetrical electrical configuration required by a R.F. sputtering system in order that material is sputtered from the target only, the variation between the ion and electron currents must be considered. Due to the much smaller mass of the electrons compared with the ions, their velocities will be greater for a particular electric field; and hence the electron current will be greater than the ion current. With the introduction of a blocking capacitor in between the generator and target, this difference in currents results in the potential at the target decaying much more quickly towards zero when it is positively charged than when it is negatively charged. Thus for the circuit shown in figure (5), the alternating target voltage will stabilise around a D.C. offset potential resulting in the target being almost continuously bombarded with ions. In the case where the target is an insulating material the introduction of this capacitor is theoretically



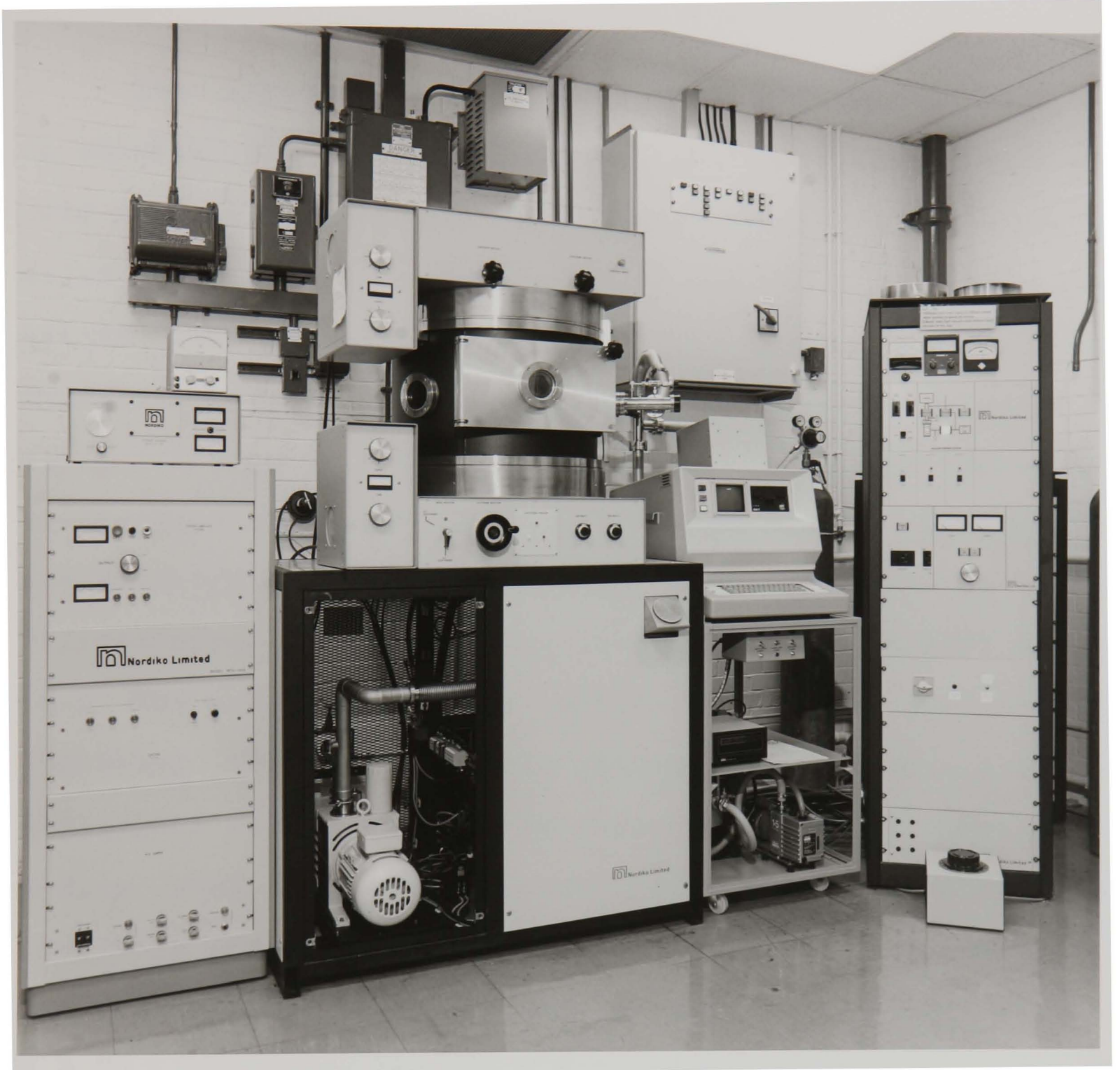


Plate 1

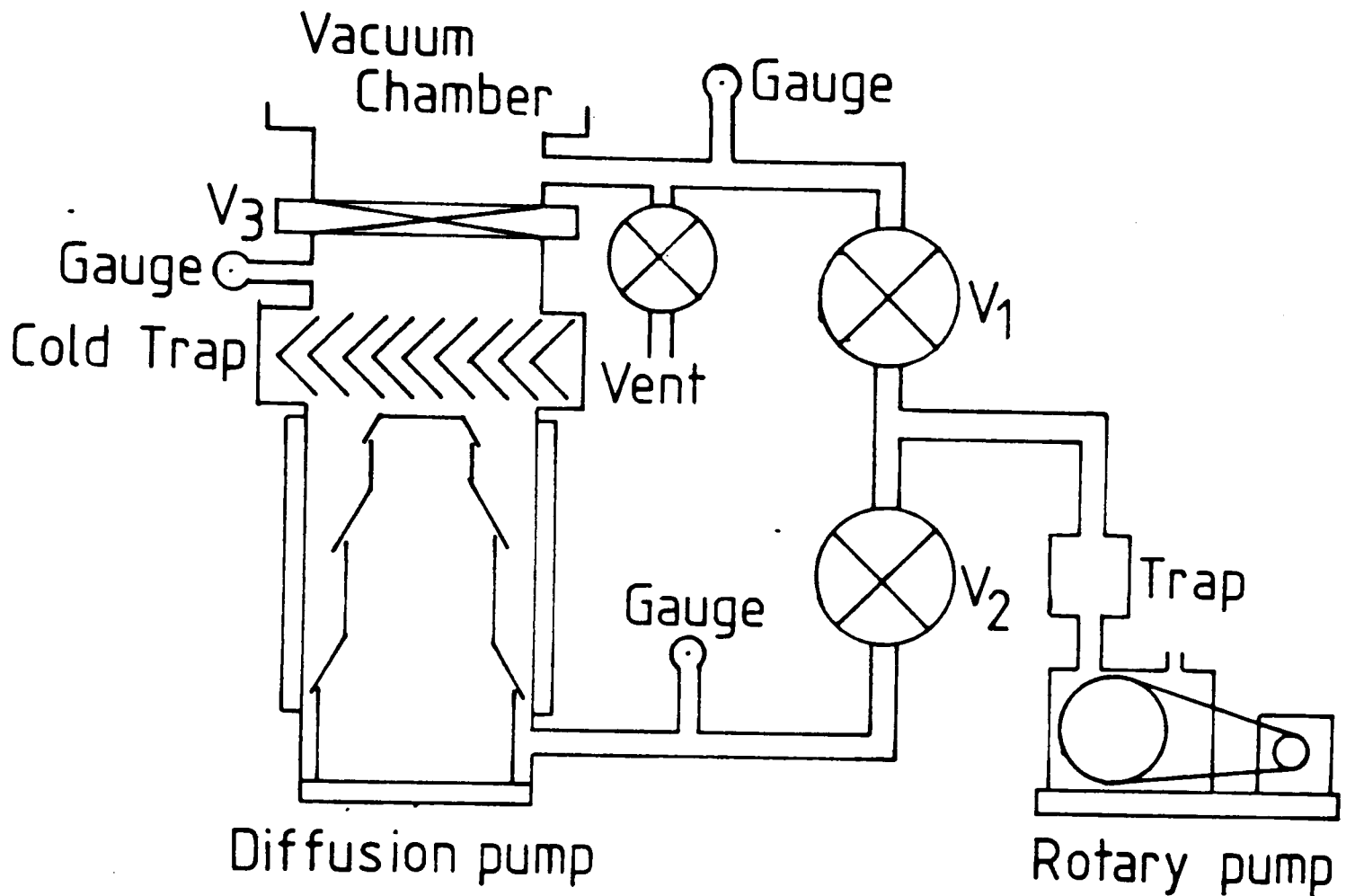
The Sputtering plant used in the fabrication of devices

not required, but its use removes any uncertainties introduced by leakage through or around the target in the plasma.

The targets used in the depositions were 99.999% pure as supplied by the manufacturer, and high purity gases were used whilst sputtering and for exhausting the vacuum chamber after sputtering. A photograph of one the two sputtering plants used is shown in plate (1). Both systems have a stainless steel vacuum chamber that is pumped using an oil diffusion pump to reach high vacuums. This is backed by a rotary pump which also serves to "rough out" the chamber to a sufficiently high vacuum for the diffusion pumps to operate efficiently. Each system has a liquid nitrogen cold trap to lower the S.V.P of residual water vapour in the chamber, improving the base pressures attainable. A schematic diagram applicable to both systems is shown in figure (6). The vacuum gauges used to measure the roughing and backing line pressures are a Hastings EVT-5 meter with DV-23 gauge heads for the Nordiko system; and a Norton N.R.C. 831 meter on N.R.C. 531 gauges for the M.R.C. system. Penning gauges were used on both plants to ascertain the base pressures; Edwards Penning-8 meter with CP25 gauge and N.R.C. 831 meter with a N.R.C. 507 gauge on the Nordiko and M.R.C. systems respectively.

Once the chamber pressure had been lowered to the required value, high purity Argon was leaked into the chamber

Schematic diagram of the pumping system used on the sputtering plant



Valves:-  $V_1$ -Roughing,  $V_2$ -Backing,  $V_3$ -High Vacuum.

Figure 6

in a controlled fashion using a micro-flow valve. The baffle valve was then partially closed to throttle the diffusion pump, causing it to operate at its most efficient point. The chamber pressure resulting from the through-put of Argon was measured using an Hastings EVT-5 gauge and VH5 meter on the Nordiko system, and M.R.C. SEM 8632 meter and gauge on the M.R.C. system. This pressure was then carefully adjusted using the micro-flow valve until the required sputtering pressure was obtained. At this point the sputtering of the target material onto the substrate could begin. When the Argon pressure had stabilised at the required value the R.F. power was turned on and the impedance matching network tuned to give a predetermined forward power, and either a very small or ideally zero reverse power. If the plasma had not been initiated at this point the baffle valve was shut for a few seconds to raise the argon pressure in the chamber. As soon as a plasma had been formed, retuning of the network became necessary to minimise the reflected power. Control of the sputtering rate by monitoring the R.F. power and electrode potential during deposition meant that film thickness could be accurately defined by simply timing the deposition. Although a simple series of depositions of differing sputtering time provided an accurate figure for the sputtering rate for each material for a fixed set of deposition conditions, the use of a nomograph supplied by the systems manufacturer provided an quick additional check. In chapter three the actual parameters and timings used to sputter each layer are given.

## 2.2) Characterisation of ferromagnetic magnetoresistive films.

As previously described R.F. sputtering provides a reliable means of producing high quality magnetoresistive NiFe films for use in the fabrication of sensors. The very low base pressures attainable with commercially available sputtering systems, together with the more advanced sputtering techniques described in chapter three; make the reproducibility of such films magnetic and electrical parameters relatively straight forward. However, in order that the sensors produced from such films are able to provide the highest possible magnetoresistive response several of their fundamental galvanomagnetic properties have to be optimised.

i) The values of the films coercivities and anisotropy fields are not only required for inclusion in the theoretical description of the sensors dynamic response; but are fundamental properties in the films magnetic behaviour.

ii) The resistivity and magnetoresistivity of the complete film have to be measured so that the maximum magnetoresistive response of the sensors can be calculated. Additionally plots of the change in resistance versus applied field, resulting from the anisotropic

Schematic diagram showing the sample to incident beam orientations used in the variety of Kerr effect examinations

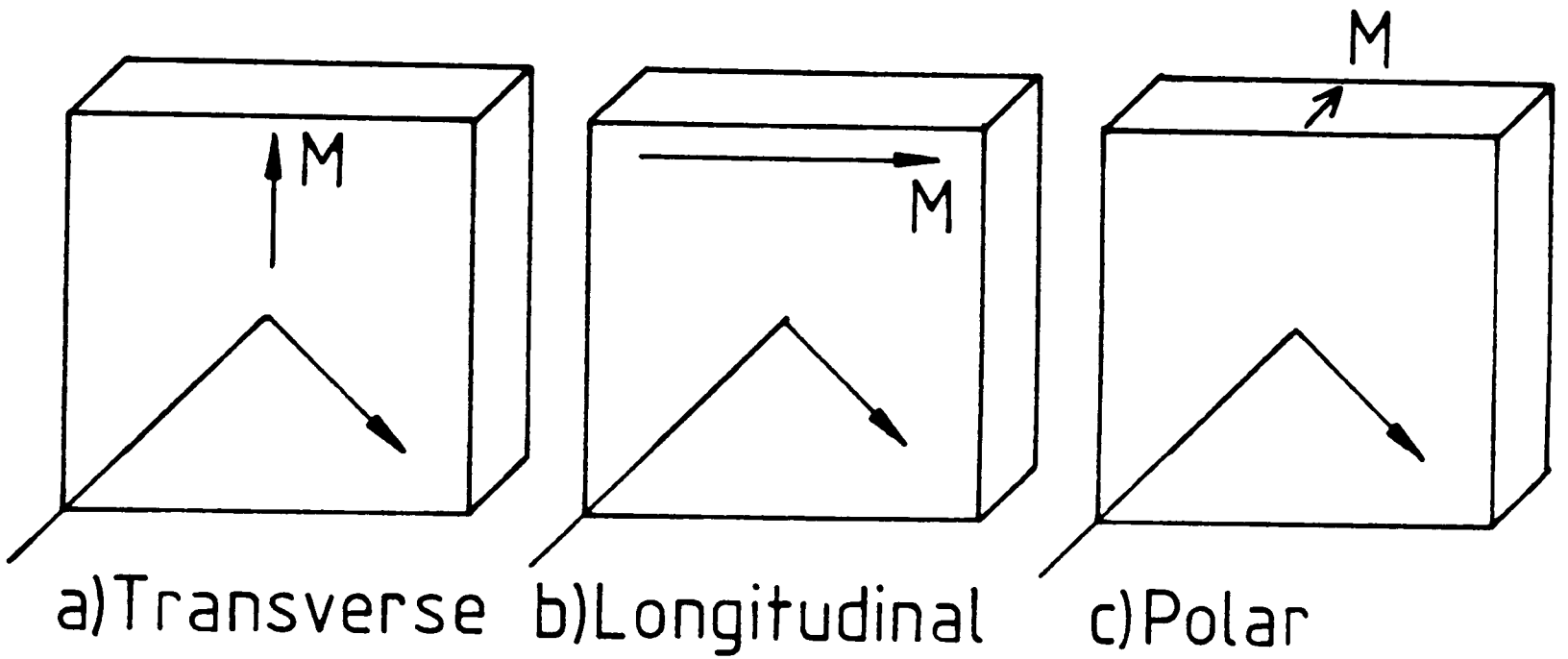


Figure 7.

magnetoresistance of the whole film, provides qualitative information on the dispersion.

As well as these basic parameters other geometrical measurements are required particularly the thicknesses of the various layers used to make up the multiple-film structure; in addition to which the lengths and widths of features on the device have to be measured to supply information on fabrication parameters such as photolithographic resolution and etch control. Other microscopic measurements can also be made on specially prepared samples providing information about the film's grain size. Finally the finished heads have to be tested dynamically using standard compact cassette tapes to provide information about their frequency response and signal to noise ratio.

### 2.3 Coercivity and Anisotropy Field Measurements

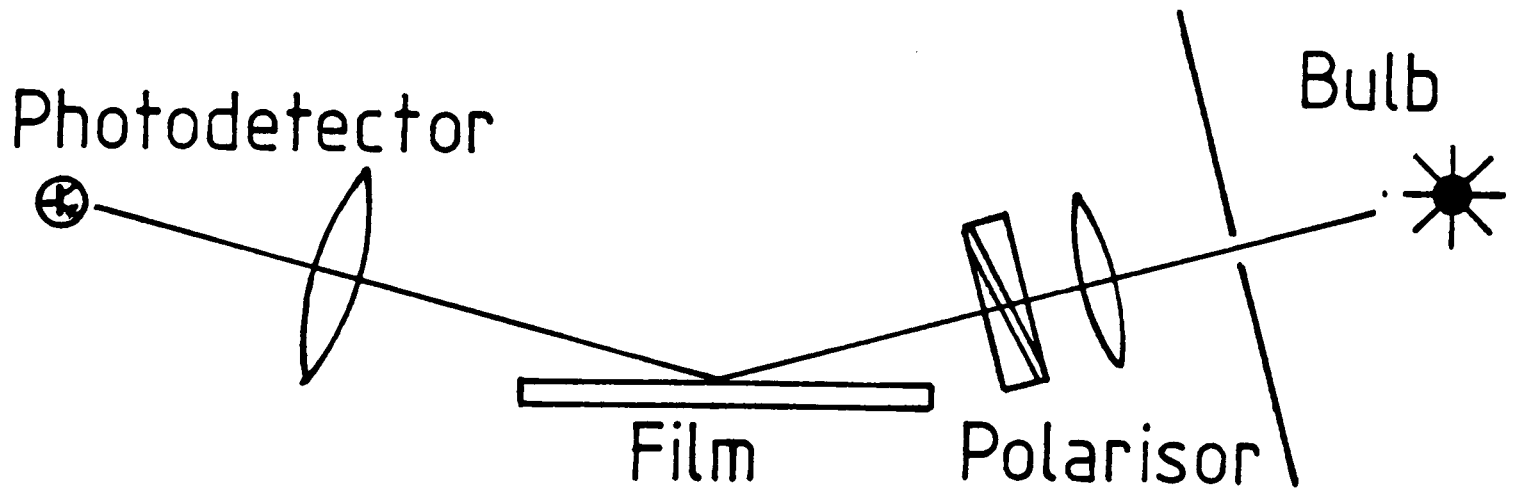
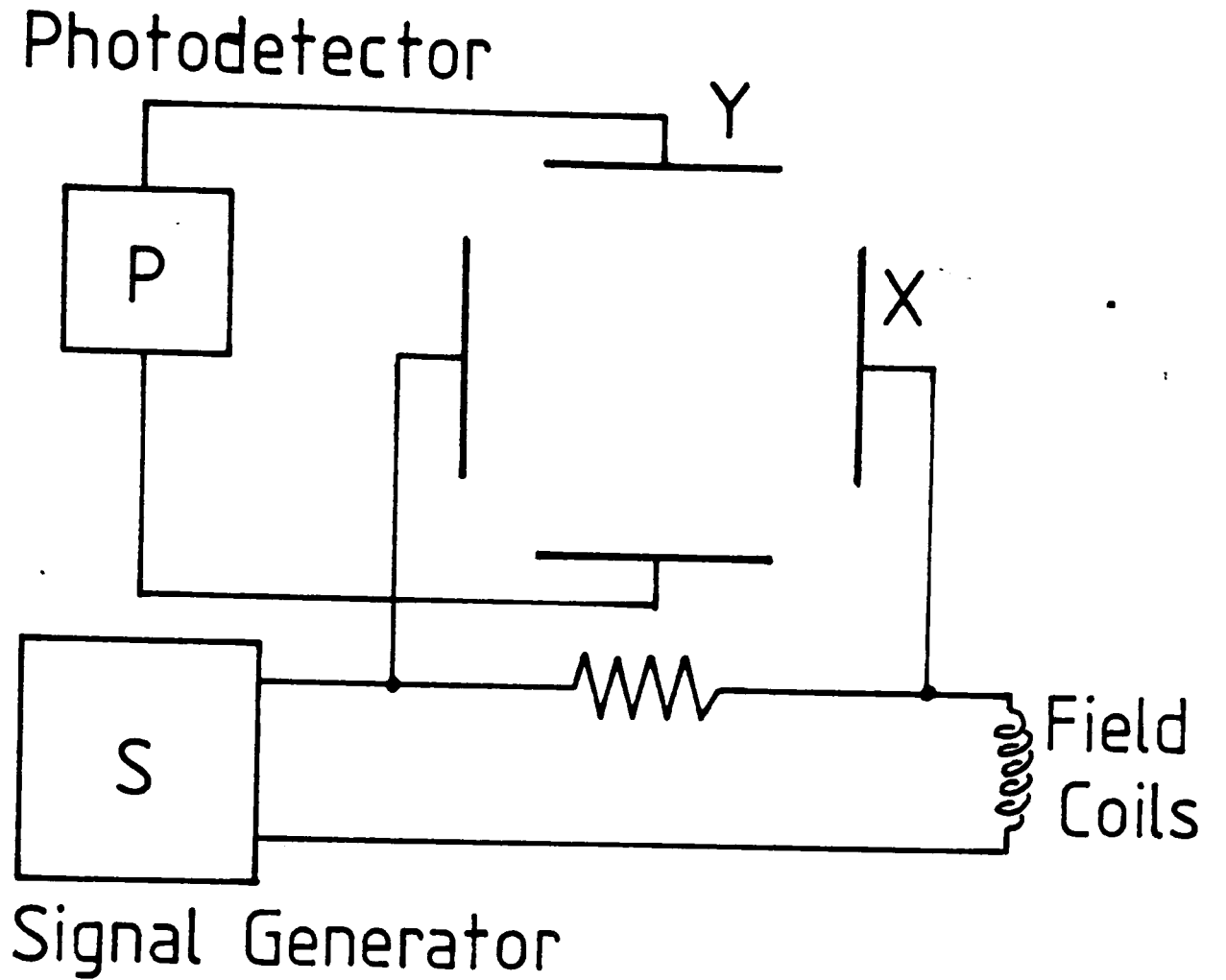
It has been shown that these properties, together with the anisotropy dispersion are instrumental in determining the magnetic behaviour of thin ferromagnetic films [1]. It is therefore obvious that in any practical device that uses an aspect of the magnetic behaviour of such films for its sensing mechanism, these properties have to be carefully optimised. To do this films have to be produced using a variety of deposition conditions, and have their coercivities and anisotropy fields accurately measured. To provide such measurements previous workers have used

inductive loop plotters [2], or torque magnetometers [3]; but these instruments have the disadvantage of only supplying information about the whole film. Due to several complete heads, each incorporating sixteen separate sensors, being fabricated from a single 2" X 2" film; with comparisons being made between elements patterned from different parts of that film; small scale determination of the coercivity and anisotropy field is necessary to check that the magnetic properties of the film are constant over its whole surface.

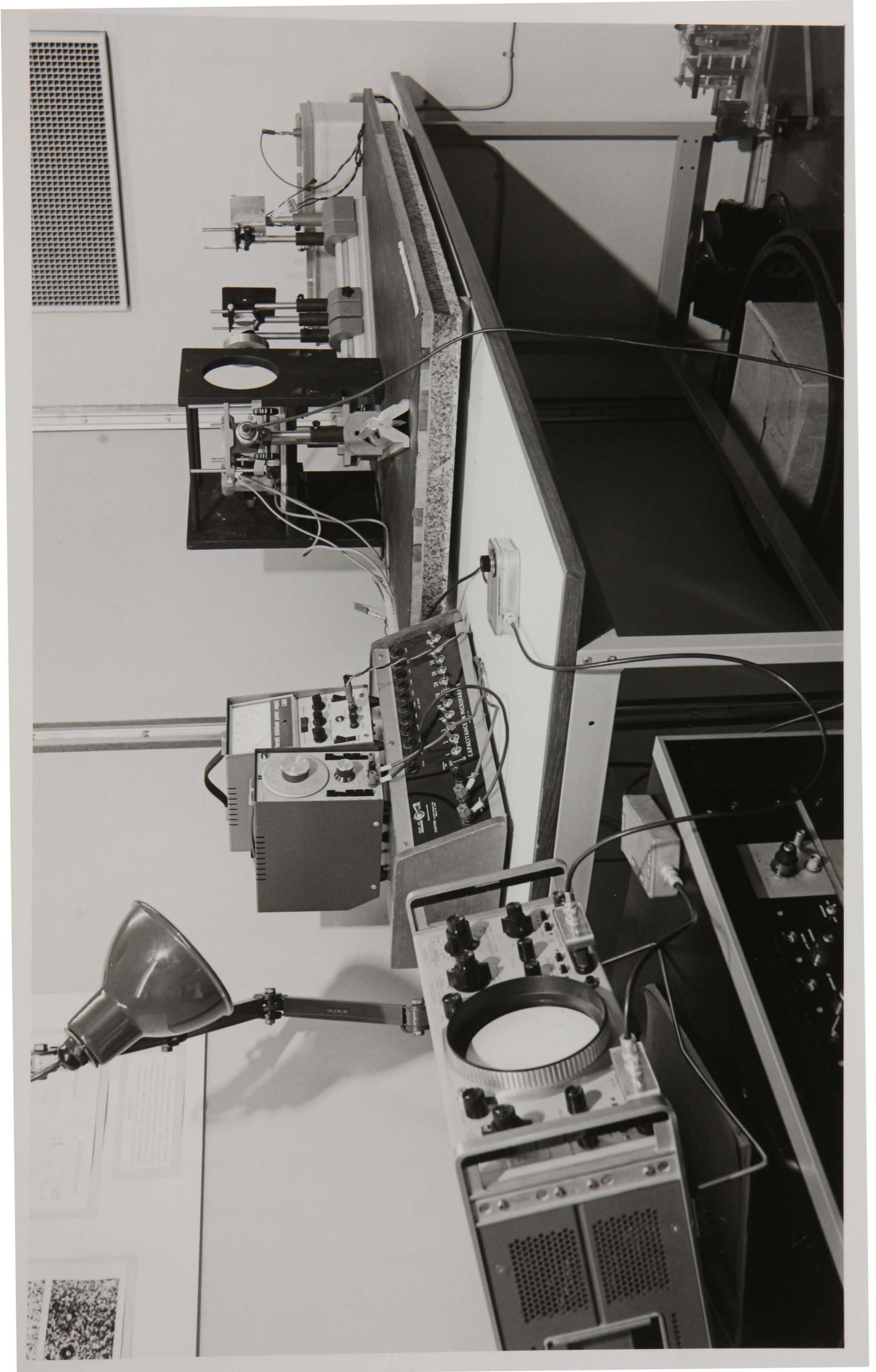
To provide such measurements an instrument has been developed that utilises the magneto-optic Kerr Effect. In this effect the reflection coefficient of a ferromagnetic surface; for obliquely incident light with its electric vector vibrating parallel to the plane of incidence, is found to be a function of the angle between the magnetisation vector and the plane of incidence. Several categories of Kerr effect exist, depending on the relative orientations of the magnetisation direction of the specimen, and the plane of polarisation of the incident light. They are, those in which the magnetisation is normal to the surface; those in which it is in the surface and parallel to the plane of incidence; and those in which it is in the surface and normal to the plane of incidence. These effects are termed the polar, longitudinal and transverse Kerr effects respectively and a schematic diagram of the relevant configurations is given in figure (7). Much work has been done on the theoretical description of the effect [4,5,6], and its use in the



Figure 8



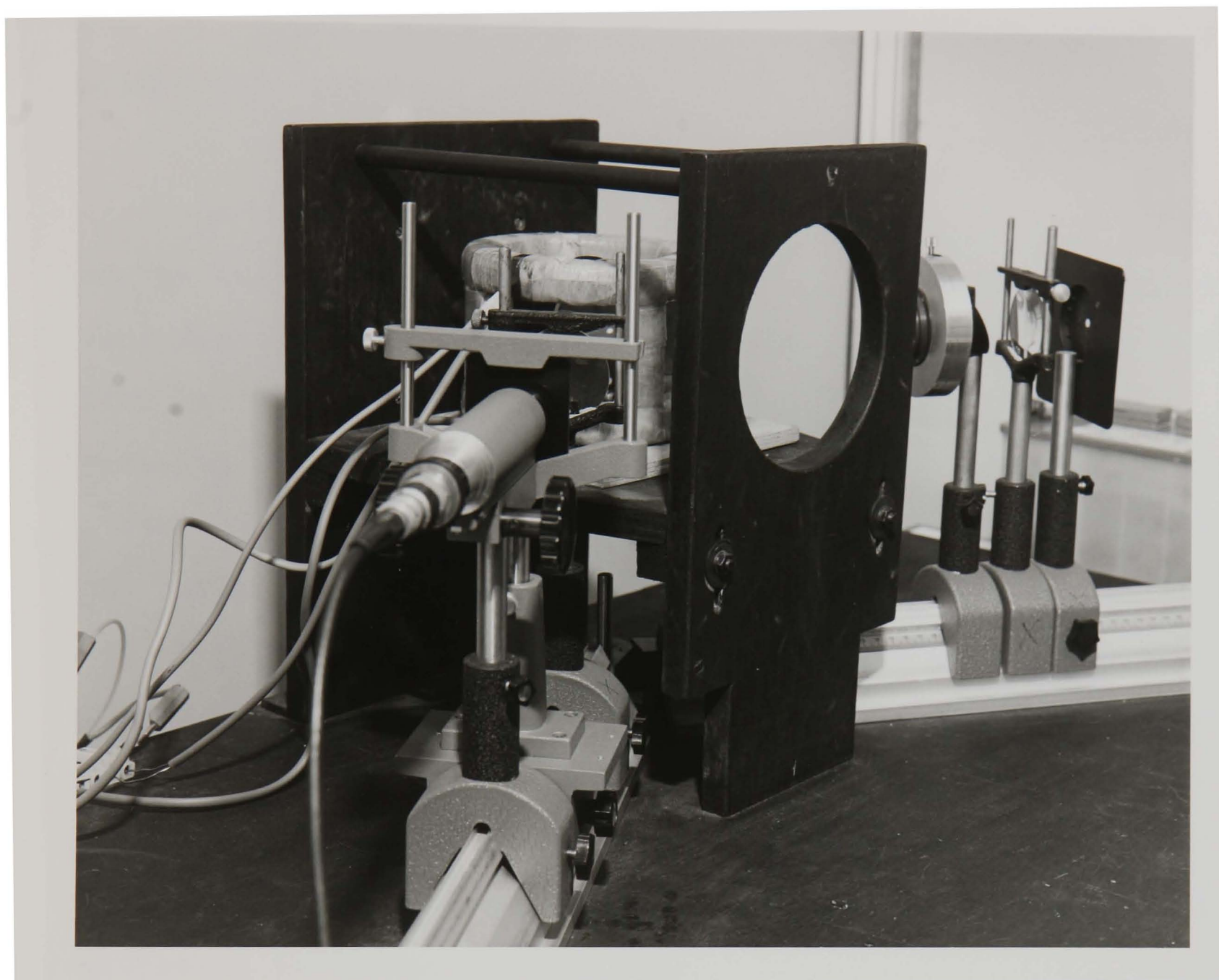
Schematic diagram showing the field coil, and optical arrangements used to examine the samples magnetic properties using the Kerr effect



examination of the hysteresis loops of thin ferromagnetic films has become common.

In the instrument constructed for use in this investigation a simple slide projector bulb is lit using a standard car battery to provide a constant intensity light source. This source is then collimated and polarised using standard optical components, and is reflected at a predetermined angle off the surface of the film. This angle is chosen to maximise the intensity of the reflected light, and is typically 80 degrees. The beam is then re-collimated and focussed onto a photodetector. Due to the effect being small in the optical part of the electromagnetic spectrum, an Infra-Red detector is used and its output amplified before being fed to the vertical terminals of an X-Y oscilloscope. Additionally the use of an infra-red filter in the optics of the reflected beam improves the signal to noise ratio of the final hysteresis loop by filtering out unwanted reflected light.

The horizontal terminals of the oscilloscope are connected across a standard resistance in series with the field coils magnetising the film. To overcome phase differences between this voltage and the magneto-optic signal a simple phase shifting network is used in this circuit to linearise the response. The field coils are arranged in a Helmholtz pair and have 50 turns on each coil. They were calibrated using a standard Hall probe placed centrally



The optical arrangement used in the Kerr-effect apparatus

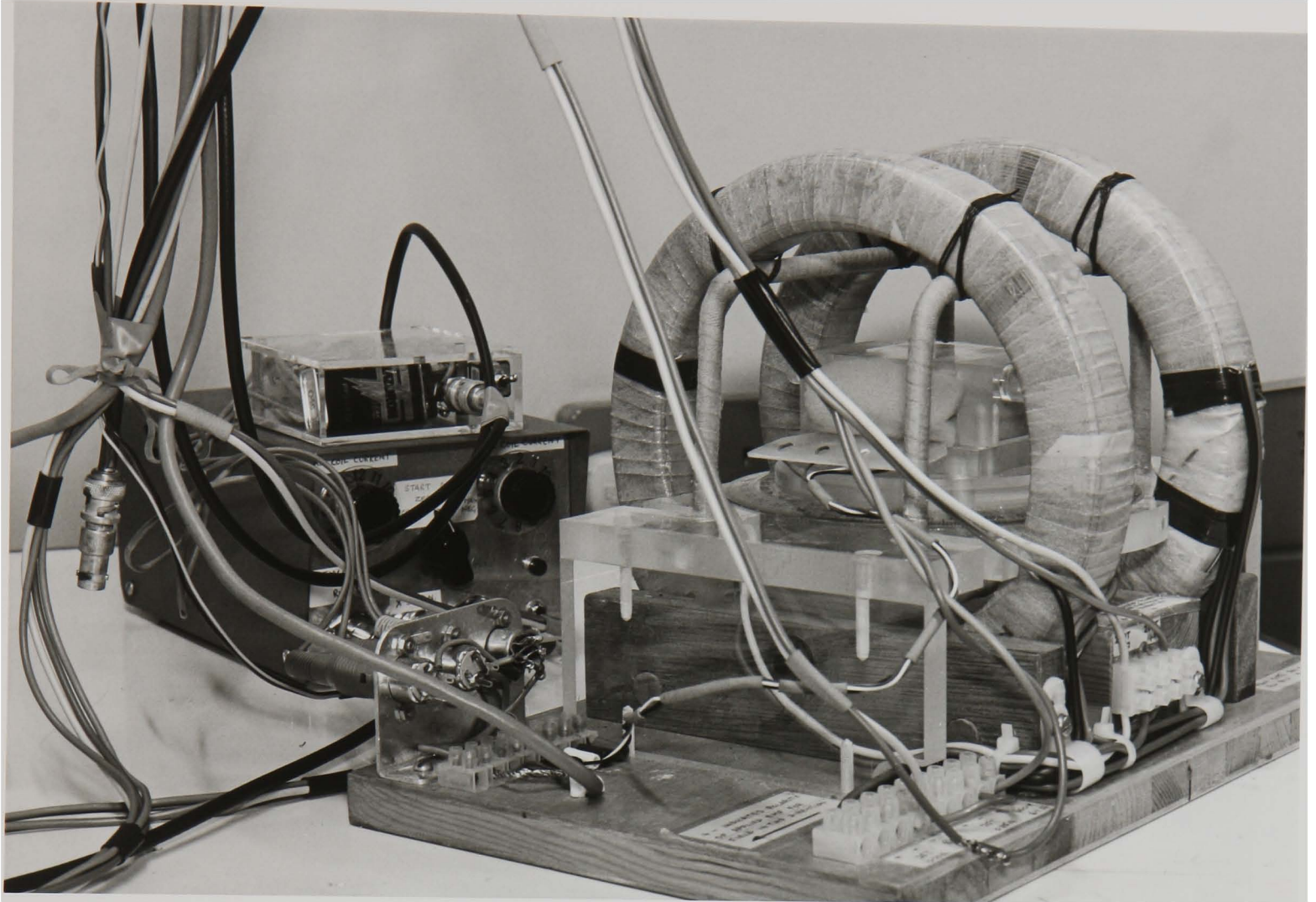
between them, and this calibration was checked using a search coil. To overcome distortion of the resulting M-H loop due to the vertical component of the earths magnetic field, a second set of coils wound onto the main magnetisation coils is driven with a direct current.

By careful collimation and focussing of the light source this instrument has enabled the hysteresis loops of very small areas, typically 1 m.m. in diameter; of a 2" X 2" film to be examined. As the substrate is mounted on a rotating goniometer stage, values for the coercivity and anisotropy field have been obtained from several locations on the surface of the films used in detector fabrication. This has meant that the the homogeneity of a particular films coercivity and anisotropy field can be ascertained in order that the response of the various elements patterned from it can be normalised. A schematic diagram of the optical arrangement is given in figure (8) and two photographs of the equipment in plates (2) and (3).

#### 2.4 Resistivity and Magnetoresistivity measurements.

In view of the fact that the flux sensing mechanism of the sensors is totally dependent on the anisotropic magnetoresistance of the film from which the sensors are fabricated, accurate measurement of this parameter is necessary. Additionally it has been shown that the

Plate 4



The field-coil, and four contact pad used in the resistivity/magnetoresistivity determination

resistivity of a particular film compared with the bulk resistivity of that material, is a good indication of its crystallinity (or poly-crystallinity) [7]. One common method for obtaining these parameters is the use of a four contact potentiometric circuit [8,9,10]. In this method a constant current is passed between an outer pair of contacts and is assumed to be isotropic across the width of the film between the contacts. An inner pair of contacts is then used to measure the voltage dropped across a portion of film in between these outer contacts. Simple calculations provide the resistance of that portion of film, from which its resistivity can be calculated after the film thickness and inner contact separation have been measured. For small elements pre-patterned gold connections have been used for the film contacts, but for large substrate size films a pressure pad has proved adequate.

To enable the instrument developed to measure the resistivity and magnetoresistivity of films produced in this investigation, a section of flexi-circuit is patterned to provide the four electrical contacts with the film. This is pressed against the surface of the film using a block of foam rubber, as can be seen in plate (4). The potentiometric circuit shown in figure (9) is then used to measure the change in resistance of the specimen due to an external applied field. In this circuit two identical current sources supply currents to the outer pair of contact strips on the flexi-circuit, and a standard resistance box. To accomodate

Circuit diagram of the bridge network used in the resistivity/magnetoresistivity measurement apparatus

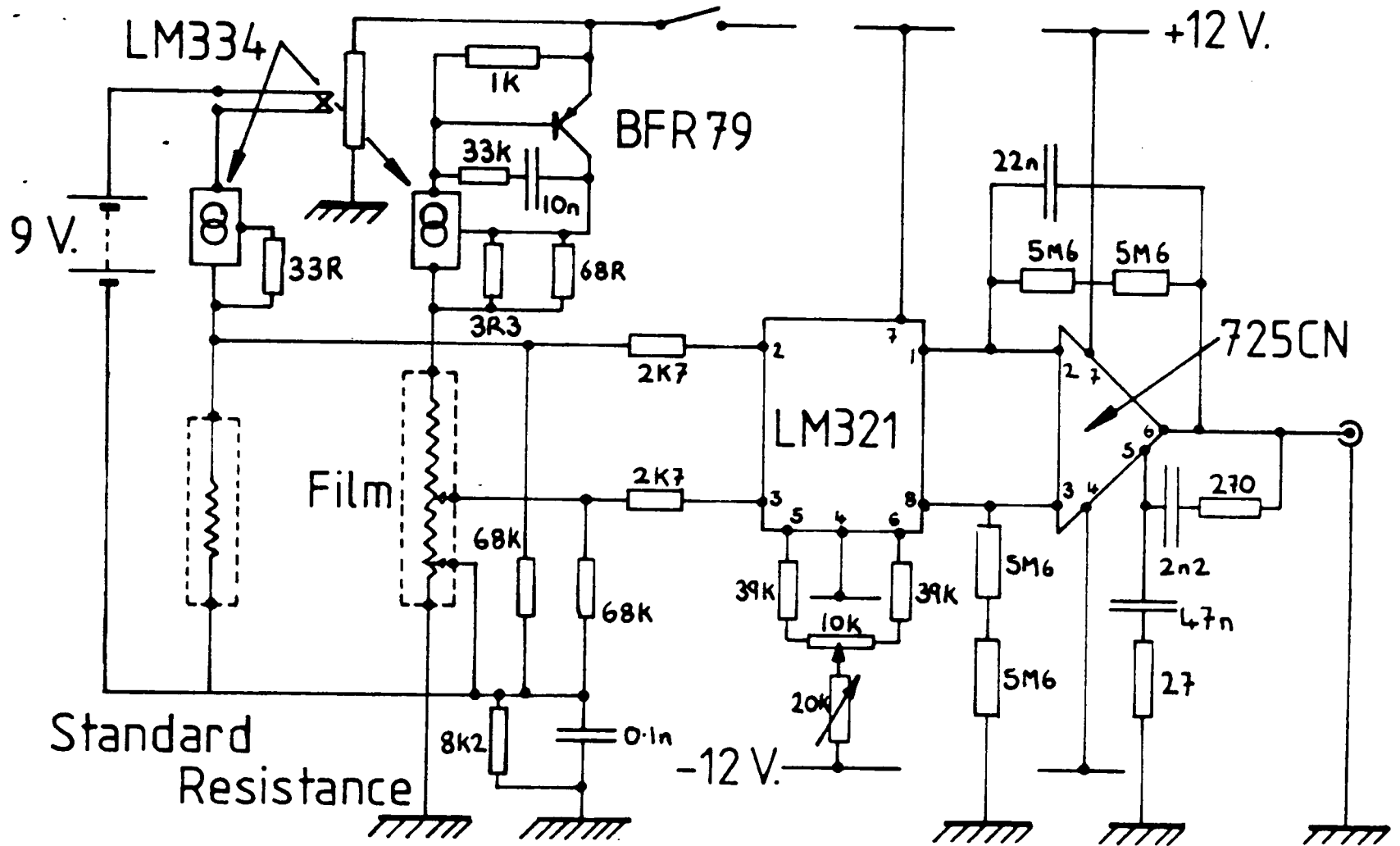
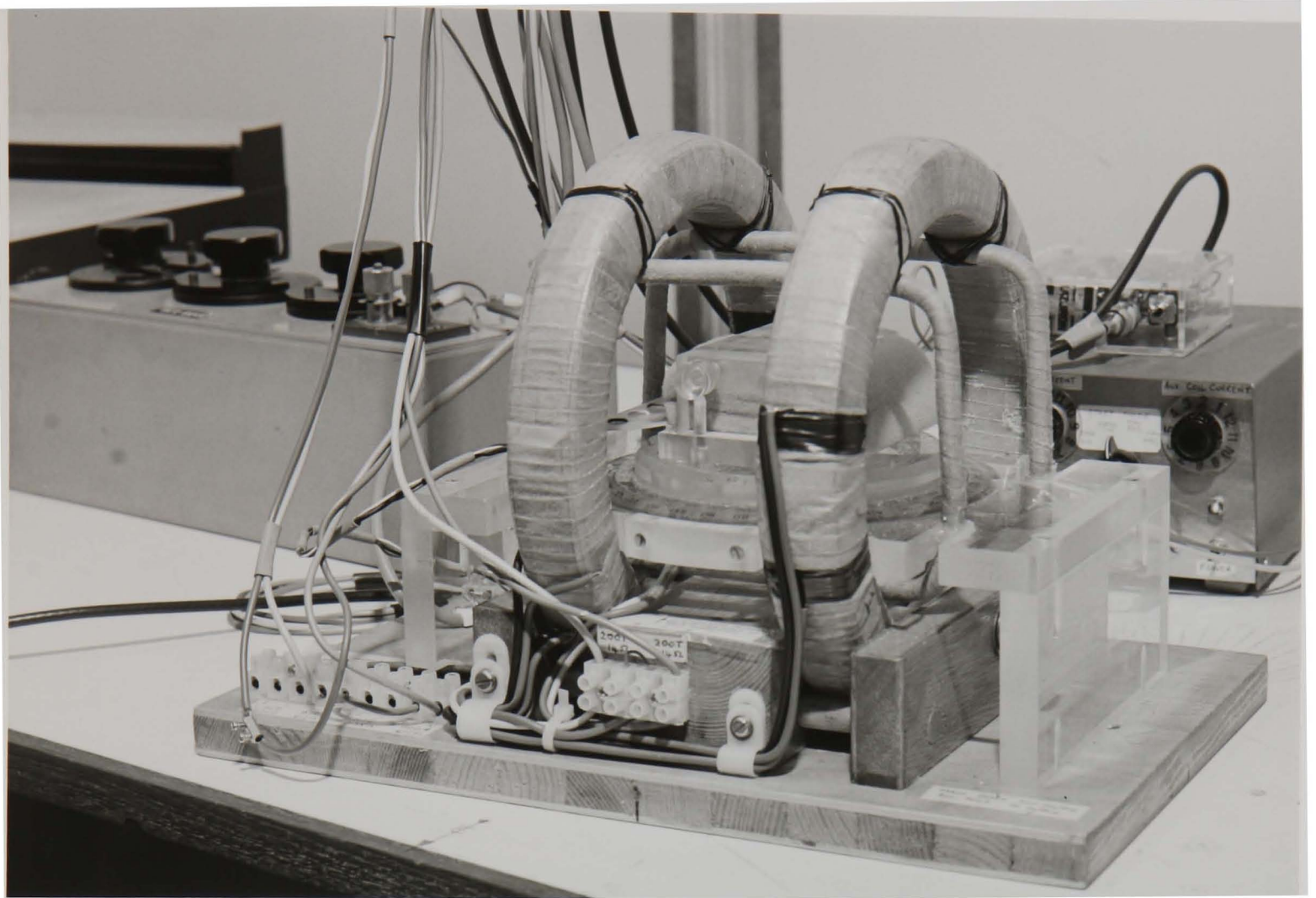


Figure 9

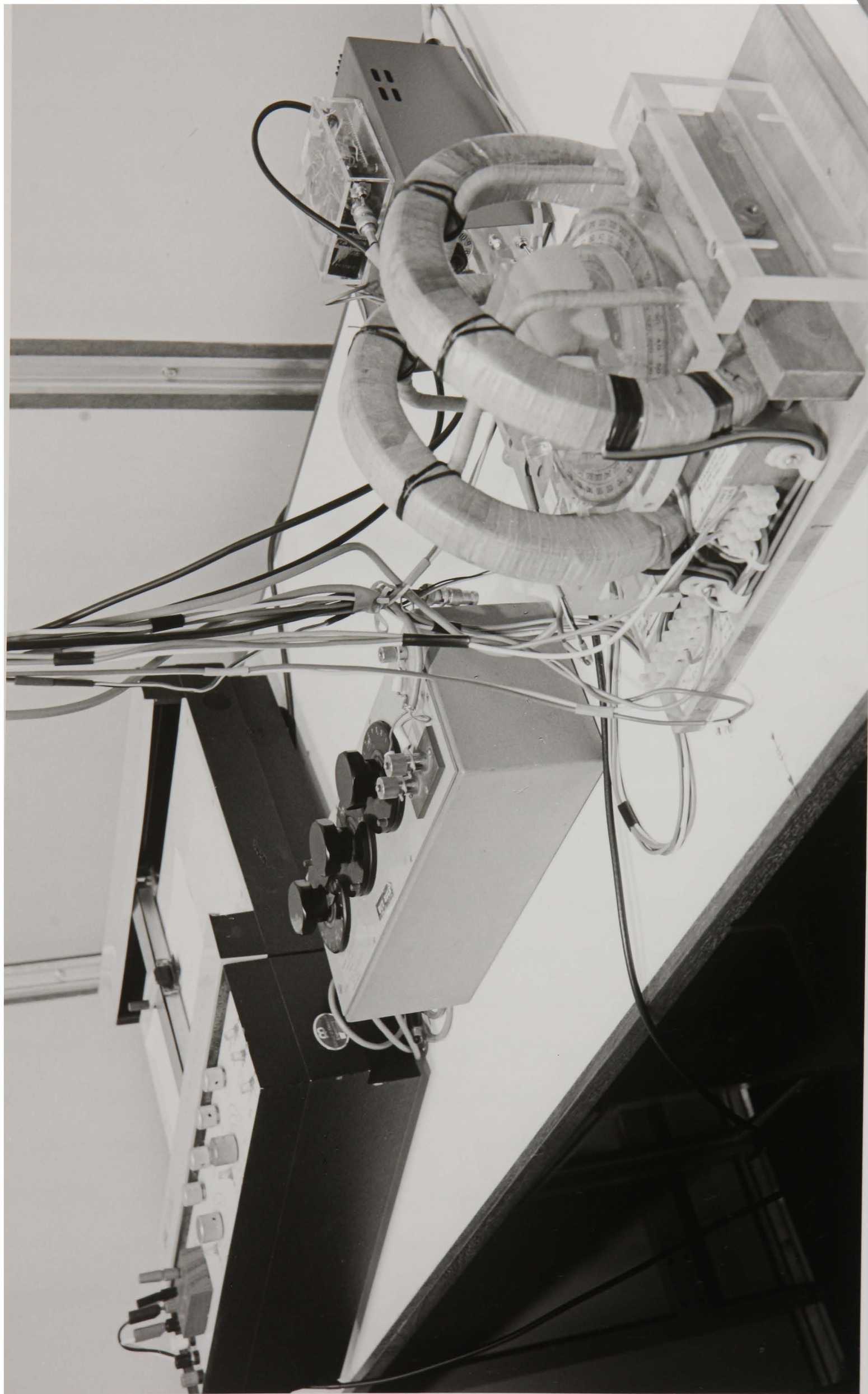


Plate 5



The field-coils used to rotate the samples magnetisation

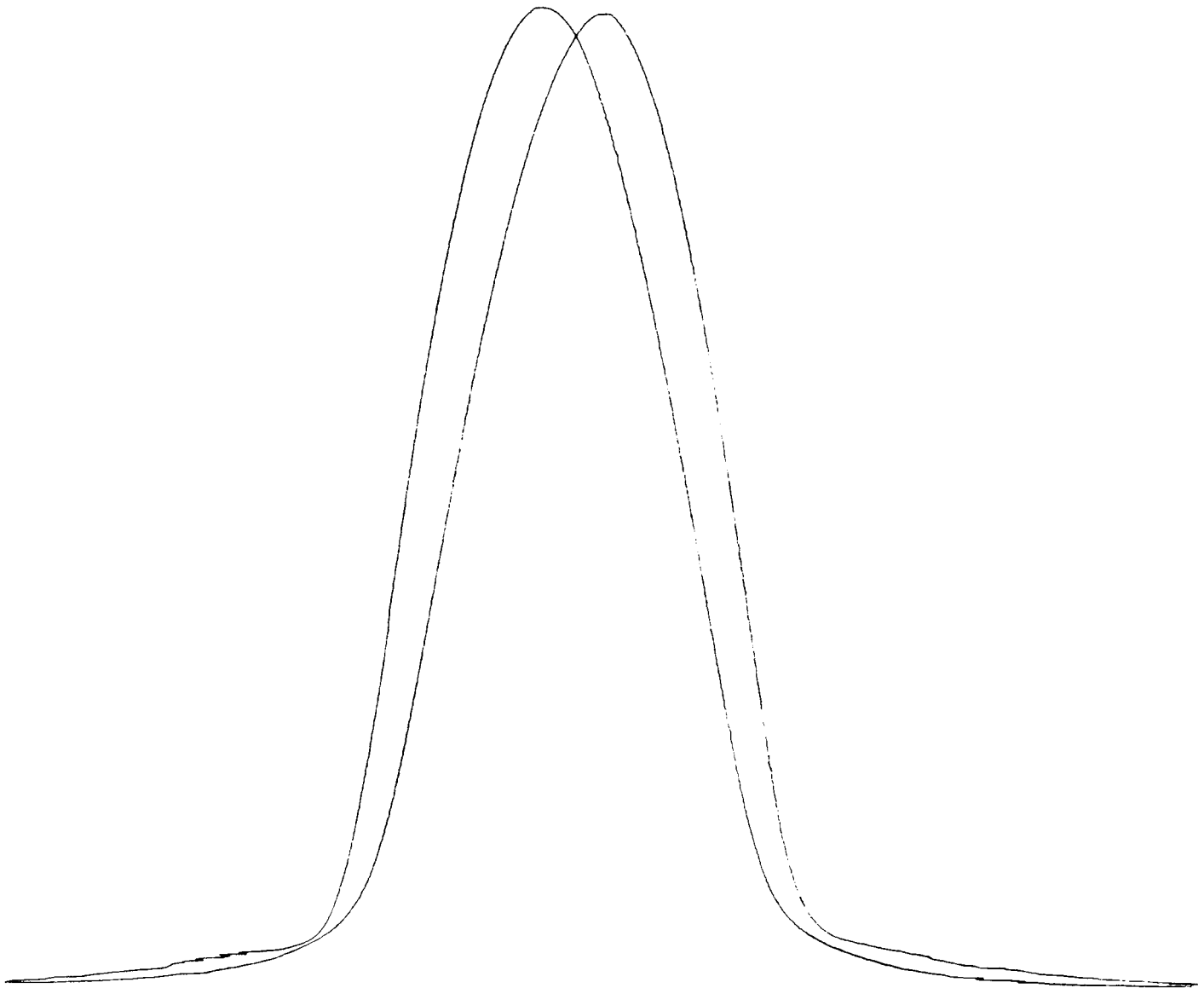
v



large variations in film resistance due to films having widely different dimensions the current to the contact strip can be set to be either identical to that through the resistance box (20 mA), or 10 times smaller. Thus for the thinner films having high resistances a balance point can still be found using reasonable values for the standard resistance. To find the film resistance between the inner pair of contacts the resistance box is simply adjusted until the bridge output is zero volts.

To measure the anisotropic magnetoresistance of a film, an external magnetic field has to be applied to it to rotate its magnetisation moment relative to the current direction. For this purpose a Helmholtz coil system surrounds the film being examined and a field is applied to saturate it first in one direction, and then after passing through zero, the other. To do this a ramp generator supplies the current to the field coils, providing a very slow change triangular waveform oscillating about zero volts at about 0.09 Hz. As the direction of the magnetisation moment is rotated by this field, the resistivity of the film changes due to the anisotropic magnetoresistance, and the resultant output from the bridge is fed to the vertical terminals of an X-Y plotter. A voltage proportional to the current in the field coils is fed to the horizontal terminals of the plotter, allowing permanent records of the magnetoresistive change of different films to be produced. Once the field has been cycled several times and the resulting plots drawn, the

Figure 10



A typical plot produced in the magnetoresistance  
determination

change in resistivity due to the magnetoresistance can be determined by reducing the external field to zero, and altering the value of the standard resistance box in fixed standard increments to obtain the same change in bridge output as that produced by the magnetoresistive change of the film. From measurements taken directly from the plot produced, the transverse anisotropic magnetoresistance can then be easily obtained. Two photographs of the system are shown in plates (5) and (6).

In addition to the main drive coils which provide the field required to saturate the film; a second set of smaller coils are wound orthogonal to them. In films having a large dispersion the the lack of a well defined easy-axis results in the magnetisation not relaxing back to its undisturbed position once the external field has been removed. This produces a "Double-Peak" magnetoresistive response, with the separation between the peaks being a qualitative measure of the dispersion [11,12]. By applying a second field perpendicular to the saturating field, a well defined direction is supplied for the films magnetisation to relax to, thus pulling the magnetoresistance peaks together. This field also has the effect of providing the maximum possible magnetoresistive change by simultaneously aligning all the magnetisation along the easy axis prior to rotating the magnetisation. Typical R-H plots are shown in figure (10) without the easy axis aligning field applied.

## 2.5 Grain Size Measurements.

As has been shown by Hoffman [13] practically all the magnetic properties of ferromagnetic films depend on their physical structure. This structure is characterised by the crystal lattice, the range of ordering (amorphous, polycrystalline, single crystal), the crystallite size, the film thickness (although for very small elements the other dimensions can have an effect), and the intrinsic stress. In the ripple theory developed by the same author [14], the effect of these structural parameters on the magnetic properties was first explained, and a new material parameter, the structure constant, was introduced.

$$S = \frac{K_s f_1 D}{n^{1/2}} \dots\dots\dots(2)$$

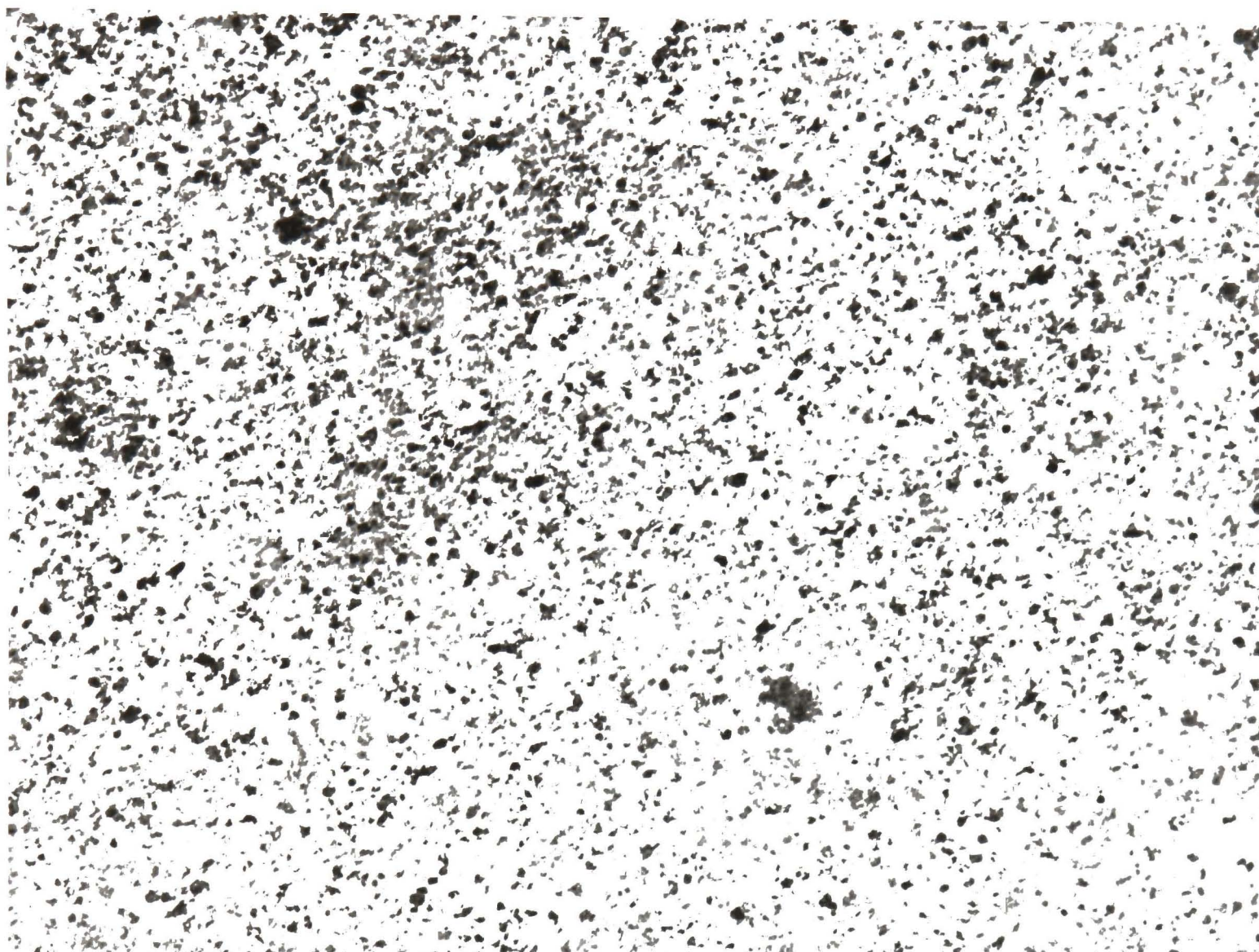
In this equation  $K_s$  is value of the local anisotropies,  $f_1$  the standard deviation of a trigonometric function determined by the symmetry of the crystallites,  $D$  is the mean crystallite diameter and  $n$  is the number of crystallites.

Doyle and Finnegan [15] showed that the value of the local r.m.s anisotropy ( $K_s, f_1$ ) could be calculated from the magnetocrystalline anisotropy constant and the magnetostriction constants for single crystals, for which the published values are  $4 \times 10^3$  erg/cm<sup>3</sup> and  $9 \times 10^{-6}$  respectively; and the intrinsic isotropic stress. Hence the

value of the structure constant could be obtained. Additionally it has been found by other workers [16] that for deposition substrate temperatures over 300 degrees centigrade, there is a marked increase in the value of this structure constant, with a corresponding increase in grain size. This results in a degraded magnetic performance for magnetoresistive sensors due to the increase in the dispersion. Hence the measurement of a films grain size provides a qualitative guide to one aspect of its magnetic behaviour.

The grain size measurements were taken from specially prepared very thin (200 Angstrom) NiFe films using transmission electron microscopy. Although practical devices are fabricated from films at least 2-3 times thicker, grain size determination was not possible at these thicknesses using the electron microscope available, as such films are opaque to the electron beam. The films to be measured were sputtered onto freshly cleaved mica substrates, onto which 2,500 Angstroms of carbon had been coated. Included in each deposition to provide a sample for grain size determination, was a standard substrate providing a control for the electrical and magnetic properties. Despite the fact that the corning 7059 borosilicate substrates have amorphous surfaces, and the mica is monoclinically crystalline, little difference was found in the magnetic or electrical properties of the films. The reason for this is felt to be the smoothing out of the mica's crystallinity by the thick carbon layer. Thus it

Plate 7



A typical micrograph, showing the grain size of a NiFe  
film



is feasible to assume that the measured grain size is the same as that of the films prepared on the standard substrates, although the extrapolation of the results to the film thicknesses used to produce sensors remains conjecture.

To mount the films for transmission electron microscopy they were floated off the mica onto the surface of a beaker of water, using the surface tension of the water to separate the film from its substrate along the carbon interlayer. Sections were then carefully lifted out onto gold grids and dried on filter paper. Although remnants of the carbon interlayer remained on the back of the film sections prepared, these are found to be transparent to the electron beam and do not affect grain size determination. Once completely dry the sections were examined in the microscope, with several micrographs being taken of different areas seen to be typical of the overall film. Grains could then be measured directly from these electron micrographs, after allowance had been made for the print enlargement.

For the films produced for this experiment, an average grain diameter of 300 angstroms was obtained, comparing well with that found by other workers for vacuum evaporated films, [16,17,18]. Additionally this grain size is significantly below that found in films which would be unsuitable for use in magnetoresistive sensors [16]. Thus, although such films are not typical, in either thickness or

substrate material when compared with the films used in device production; it can be assumed from the micrographs of their grain structure, that there is no fundamental problem with the depositon methods. It was consequently assumed that this conclusion would also be valid for the thicker sputtered films, which were patterned into the heads detection elements. A typical micrograph is shown in plate (7).

## 2.6 Other Physical Dimension measurements.

To characterise a particular sensors dynamic performance its length, width and thickness must be known. The measurments in the plane of the device were taken using an Olympus BH2 optical microscope fitted with a vernier eye-piece. Values for the thicknesses of the various films used to make up the sensors, conductors and insulation layers were obtained from a Rank, Taylor, Hobson type Tallystep 1 stylus measuring instrument.

REFERENCES CHAPTER TWO  
-----

- 1) M. Prutton. Brit. J. Appl. Phys. vol.15 pp815 (1964)
- 2) T.S. Crowther. J. Appl. Phys. vol.34 no.3 pp580 (1963)
- 3) W.D. Doyle. J. Appl. Phys. vol.37 pp1769 (1962)
- 4) C.C. Robinson. J. Optical. Soc. of America. vol.54 no.10 pp1220 (1964)
- 5) R.P. Hunt. J. Appl. Phys. vol.38 no.4 pp1652 (1967)
- 6) D.O. Smith. Opt. Acta. vol.12 pp13 (1965)
- 7) A.F. Mayadas, J.F. Janak, A. Gangulee. J. Appl. Phys. vol.46 no.6 pp2780 (1974)
- 8) E.N. Mitchell et. al. J. Appl. Phys. vol35 no.9 pp2605 (1964)
- 9) K. Kuwahara. Trans. Jap. Inst. Metals vol.6 pp192 (1965)
- 10) S. Krongelb. Jnl. of Electronic Materials vol.2 no.2 pp228 (1972)
- 11) F.G. West. J. Appl. Phys. vol.32 pp290s (1961)
- 12) J.H.J. Fluitman. Thin Solid Films vol.16 pp269 (1973)
- 13) H. Hoffman. Thin Solid Films vol.58 pp223 (1979)
- 14) H. Hoffman IEEE Trans. Mag. vol.MAG-4 pp32 (1968)
- 15) W.D. Doyle, T.F. Finnegan. J. Appl. Phys. vol.39 pp3355 (1968)
- 16) V.B. Chapman, A.S. Marwaha. Thin Solid Films vol.76 pp77 (1981)
- 17) S.G. Fleet. Mullard Res. Lab. Rep. pp466 (1963)
- 18) M. Rheinbold, H. Hoffman. Phys Status Solidi A, vol.2 ppK69 (1970)

### CHAPTER THREE

-----

" The design, optimisation, and construction of a six-element multiple-film magnetoresistive replay head for audio applications "

3.0) Design and fabrication of the multiple film head.

3.1) The use of Multiple-Film elements in magnetoresistive heads.

There are many advantages associated with the use of the anisotropic magnetoresistance effect in the reading of magnetically recorded information. Firstly the magnetoresistive element is a parametric device, where the voltage is scaled by the applied sense current, which in turn is limited only by thermal and electron migration considerations. This means that much larger sensor outputs are typically available compared with inductive read elements. Secondly good linear density resolution can be obtained by implementing one of the variety of design configurations that have been considered in chapter one. Finally as the use of the phenomena results in the sensor being a flux ( $\phi$ ) sensing device, rather than a rate of change of flux ( $d\phi/dt$ ) sensing device; the sensor output is independent of medium velocity.

A detailed description of the use of the effect in magnetic recording and of the various designs that have been proposed to most usefully exploit the phenomena has been given in Chapter One. However the main improvement offered by sensors using the effect over standard inductive heads; that

of reduced trackwidth whilst retaining a good signal to noise ratio, becomes increasingly difficult to obtain as the trackwidth becomes very small. This is due to the resistance of the element being reduced linearly with the reduction in trackwidth and hence the available signal becoming unacceptably small. To overcome this problem the design proposed here retains the ability to read small trackwidths whilst providing a high signal to noise ratio by "folding up" the magnetoresistive element. Additionally it has proved possible to fold together two magnetoresistive elements in such a fashion that the sense current in each element provides the bias field required to linearise the response of the adjacent element. A schematic diagram of the design is given in figure (4).

As can be seen from this diagram the length of available sensing element is three times the trackwidth, and by differentially sensing the element outputs a possible sixfold increase in signal is possible over a single sensor of the same length as the recorded track. The ability to differentially sense the two arms of the structure also acts to cancel second harmonic distortion introduced by the quadratic component of the magnetoresistive response function. Due to the compact nature of the sensor structure this use of a differential sensing mechanism has the additional advantage of limiting thermally induced noise. However a problem arises from the spatial separation of the array required to electrically insulate each of the layers;

in that as the length of the recorded wavelength approaches that of the array height a reduction in signal is created as each element in the array starts to sense radically different tape fields. The differential sensing mechanism then works to cancel the outputs from the elements as the length of the recorded wavelength is progressively decreased. Indeed a point is reached when the recorded wavelength becomes one and one-sixth the height of the sensor array when a null in the signal voltage is obtained. As shall be shown later, although this effect limits the sensitivity of the device in reading short recorded wavelengths, its superior performance at longer recorded wavelengths makes it ideal for Audio-Frequency recording applications.

In addition to the improved signal to noise ratio at long recorded wavelengths the design has a second advantage over either conventional or other magnetoresistive read heads, in that its bias field is internally generated. With the sense current in each of the elements supplying the field required by the adjacent element to linearise its magnetoresistive response no additional fabrication steps are required. By tailoring the thickness of the insulation layers between the elements in the array, the optimum bias for each element can be provided by the maximum realistic sense current that can be used. Although to some extent this becomes a trade between the reduced high frequency response caused by the increased insulation thicknesses required at higher currents, and the increased output at lower

Schematic diagram of the six-element sensor

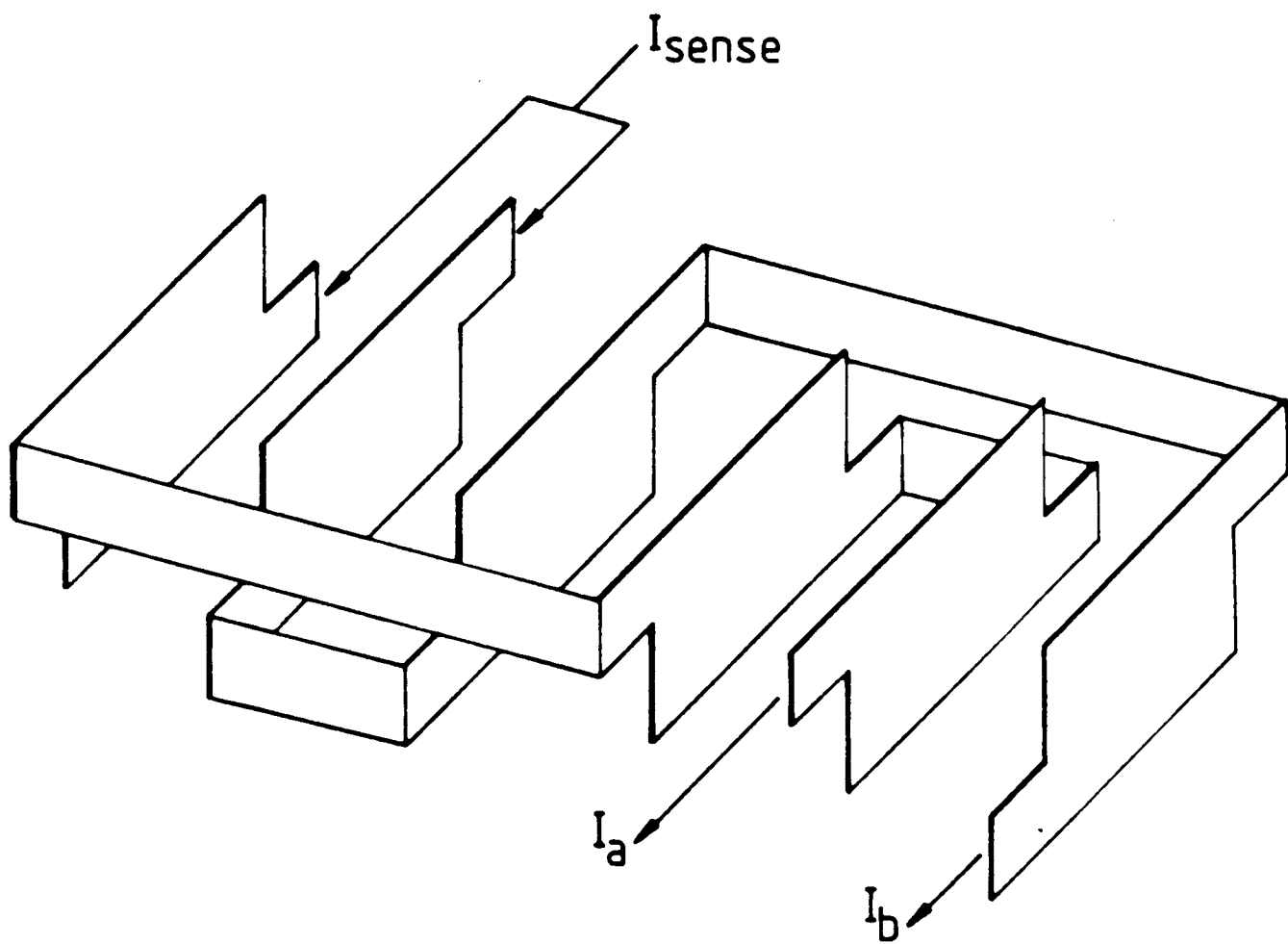


Figure 4



frequencies. As the device output is scaled linearly with the sense current the larger the current the greater the signal. Thus the use of an internally generated bias field scaled only by the sense current is a major advantage over the more complicated schemes that have been proposed elsewhere.

### 3.2 Design of the Multiple-Film magnetoresistive head.

Although the theory governing the response of the multiple-film head predicts a superior response at audio-frequencies than either conventional, or previously described magnetoresistive heads; and the ability to construct an element array in which the bias requirement is met by an internally generated field is conceptually possible; the design and fabrication of actual devices presents several practical difficulties. The format chosen for this project was the production of a sixteen track multiple film head for reading the information stored on a standard compact cassette. Not only does this considerably aid the testing of the finished devices, in that standard commercially available tapes and machines can be used; but in the event of commercial applications proving possible, the design would require little or no modification before manufacture. However this choice immediately constrains the trackwidth available, and hence the length of each of the magnetoresistive elements in the array; if a sufficiently large guard band is to be placed between tracks. Additionally

with each of the sixteen tracks being read simultaneously , the large number of connections required to provide the sense/bias current to each set of detectors limits the size and geometry of these connectors if crosstalk between tracks is to be kept within acceptable limits. With these constraints, together with the difficulties inherent in the interconnection of the multiple films to provide the bias field required, and the need to keep the number of process steps in the device fabrication to a minimum; much consideration had to be given before a final design configuration could be chosen. Basically the head can be broken down into three categories :-

i) The head element assembly.

ii) The conductor pattern.

iii) Fabrication aids included in the design.

Each of these will now be described separately.

3.2) i) The head element assembly.

From the schematic diagram given in figure (4) it can be seen that a six element configuration was chosen in which the electrical interconnection between adjacent elements was provided by tags protruding from their sides. Although one result of this is to reduce the available trackwidth in that

Two geometries used to determine the optimum connecting tag to element height ratios

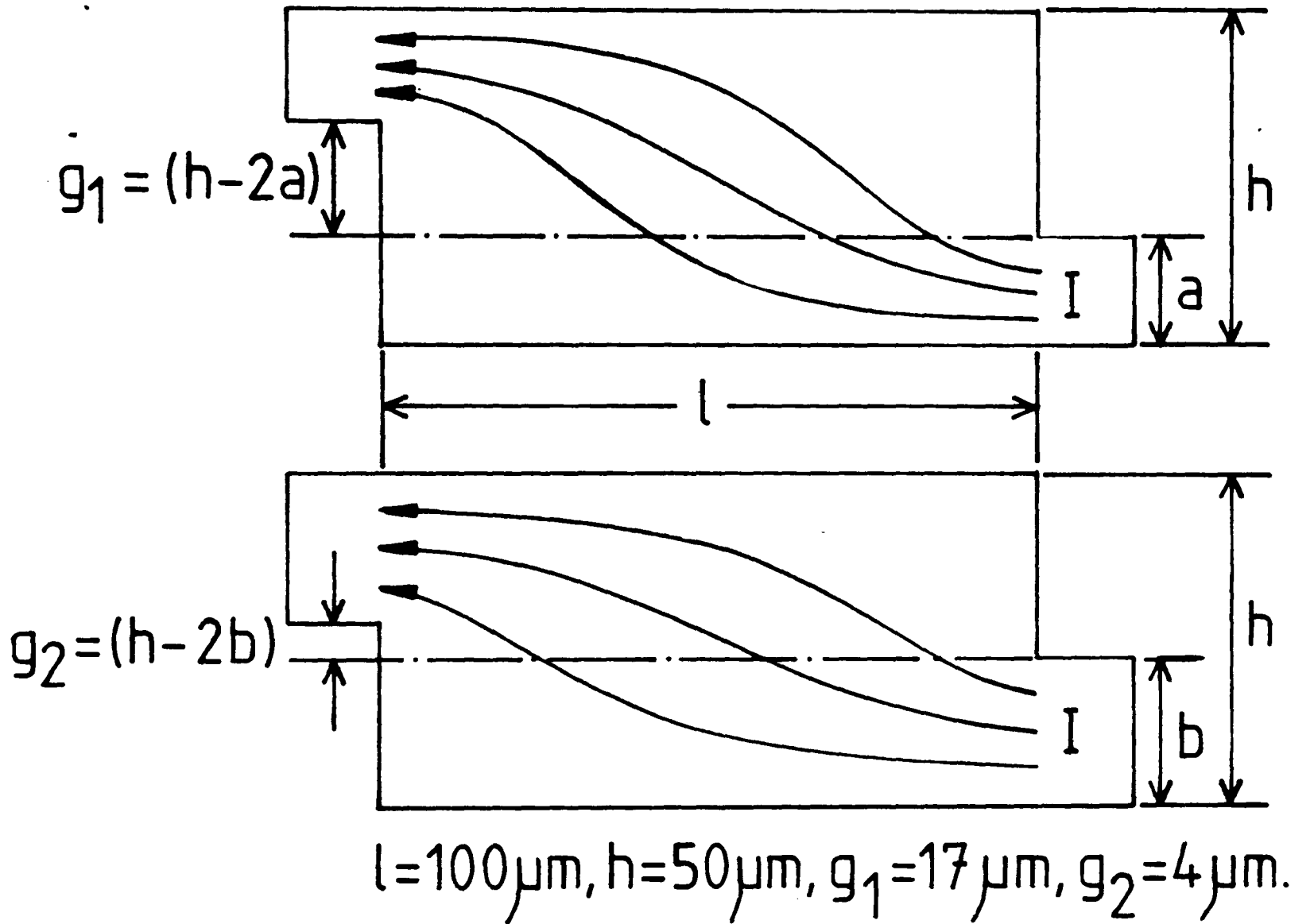


Figure 11

more space has to be allowed between the tracks in which to place each elements electrical connectors, it has several advantages over inter connection of the elements either on the main body of each sensor, or at either of the other two sides. By separating the magnetoresistive layers with Silicon Dioxide insulation layers, interconnection between elements becomes possible by etching windows through these layers only at the protruding tags thus keeping the six elements parallel, and reducing the danger of electrically shorting the wrong layers together. With one set of three detectors being the mirror image of the other, possible geometry induced variation in the electrical and magnetic behaviour of the two sets is reduced, and the differential sensing mechanism improved in that asymmetry in the performance of each set of sensors is only process dependent.

In figure (11) two of the widths of connecting tags considered are shown. In the first diagram the tag width shown was set at one third of the total element width for all widths of element; and the second diagram shows the geometry used to produce the actual device. In this case the connecting tags on different sensors are separated by a fixed constant distance of five microns regardless of the width of the elements. Field plotting experiments showed that the direction of the current vector in the second case was closer to the idealised direction (parallel to the anisotropy direction of the sensor), used in the theoretical descriptions. As well as this advantage variations in the

Figure 12

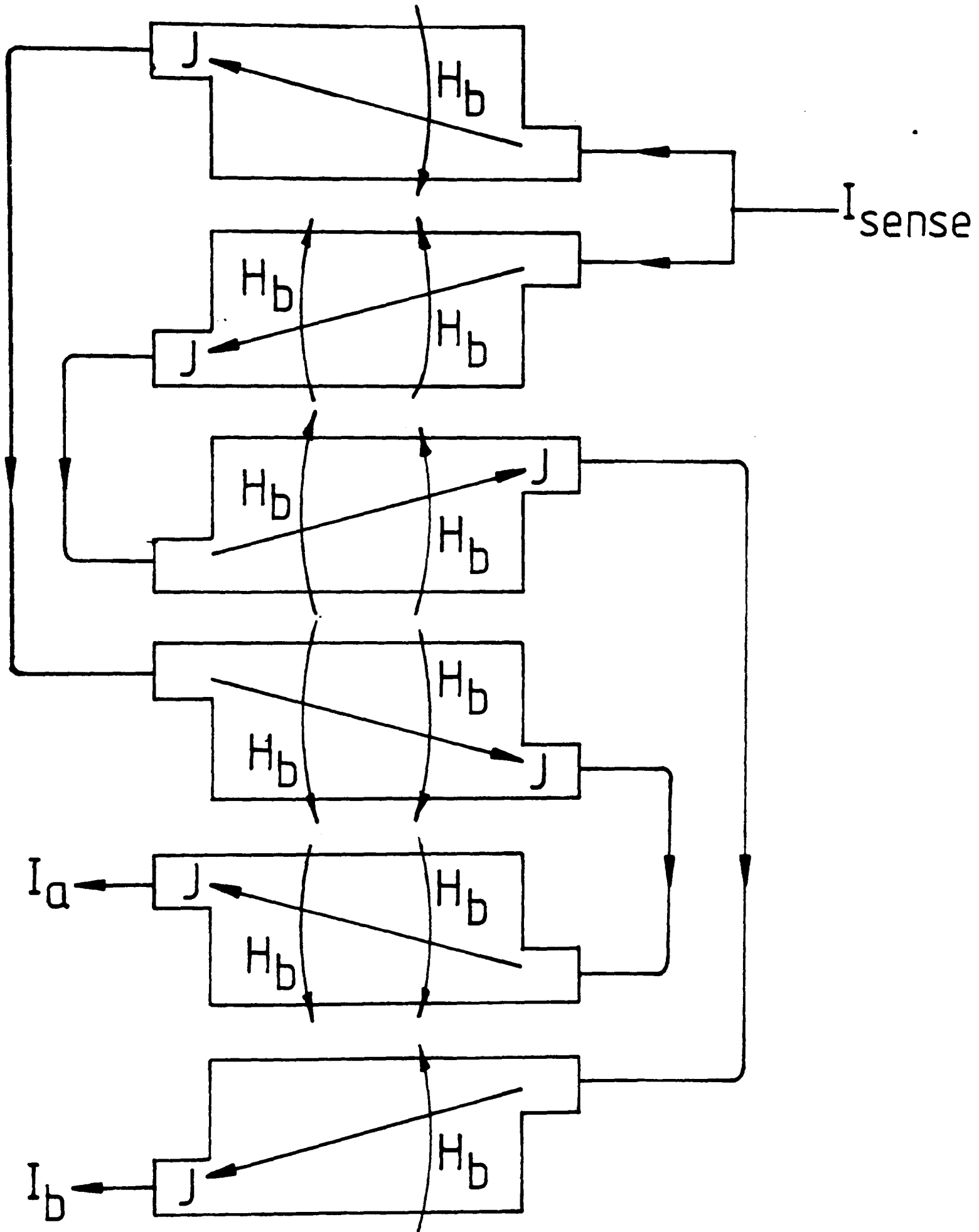


Diagram showing the element current directions, and bias fields used in the multiple-film sensor

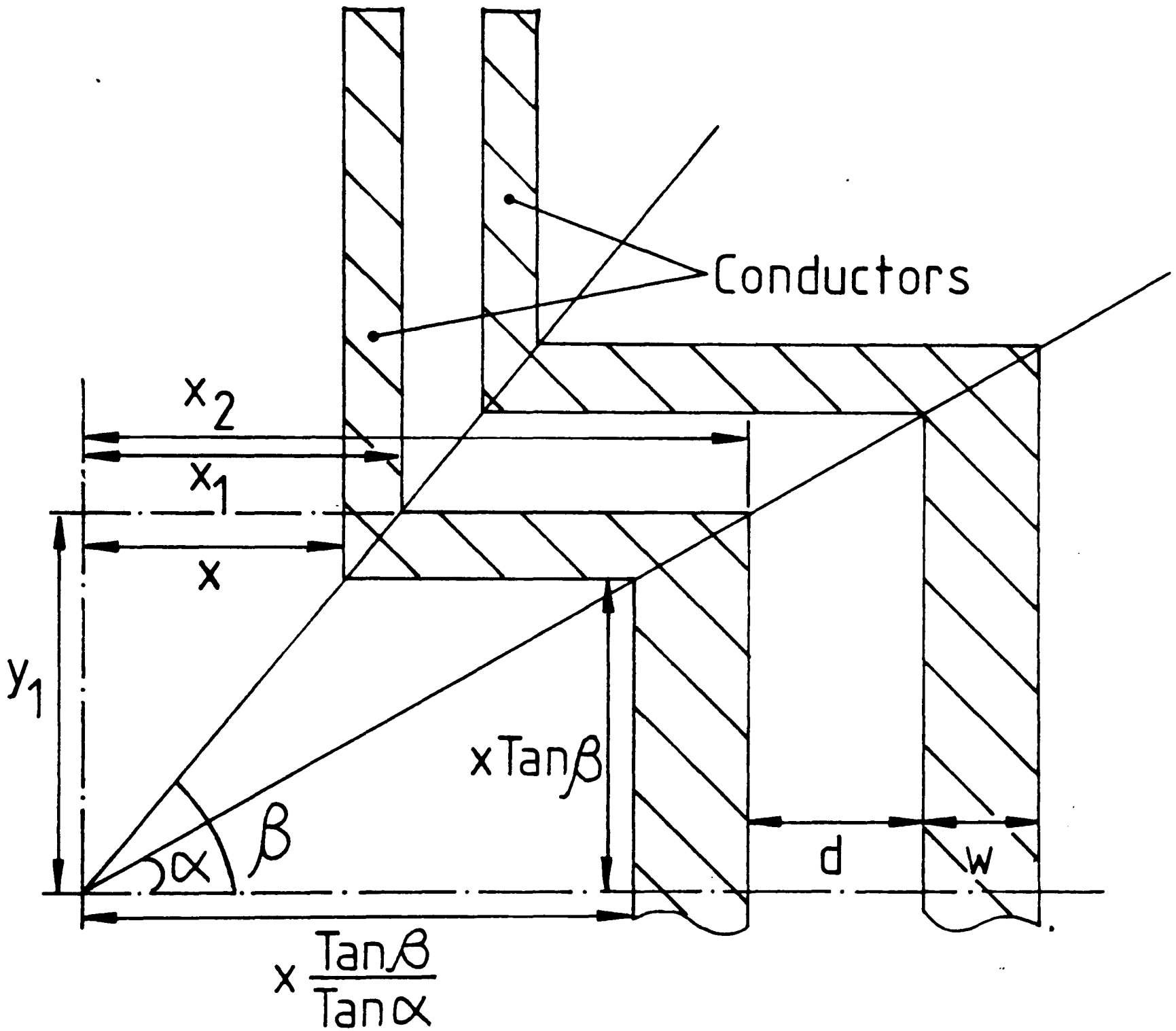
current angle between sensors having different widths were smaller for the chosen configuration than those of the one third of element width tag design. A third configuration in which the tag width was made a fixed distance regardless of the total sensor width performed worse than that shown in the first diagram, and was thus not considered further.

As can be seen in figure (12) with the exception of the end two elements, the bias field in each sensor is jointly produced by the field of the sense currents in the elements immediately adjacent to it. This results in a smaller sense current being needed to linearise the response of the head than would be required for a two-element structure. Such a reduction in current density lowers the risk of damage to the sensors due to Joule heating, and allows relatively large thicknesses of silicon dioxide to be used to electrically insulate the elements, reducing the possibility of element interconnection elsewhere on the sensors than the connecting tags.

### 3.2) ii) The conductor pattern.

With each of the sixteen sets of sensors requiring three electrical connections to be made to them to supply the sense/bias current a total of forty-eight connections must be made. As the overall chip size is limited to a width of seven millimeters by the constraint that it fit into a standard compact cassette head package; it can be seen that either a

Figure 13



Schematic diagram used to calculate the conductor dimensions required to optimise the lead resistances

reduction has to be made in the number of connections, or their width has to be reduced. If the lead out width is reduced its electrical resistance is raised, and if it is large compared with the element resistances; then the magnetoresistive signal is made unrealistically small. To attempt to overcome this problem the common connection for each array was joined to the common for the neighbouring array, which reduces the number of connections still required to forty. However the lead-out resistance can still be comparable with the element resistance for thin lead-out connectors. As the design calls for the capability for all sixteen tracks to be read simultaneously, any variation in the lead resistance across the width of the head will create an undesirable apparent variation in head performance. It therefore becomes necessary to evaluate the resistances used and design the connections such that they are all identical.

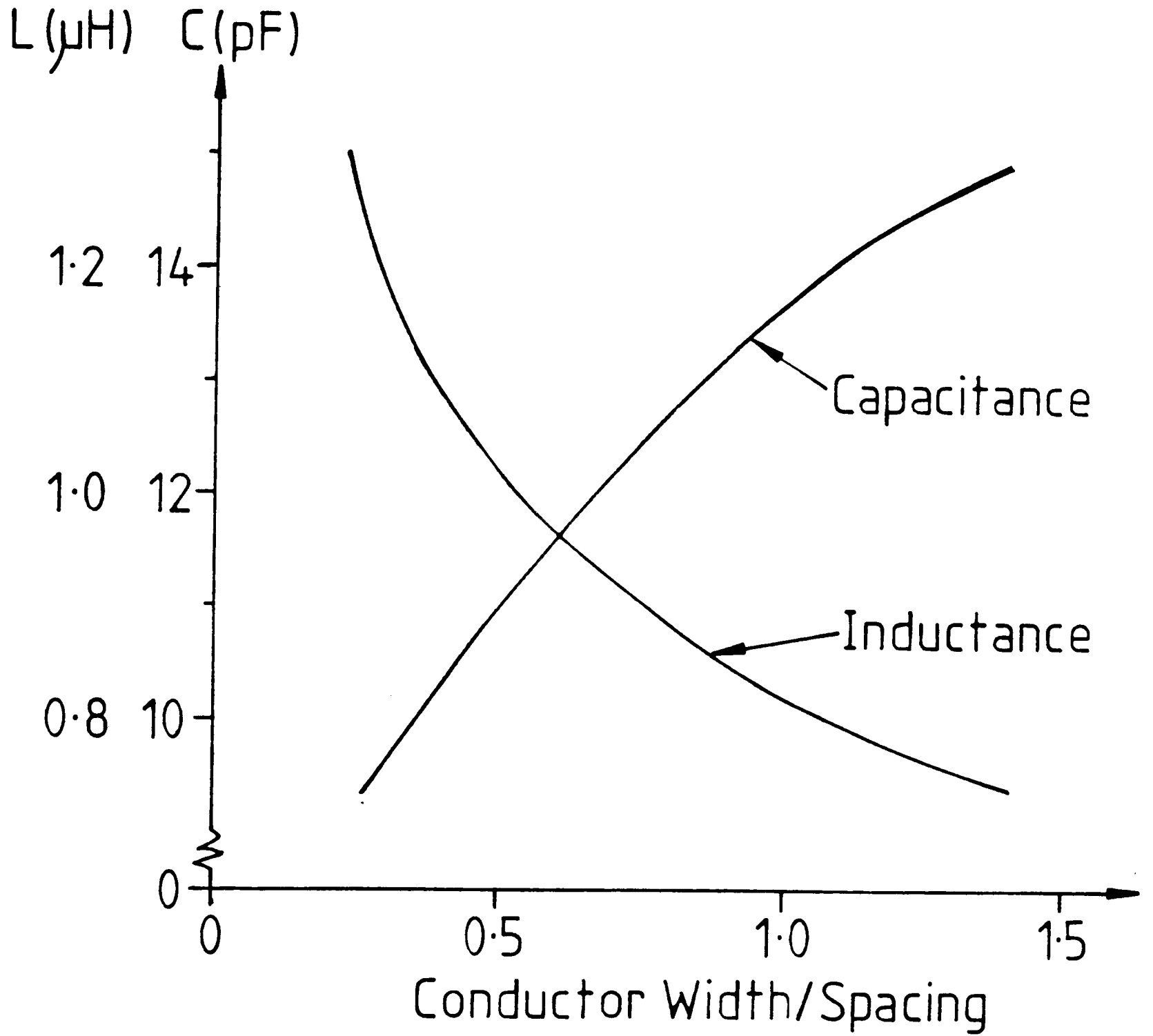
If a pair of connectors from an arbitrary point on the connector pattern are chosen, as shown in figure (13), the resistance of one connector is found to be:-

$$R = \frac{P}{t} \left( \frac{Y - X \tan \beta}{W(\tan \alpha / \tan \beta)} + \frac{(X(\tan \beta / \tan \alpha) - X)}{W \tan \alpha} + \frac{X \tan \beta}{W} \right) \quad (3)$$

where all of the X measurements are from the centre of the connector pattern, and Y is from the arbitrary point "O". R is the lead-out resistance, P the resistivity of the material from which it is made, t its thickness and the remaining



Figure 14



Graph showing the variation of lead capacitance and Inductance calculated from the field plot experiments

dimensions are taken from the figure. If the resistances for the two adjacent connectors are to be equal then:-

$$\tan(\alpha) = (Y_1/X_2) \quad \text{and} \quad \tan(\beta) = (Y_1/X_1)$$

If these values are substituted into equation (3), an equalised resistance for each resistance is obtained.

$$R = \frac{P}{Wt} \left( \frac{Y_1 (1 - (X_1/X_2))}{(X_1/X_2)} + \frac{X_2((X_2/X_1) - 1)}{(Y_1/X_2)} + X_1(Y_1/X_1) \right) \quad (4)$$

By differentiating this result with respect to X, and putting the resulting equation equal to zero; the variation of Y with changing X<sub>1</sub> and X<sub>2</sub> can be found.

$$\frac{dR}{dX} = 0 = \frac{P}{Wt} \left( 0 - \frac{(Y_1 \cdot X_2)}{(X_1 \cdot X_1)} + \frac{X_2}{Y_1} ((X_2/X_1) - 1) + \frac{Y_1}{X_1} \right) \quad (5)$$

from which it can be shown that:-

$$Y_1^2 = (X_1 * X_2) \dots \dots \dots (6)$$

if each of the electrical connections to the sensors have the same resistance.

A computer program was then developed based on this result which produced the relevant dimensions for each leg of the connector pattern based on the lengths fixed by the head width constraints. In addition to giving these dimensions it

also provided the electrical resistance given the resistivity of the connector material. A print out of the program is given in appendix (I).

To evaluate the inductance and capacitance between the leads, a series of field plotting experiments were performed in which the equipotential lines between the leads were plotted. From these plots calculations could be made to supply the values required and based on this the paper given in appendix (II) was published. A graph of the experimental values obtained is given in figure (14).

3.2) iii) Fabrication aids included in the design.

As the devices are deposited in successive layers onto Corning 7059 Borosilicate glass substrates, and patterned into the shapes required using Photolithographic techniques; it becomes possible to fabricate a large number of sixteen track heads at one time. This reduces the possibility of introducing deposition or fabrication variations in the electrical and magnetic characteristics of different widths of sensor when tested. To facilitate this, several novel features were included in the mask design allowing easy recognition of each type of head, its dimensions and construction history. Additionally various other features were included to enable easy assembly of the finished chips into testable devices; thus reducing the possibility of damage in the final stages of construction. With an overall

Figure 15

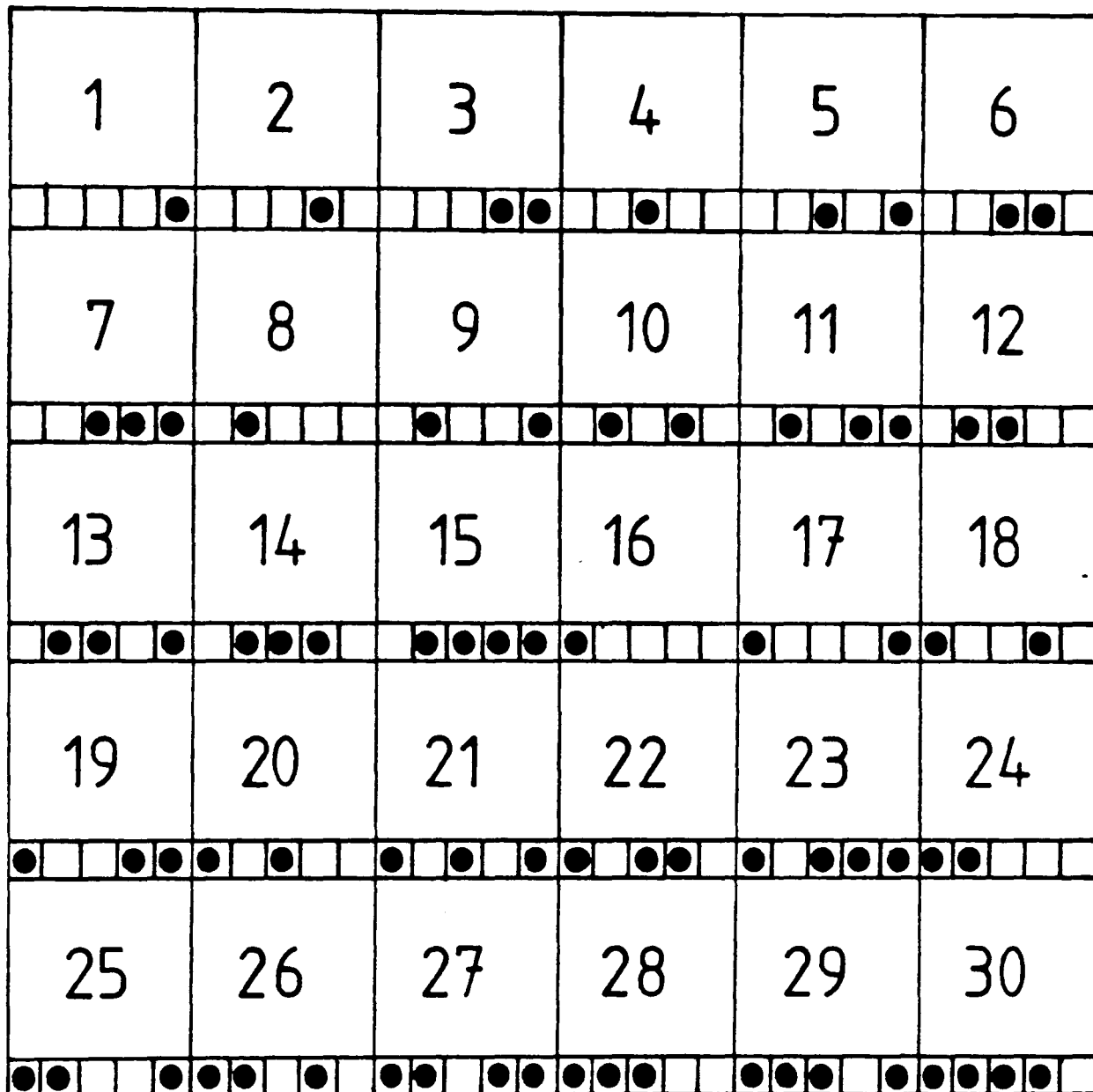
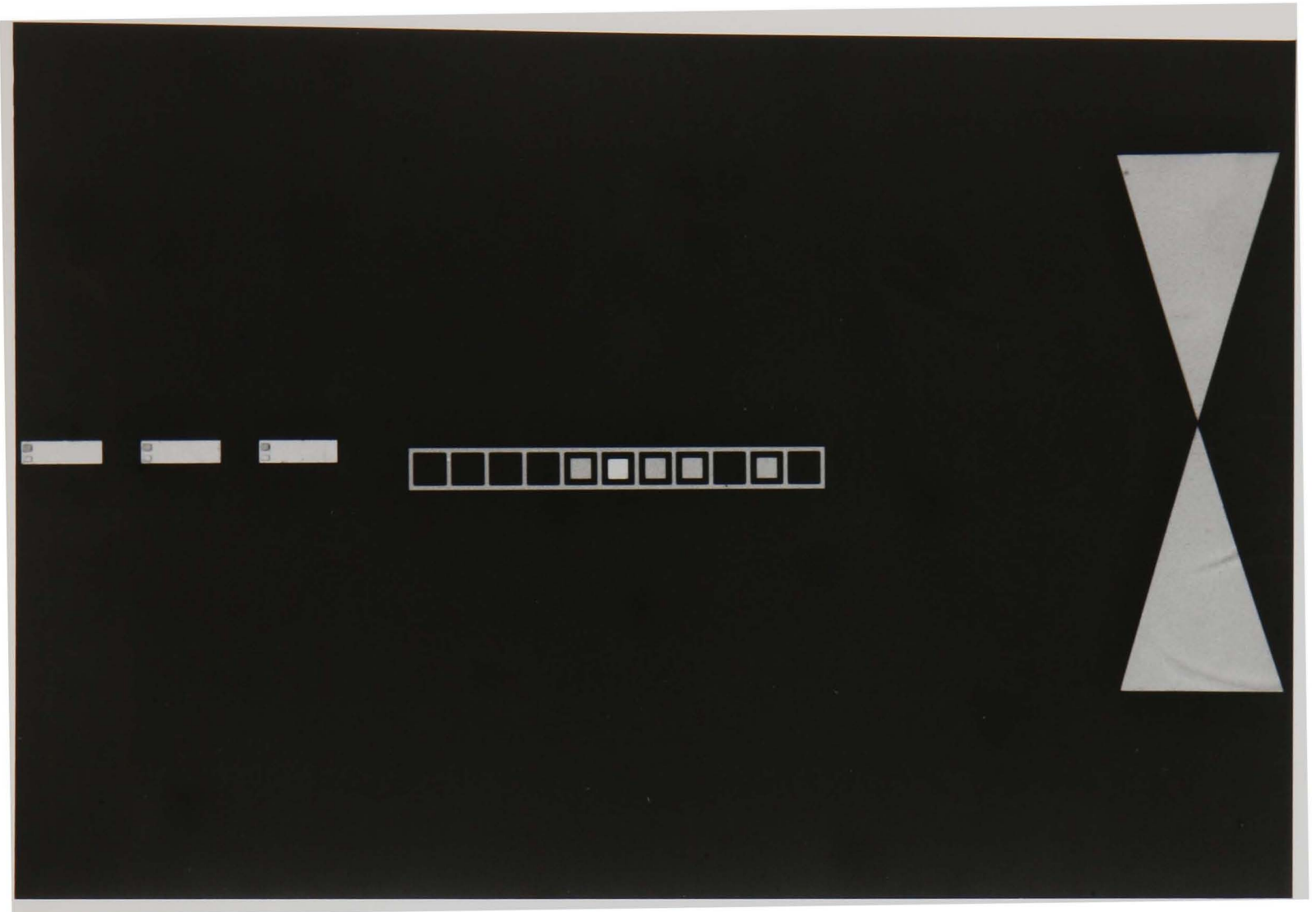


Diagram showing the coding scheme used on the substrate to identify individual chips

Plate 8

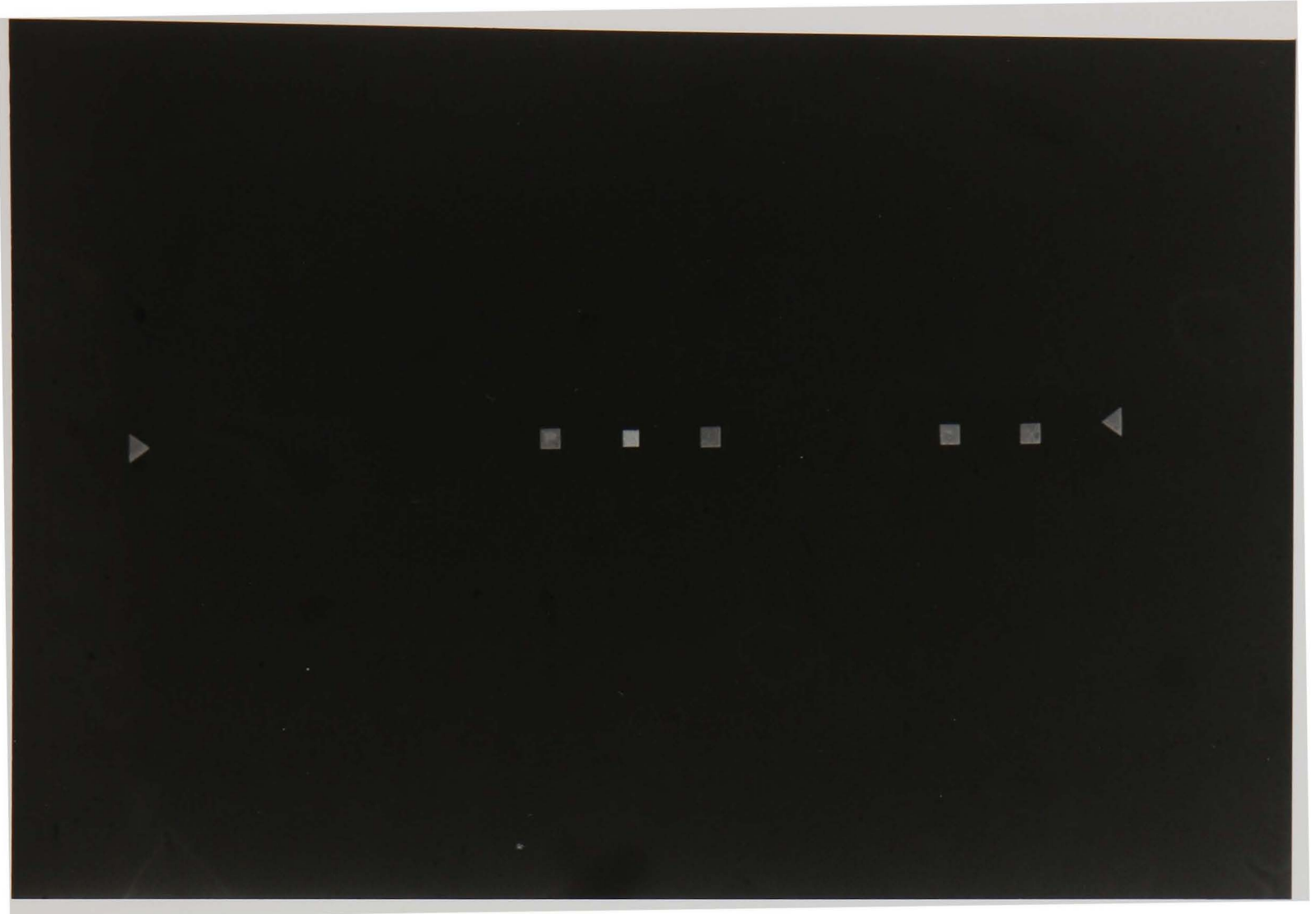


The coding scheme in use on an actual chip

chip size of 7 mm x 9 mm being necessary for the heads to fit into a standard cassette head package, allowing for sufficient space between each device to dice them once completed; a total of thirty-six heads can be fabricated at one time. Although it was tempting to make each head unique, a realistic assessment of possible losses in the manufacturing process resulted in six different designs per substrate being chosen. Thus for the very worst case, any given substrate should produce at least one working sixteen track head of width 15, 20, 25, 30, 40 or 50 microns.

To the naked eye each chip once diced is indistinguishable from any other chip from that substrate. To overcome this a binary coding scheme was introduced into the design, which is of sufficient size that it can be seen with an ordinary magnifying glass. The coding scheme is shown in figure (15) and a photograph of it in use on an actual chip in plate (8). Beginning from the right blocks are placed in the windows counting up in binary code from one to thirty-six in rows across the chip. The remaining windows are filled with a square if certain key masks have been used in that particular devices fabrication. The same coding is placed between the electrical connections to the elements near the pads at the rear of the chip with two triangles marking the ends of the pattern as shown in the photograph in plate (9). In this fashion each of the chips can be readily identified even after dicing, its position on the complete substrate pin-pointed, and its construction noted.

Plate 9

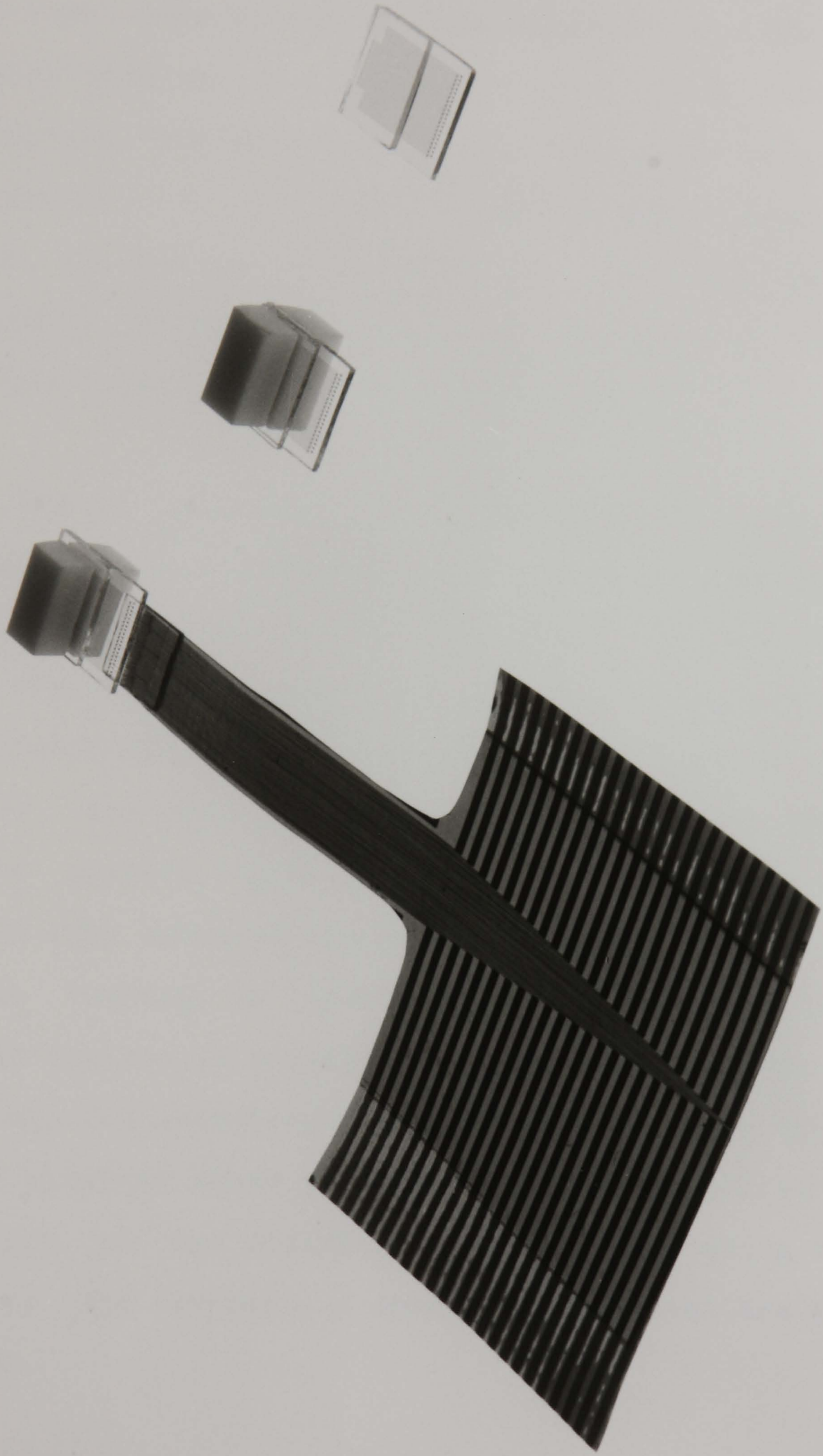


The coding scheme as placed between the connecting leads

After dicing, a cover slip is glued in place over the front portion of the chip leaving the bonding pads exposed as shown in plate (10). At this point the coding marks on each side of the sensor array are obscured, but the pattern between the electrical connectors is visible. The head is then Wire-Bonded using a Dage-Precima pulse-tip wire bonder, to a flexi-circuit patterned from "Kapton" a commercially available material. This consists of a thin copper sheet bonded onto a plastic backing, and is widely used in the electronics industry. To provide the same pitch of conductor on the Kapton as on the chip, the material is photolithographically processed in a similar fashion to the substrates, except that a hand drawn mask is used, and P.C.B standard Ferric Chloride etchant used to pattern it.

As the substrate and cover slip are both made from relatively soft borosilicate glass, an extra degree of wear resistance has to be provided to reduce damage to the sensors by the magnetic tape passing over the finished head. To this end two ceramic side-cheeks, pre-profiled to the correct nine millimeter radius are glued on top of and under the chip/cover-slip sandwich as shown in the photograph in plate (10). Due to the high wear resistance of these side cheeks large amounts of post-assembly lapping of them to align the front edge of the sensors with the front edge of the finished head is impractical. They thus have to be glued in place with a degree of accuracy for which two large triangular shapes are



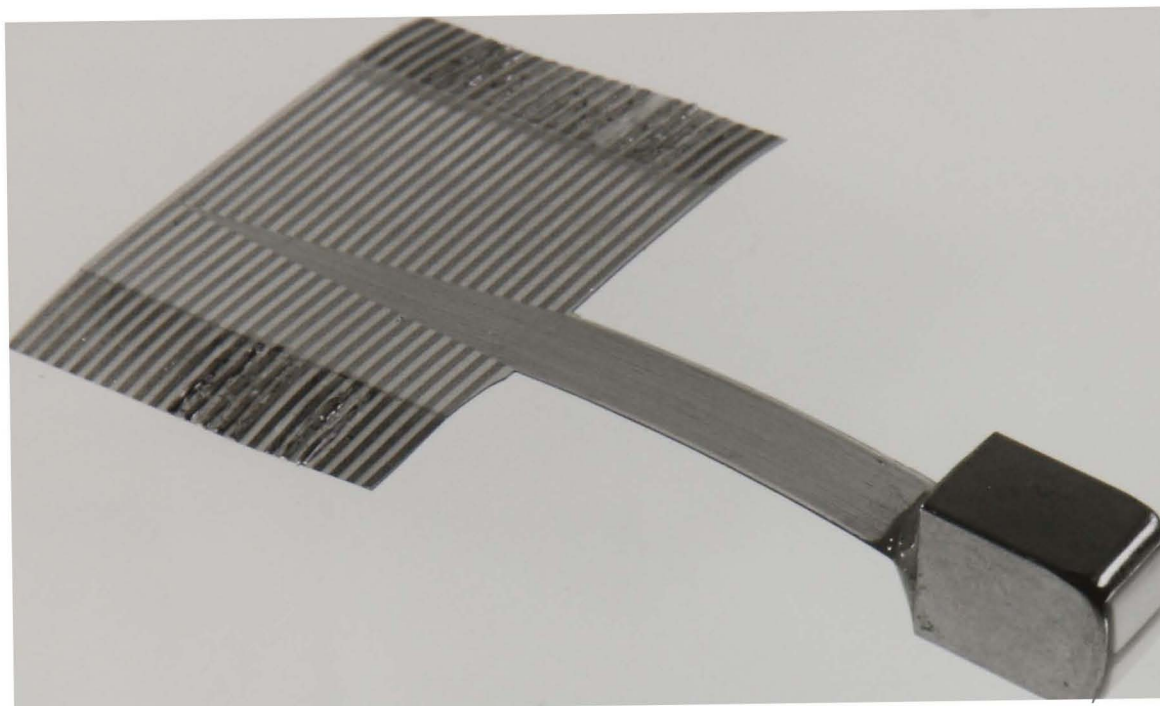


patterned onto the substrate at either side of the sensor array, as shown in the photograph in plate (9). The point at which the apexes of the triangles meet is placed two microns from the front edge of the sixteen elements, and the edges of the ceramic side-cheeks are aligned using these centres. Once the cover-slip, and side-cheeks have been glued in place, the whole assembly is packaged using a standard cassette head container, and the space remaining at the rear of the can filled with a potting compound. A photograph of a head prior to its final lapping is shown in plate (11).

In the introduction, one of the limiting factors in the performance of magnetoresistive read heads, that due to the sensor to tape separation; was discussed. As shall be shown in the theoretical description of the multiple-film heads large separations result in significantly reduced outputs at short recorded wavelengths. If all sixteen tracks are to perform equally this parameter must be made constant across the full width of the head. It is thus imperative that the final lapping of the finished structure be in as a controlled fashion as possible. This is achieved by placing in front of, and attaching to the magnetoresistive sensors, a series of elements whose resistance can be monitored during the lapping of the finished head assembly, using the same circuit as the sensors. A photograph of these are shown in plate (12).

As the front surface of the head is removed these

Plate 11



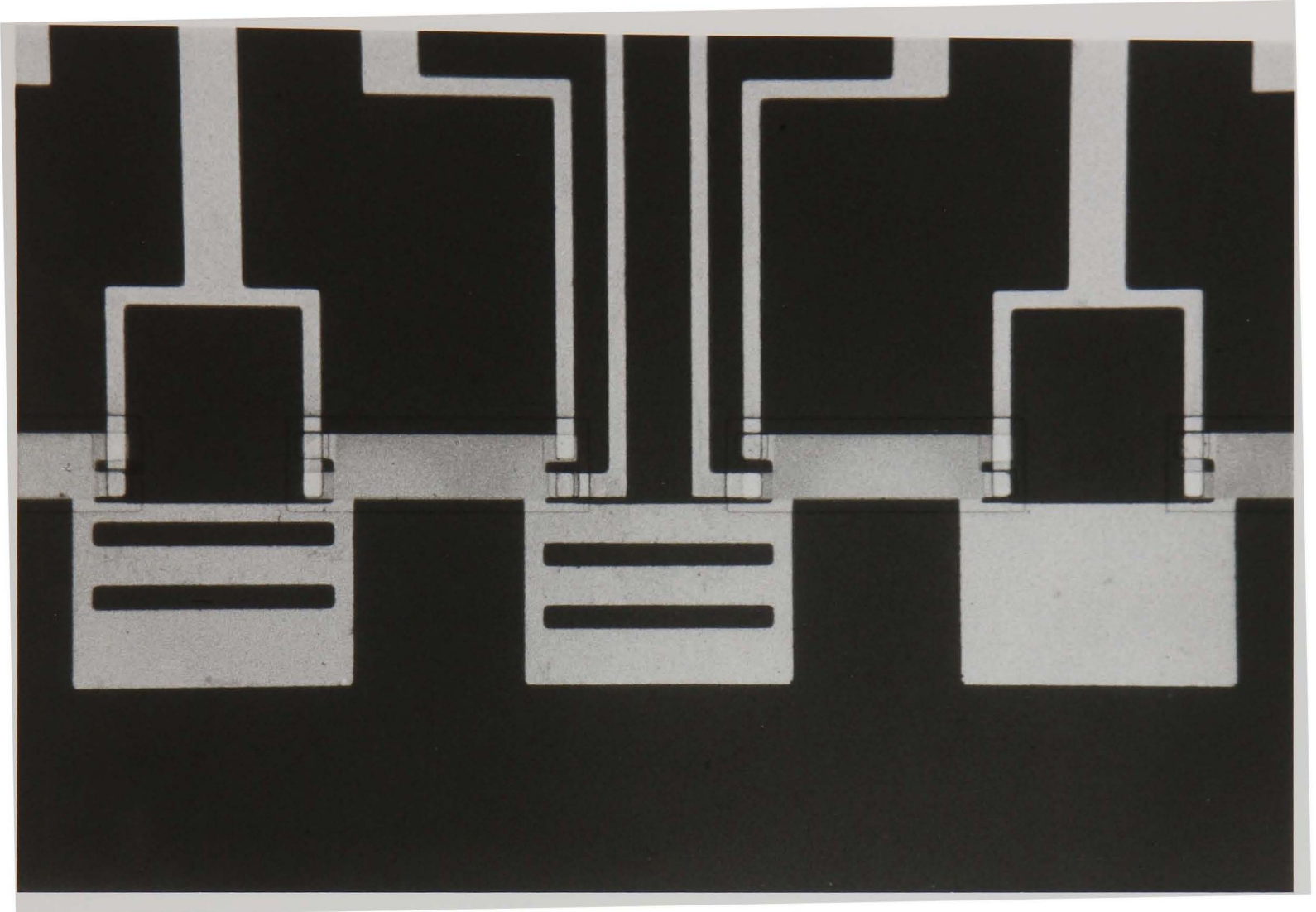
A finished sixteen-track magnetoresistive read head

elements are gradually worn away, and their resistance thus increases in a measurable fashion. If one edge of the head is being lapped at a faster rate than the other, the resistance of these "sacrificial" elements will be increasing faster than those at the other edge, and adjustments can be made to equalise the erosion rate. Once the front edges of the sensors and the head assembly are parallel and the rate of removal has been equalised for each sacrificial element, lapping can proceed until each of the elements goes open circuit. At this point the front edge of the head is two microns from the front edges of the elements, and after a final polish of the finished surface with cerium oxide powder to reduce damage to the standard tapes during testing, experimentation can begin. Although at this separation the head performance is not at its maximum, careful lapping in small stages acts to significantly improve it; and testing can continue until eventually the sensors themselves go open circuit.

### 3.3) Micro-Fabrication of sensor array.

With the magnetoresistive elements used as sensors in this device being constructed from thin films of NiFe, and only small separations being needed between each sensor; Photolithographic techniques are ideally suited to their fabrication. Each successive layer is sputter deposited and then chemically etched after a photoresist layer has been applied, pre-baked, exposed to U.V. light through a chrome

Plate 12



Micrograph of the sensor array, showing sense elements,  
electrical connections, and sacrificial elements

photomask, and developed to provide the shape required. With the production of micron size features routinely possible with this technique, the main difficulty in the fabrication of such devices becomes the mask design required to assemble the multiple-film array; and the choice of etchants to selectively etch successive layers without damaging the features previously patterned.

To obtain the photolithographic masks used in the fabrication of the heads, a computer programme was generated using the micro-circuit design facility on the S.E.R.C Rutherford and Appleton laboratories prime F. This program is written in a low-level graphics language called GAELIC, which defines a series of points, lines, and shapes, defining the features used to construct the sensors, insulation layers and electrical connections of the heads. Various software routines are included in this package, that allow interactive editing of the mask features, enabling complicated designs to be viewed, and mask alignment checked. Once finished the design is written onto the original mask plate using an electron beam pattern generator, driven from the instructions encoded in the original program. A copy of the program used to define the shapes on the masks used is given in appendix (III).

The order of deposition and etching is given in appendix (IV), together with an example of a single shape having a particular width from that mask. A total of eleven masks were

used, with the long electrical connectors being broken into two sections. This allows low resistance leads to be fabricated by making the second lead sections very thick ( 2-3 microns ), but keeps the height of the sensor array at the front face of the head assembly by making the first section relatively thin ( 0.2-0.3 microns ). Additionally changes in the detail of the sensors can be easily made without having to include a whole new conductor pattern, as modifications need only be made to the first set of leads. The use of a chrome under-layer beneath the gold on the electrical connectors to the sensors improves the adhesion of these features to the substrate. This reduces the problems associated with the wire bonding of the chip in the final assembly stage, whilst keeping the low resistivity leads provided by the use of a thick gold layer for these long lead-outs.

It can also be seen in this appendix how care has been taken to cover with Silicon Dioxide all the Nickel Iron shapes previously patterned, protecting them whilst subsequent magnetoresistive sensors are etched. Although the first connecting layer patterned is exposed to the chemical etchants used in the patterning of the Nickel Iron and Silicon Dioxide layers during the remaining fabrication steps; the careful choice of these solutions ensures that damage to these features does not occur.

To provide the etch selectivity required, four main

chemical solutions were used:-

- 1) NiFe etch - 100 ml. Orthophosphoric Acid, 100 ml. Nitric Acid, 50 ml. Nickel Nitrate solution and 500 ml. DeIonised water. Etch temperature 30 degrees centigrade. Etch rate 1000 Angstroms/minute
- 2) SiO<sub>2</sub> etch - Countdown high yield system. Iso - Electronic grade, Iso-form Silicon - Dioxide etch. Available from Micro - Image Technology Ltd. Etch temperature 20 degrees centigrade. Etch rate 1000 - 2000 Angstroms / minute, depending on impurities.
- 3) Au etch - 500 g. Potassium Iodide, 100 g. Iodine and 400 ml. DeIonised water. Etch temperature 20 degrees centigrade. Etch rate 2000 Angstroms / minute.
- 4) Cr etch - 25 g. Ammonium Ceric Nitrate, 15 ml. Nitric Acid and 85 ml. DeIonised water. Etch temperature 20 degrees centigrade. Etch rate 1000 Angstroms / minute.



As described in chapter two each of the layers making up the device was sputter deposited using either a Nordiko or a Materials Research Corporation Sputtering machine. The two materials used to make up the connections to the sensors, and the silicon dioxide insulation material were both R.F. sputter deposited in the conventional manner. However, to optimise the electrical and magnetic performance of the magnetoresistive layers, the technique of "Bias" sputtering was used. In this method the R.F. power from the generator is divided between the substrate, and the target to produce a fixed voltage at the substrate surface. This voltage can be controlled by varying the power division and acts to allow material to be re-sputtered from the substrate whilst the film is nucleating and growing. Careful control of this bias voltage results in the preferential re-sputtering of selected atoms or molecules from the film during its deposition resulting in a purer material than possible with the normal electrode configuration. (1,2)

The sputtering details for each layer are:-

- a) NiFe - Target sputter cleaned for 10 minutes at 400 watts forward, 0 watts reverse. Substrate etch cleaned for 5 minutes at 200 watts forward, 0 watts reverse NiFe sputtered for 3 minutes at 400 watts forward 0 watts reverse. Bias voltage set to 60 volts.

- b) SiO<sub>2</sub> - Target pre-cleaned for 10 minutes at 400 watts. No pre-clean of substrate. Material sputtered for 30 minutes at 400 watts forward, 0 watts reverse.
- c) Au - Target pre-cleaned for 10 minutes at 400 watts then Gold sputtered for 30 minutes at 400 watts forward, 0 watts reverse. No substrate pre-clean.
- d) Cr - Target pre-cleaned for 5 minutes only, at 200 watts forward 0 watts reverse. Magnetron sputtering used on this target. Chrome then sputtered for 5 minutes at 100 watts forward, 0 reverse.

All depositions were performed in a plasma pressure of 5 microns of 99.99% pure Argon, after the chamber had been pumped down to a base pressure of better than  $2 \times 10^{-7}$  mBar. To align the easy axis of the magnetoresistive stripes in a predetermined direction, a magnetic circuit was built using bar magnets and a mild steel former. This was attached to the substrate plattern and provided a constant direction magnetic field of no less than 60 Oe across the substrates during sputtering. The substrate plattern was also water cooled to reduce temperature effects in the growing films, and after deposition all the sputtered films were left under a high

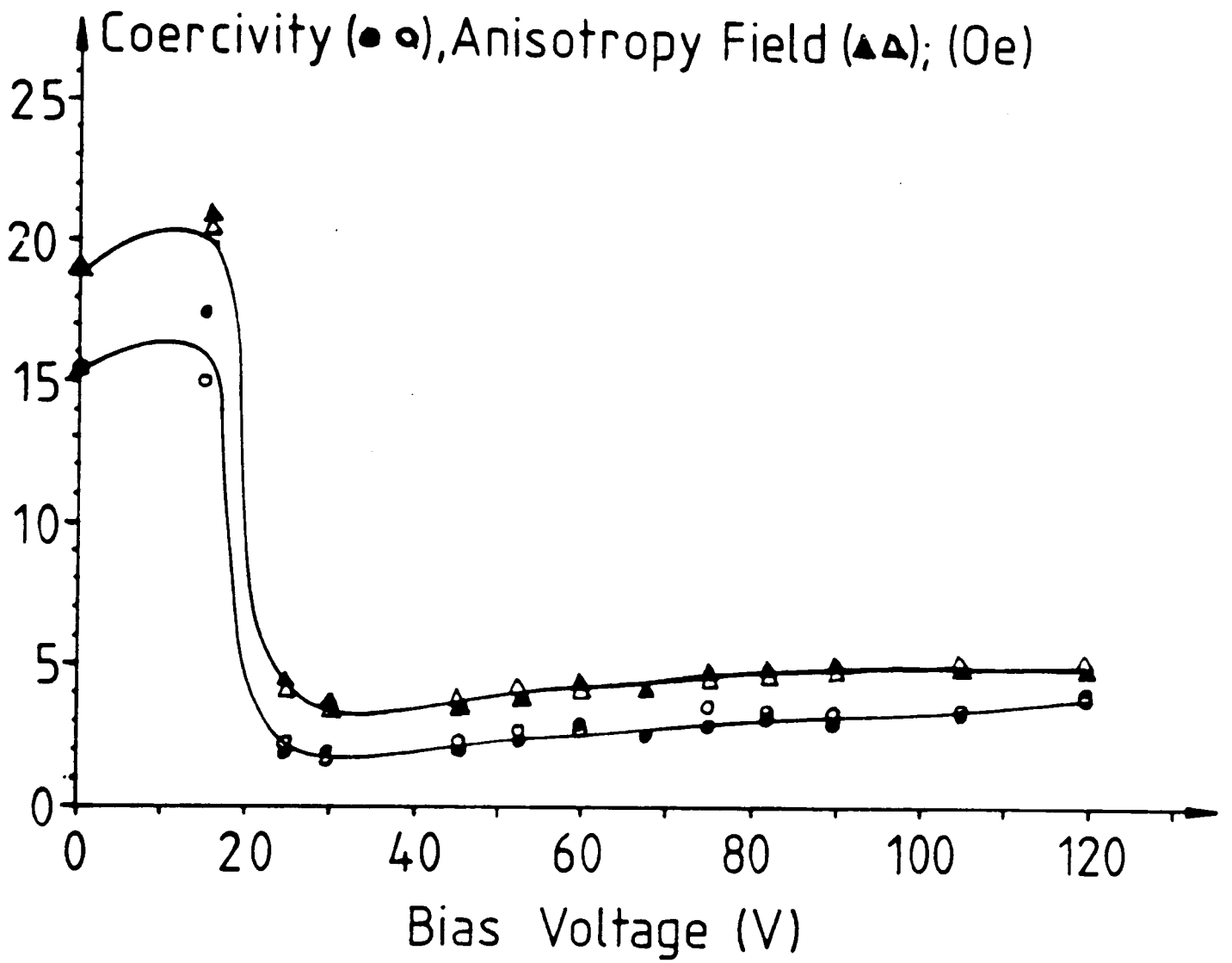
vacuum to cool to ambient temperature for at least one hour. In each case the substrates were prepared by ultrasonically cleaning in a 2% solution of Decon 90, an industrial cleaning fluid, at 65 degrees centigrade, rinsing in deionised water, degreasing in an Isopropyl Alcohol bath, re-rinsing in DeIonised water and force drying in an oxygen free nitrogen jet.

#### 3.4) Optimisation of the anisotropic magnetoresistance effect.

With the performance of the multiple-film head relying on the percentage magnetoresistive change in the films sputter deposited to provide the sensors, a high degree of reproducibility is required in their production. It has been found by other workers (3,4,5) that the presence in the vacuum chamber of even small quantities of residual Oxygen or Water Vapour can have a marked detrimental effect on the magnetic properties of the films produced. To overcome this, and provide a well regulated method of sputtering films having consistent electrical and magnetic properties a series of experiments were performed to investigate these variations with changing deposition condition.

When considering the data published on the production and performance of thin magnetoresistive NiFe films, several points emerge as being critical:-

Figure 16



Graph showing the variation in film coercivity and anisotropy field as a function of Bias voltage used during sputtering

i) The anisotropic magneto-resistance ratio depends on thickness, grain size and film surface conditions.

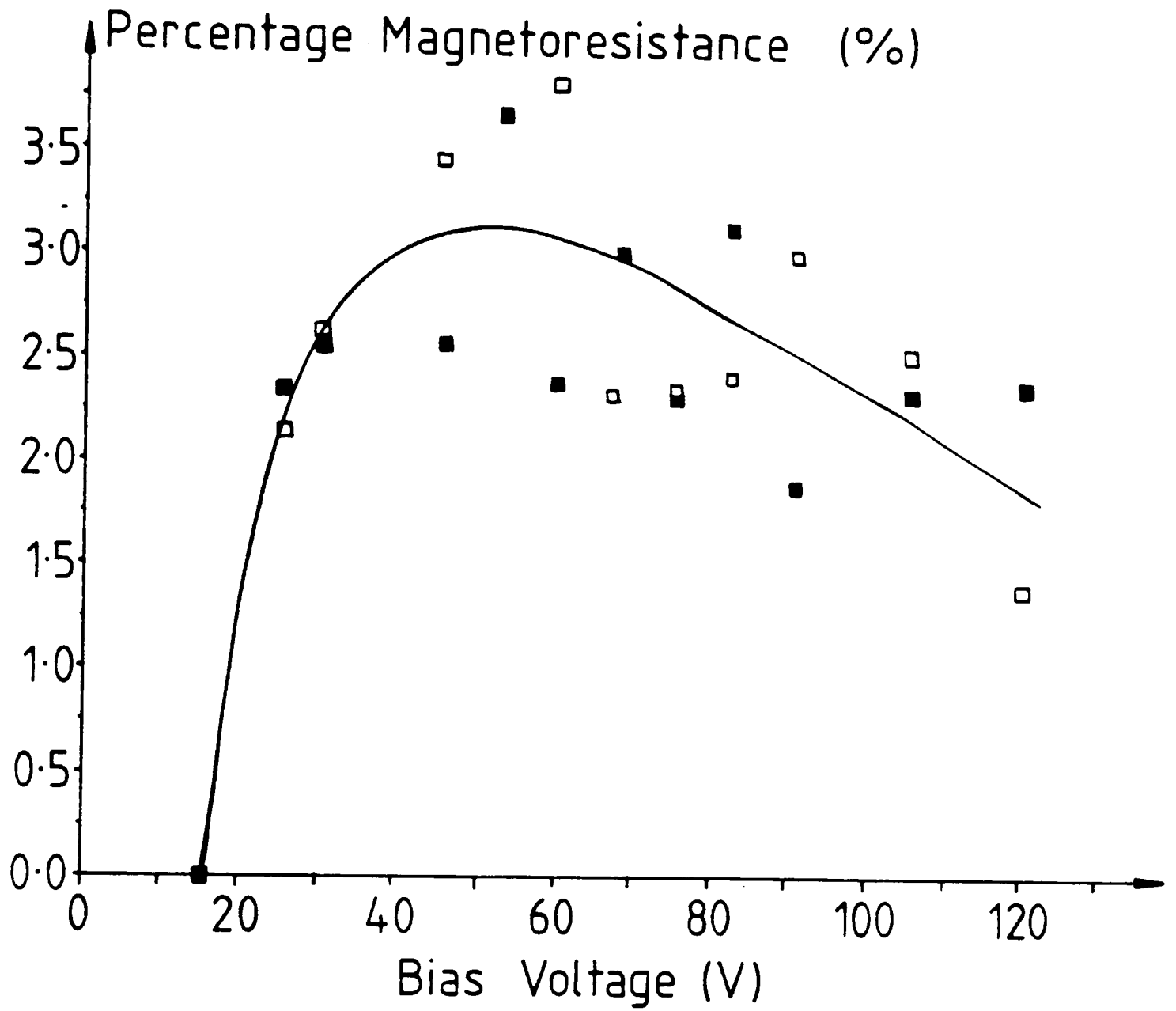
ii) There is a large preparation dependent variation in the anisotropic magnetoresistance involving parameters such as vacuum purity, substrate temperature, and deposition rates.

iii) Due to the surface scattering of conduction electrons dominating the resistivity measurements at lower temperatures, making interpretation of the magnetoresistive data difficult; film measurements tend only to be taken at room temperature.

iv) Associated electromagnetic properties such as coercivity, anisotropy field, and resistivity are also difficult to control.

As the sputtering apparatus used to produce the films used as sensors is not capable of achieving an ultra-high vacuum (better than  $10^{-10}$  mBar), the use of bias sputtering to reduce the contaminant gases in the films becomes a necessity. However the increase in bias voltage can result in other performance limiting effects, and it is found [6] that for any given sputtering system there is in general only a narrow range of substrate bias that yields the optimum physical film properties. To discover the optimum bias for this particular system and material a series of experiments

Figure 17



Graph showing the variation in film magnetoresistance as a function of Bias voltage used during sputtering

were performed in which several substrates were sputtered at bias voltages from 0 to 120 volts. Two results at each substrate bias voltage were taken with each film in the pair sputtered separately, in some cases several days apart. Prior to each film being deposited the vacuum chamber was pumped down to a fixed and easily obtainable pressure of  $1 \times 10^{-5}$  Torr. During sputtering a plasma pressure of 5 microns of 99.99% Argon was maintained, and the substrate bias voltage was measured directly from the substrate voltmeter on the sputtering system. After deposition and cooling to room temperature under vacuum, the films coercivity, anisotropy field, resistivity and anisotropic magnetoresistance were measured using the apparatus described in chapter two. The results are given in the graphs shown in figures (16) and (17).

In addition to these results which point to a choice of substrate bias voltage of 60 volts as providing the optimum film properties; several other points were noted during the experimentation.

a) The base pressure for unbiased films was critical to their magnetic behaviour. Above  $5 \times 10^{-5}$  Torr large coercivities were found ( $>15$  Oe), together with large anisotropy fields ( $>20$  Oe) and virtually no detectable anisotropic magnetoresistance. As the base pressure is decreased, and especially below base pressures of  $1 \times 10^{-5}$  Torr the coercivity and anisotropy field falls to typically 2

Oe and 10 Oe respectively. However, although the percentage magnetoresistive change improves slightly (generally becoming a few tenths of a percent); not until base pressures in the region of  $10^{-6}$  Torr are reached does it approach the values obtained from Bias-Sputtering.

b) Annealing of the films after deposition could result in a marked lowering of the coercivity and anisotropy field; together with a slight improvement in the anisotropic magnetoresistance. The results were however very inconsistent, possibly due to the incorporation of residual gases from the vacuum chamber during the annealing process and subsequent cooling of the films.

c) Several very thin films were produced in conjunction with those sputtered to provide the transmission electron micrographs as shown in plate (8). The electric and magnetic performance of these films was characterised by high coercivities, high anisotropy fields, high resistivities and no detectable anisotropic magnetoresistance, irrespective of base pressure or substrate bias voltage used to sputter them. However, these properties were consistent for both the films sputtered onto carbon coated mica for use in electron microscopy, and those sputtered onto the standard glass substrates.



REFERENCES CHAPTER THREE  
-----

- 1) J.J. Cuomo, R.J. Gambino J. Vac. Sci. Technol. vol.14 no.1 pp152 (1977)
- 2) J.L. Vossen J. Vac. Sci. Technol. vol.8 no.5 ppS12 (1971)
- 3) M.C. Paul, M.M. Hanson. J. Appl. Phys. vol.37 no.10 pp3743 (1966)
- 4) K. Kempter, H. Hoffman J. Phys. (Paris) vol.32 Suppl.C1 pp396 (1971)
- 5) V.B. Chapman, A.S. Marwaha, A.J. Collins Thin Solid Films vol.58 pp247 (1979)
- 6) B. Chapman "Glow Discharge Processes" John Wiley and Sons. (1980)

#### CHAPTER FOUR

-----

"The theoretical description of anisotropic magnetoresistance and various theories describing its use in magnetoresistive replay heads."

#### 4.0) Theoretical analysis of Multiple-Film magnetoresistive head.

##### 4.1) Origins of the anisotropic magnetoresistance effect.

Although it is now felt that both the magnetoresistance and anisotropic magnetoresistance effects are understood, detailed theoretical calculations are still difficult, particularly for the anisotropic effect. Early theories describing the phenomenon discussed it in terms of spin-orbit coupling [1] in which a spherically symmetrical perturbing potential was used to calculate the transition probability for an electron transition from an s to d state. This then allowed the anisotropy in the resistivity to be evaluated. Later work [2] revealed certain inconsistencies between this theory and experimental results, and an additional mechanism in which the density of antiparallel states in the 3d band becomes the determining factor was proposed. Recently a more rigorous theoretical analysis has been given [3] in which the effect is discussed both from the considerations of symmetry, and from a microscopic, quantum-theory point of view.

Although such a detailed approach results in a better understanding of the origins of the effect, it is possible to calculate the performance characteristics of actual devices

using only the simplistic phenomenological equation:-

$$R = R_0 + \Delta R \cos^2(\theta) \dots\dots\dots(7).$$

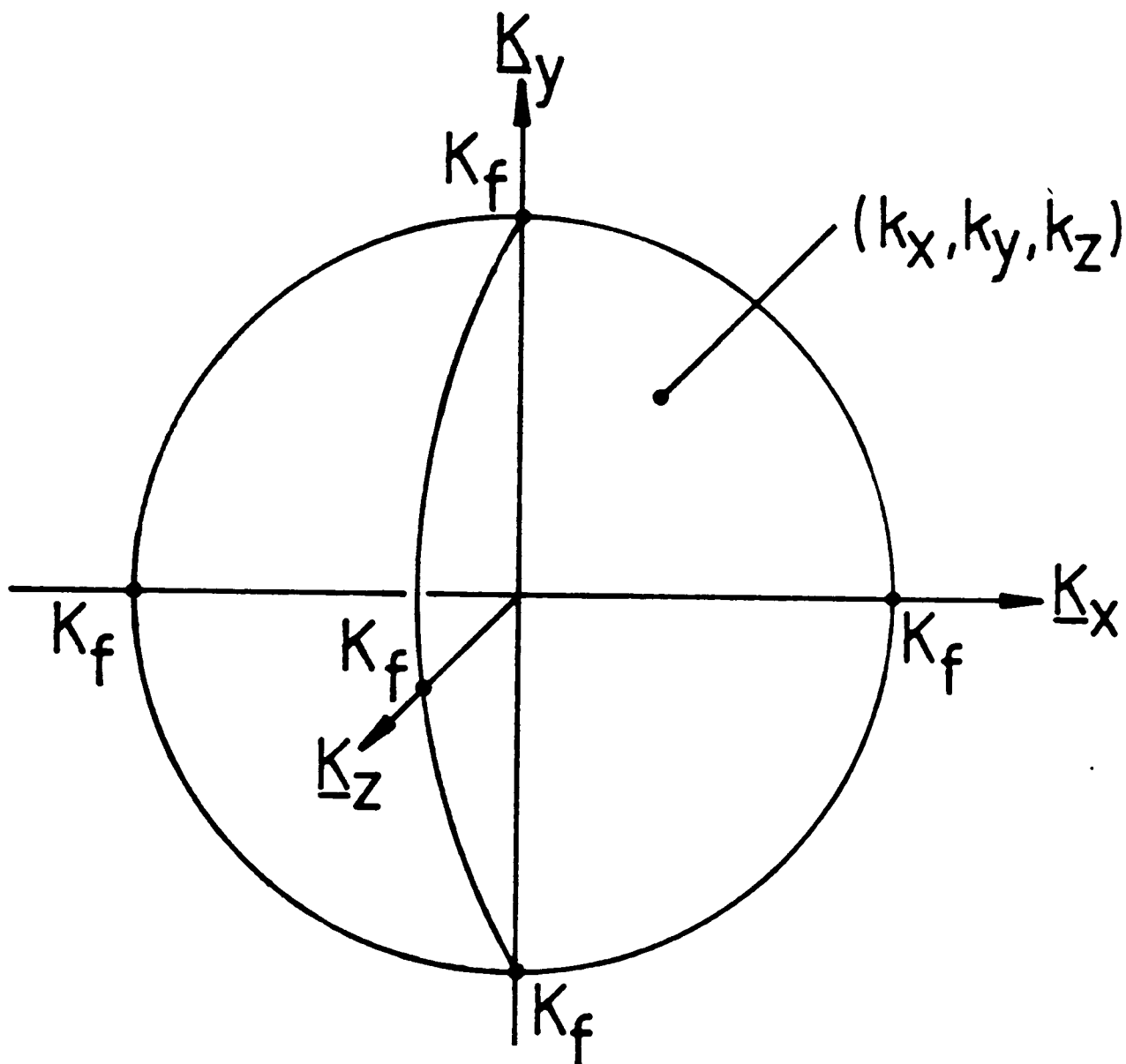
Where  $R$  is the resistance measured,  $R_0$  the resistance of the sample in the absence of an applied field, and  $\theta$  the angle between the current density vector and magnetisation direction in the sample. Despite the viability ( and attraction ) of this practical approach to overcoming the problems encountered in giving a detailed theoretical description of the performance of experimental devices utilising the effect ( thereby overcoming the difficulties imposed by the complexities of electron transport processes in magnetic materials ), a brief description of current theoretical understanding of the problem is given.

It is often pointed out in texts, varying from those on theoretical solid state physics to experimental handbooks describing the properties of electronic materials; that among the observed physical properties of solids, the electrical resistivity displays possibly the widest range. This range of  $10^{32}$  is found to be intimately tied to the behaviour of electrons in solids, an understanding of which leads eventually to a description of the anisotropic magnetoresistance observed in thin NiFe films. The first attempt to provide a realistic description of electron transport processes in metals was given by Drude [4]. In this theory the conduction electrons were assumed to be a free electron gas, obeying classical Maxwell-Boltzmann

statistics; in which, for an electron travelling freely between collisions, no interactions between the other electrons in the gas or the ion cores of the metals atoms was possible. It was further assumed that the collision processes with the ion cores predominated ( electron/electron collisions being ignored ), and that the electron gas achieved thermal equilibrium with its surroundings through these interactions. The time between collisions was termed the relaxation time. Additionally each electron in the assembly is assumed to have the same thermal speed, one consequence of which is that the observed magnetic field strength dependence of the magnetoresistance, and the field dependence of the resistance on the orientation and preparation of the specimen cannot be predicted by this theory.

To explain these inconsistencies Lorentz [5] modified Drudes original theory to allow for a distribution of electron velocities in the gas; and described the perturbation due to an external applied field gradient, by solving the Boltzmann transport equation for the system. This theory of Lorentz can be used to predict the observed increase in sample resistance dependent on the square of the applied field, but other major limitations involving the specific heat and susceptibility of metals are not overcome. Only by applying a much more rigorous quantum mechanical approach involving Pauli's exclusion principle and the Fermi-Dirac statistics developed during the 1920's to

Figure 18



Schematic diagram showing the Fermi surface at zero degrees kelvin.

describe the behaviour of quantum particles can these problems be resolved. As well as providing a better understanding of such experimentally observed phenomena, several new parameters, such as the Fermi surface, are introduced by the incorporation of quantum mechanics into the free electron theory.

From the basic postulates of quantum mechanics, an electron can be described as having both particle aspects and wave aspects, from which it can be deduced that any individual particle has a wave-vector  $K$ , which is only allowed to take certain fixed values. Thus in a system having macroscopically large dimensions, such as a real metallic film, there is a large but not continuous, number of possible states available for the electrons in the film to occupy. If a co-ordinate system is drawn having three orthogonal axes, each of which takes the value of one of the three components of the assembly of electrons wave-vectors; then this system can be regarded as describing a  $K$ -space ( see figure (18)). At 0 degrees Kelvin the energy of the system is minimised and the array of the wave vectors of the the assembly of electrons will fill a sphere of radius  $E_f$ , known as the Fermi radius. It can be shown from analysis of the Fermi-Dirac statistics describing the system, that even at room temperatures the velocities of the electrons on the edge of the Fermi surface are not significantly different from those postulated by the energy minimisation argument for a material at absolute zero. The behaviour of the electrons in

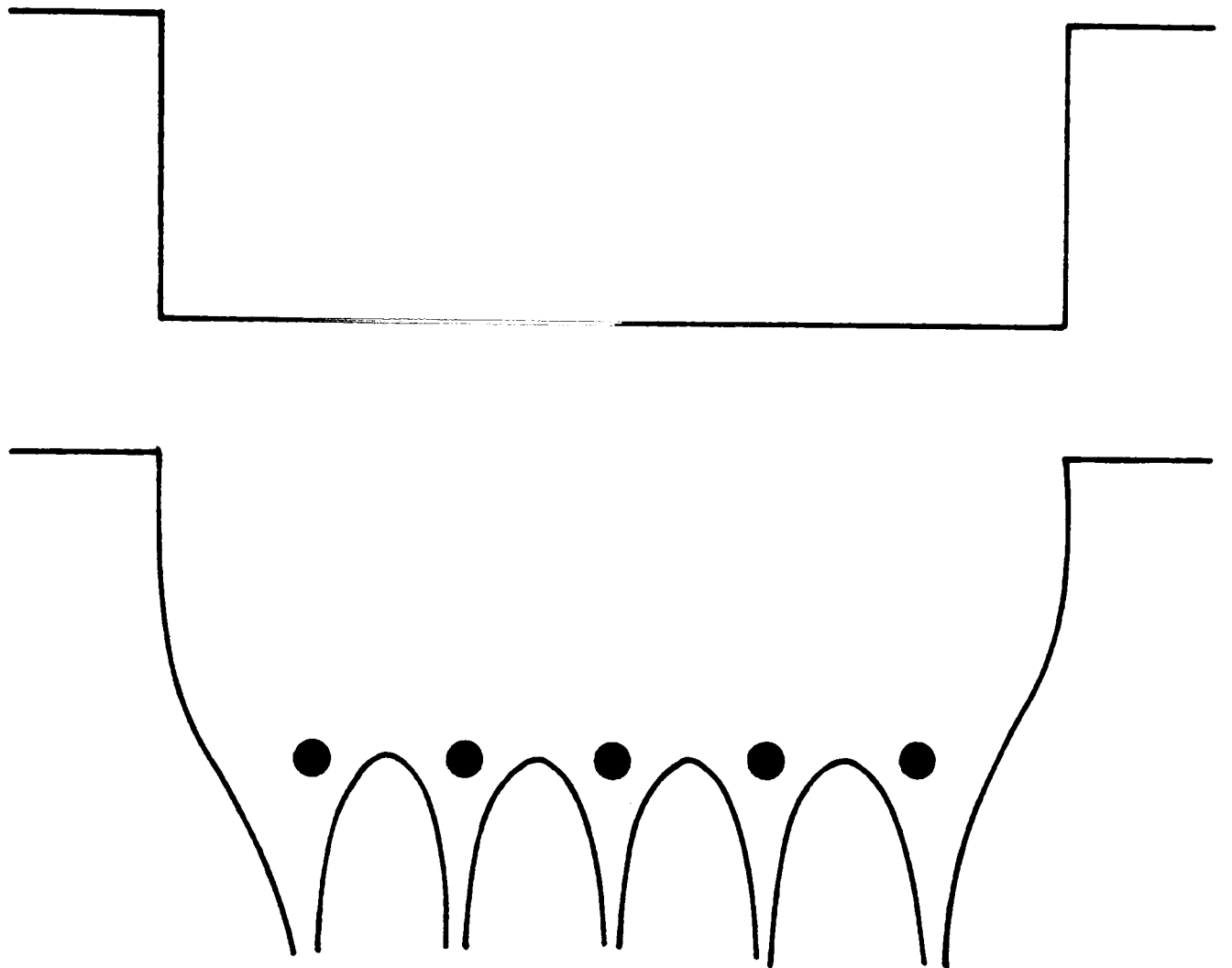
the metal can thus be described by solving Shrodingers equation for the system using the necessary boundary conditions to confine the electrons within the sample.

Despite the improved understanding of this modified theory, some basic fundamental properties of materials remain unexplained. One major problem is the lack of an explanation of the observed differences between the resistivities of metals, semi-metals, semi-conductors and insulators; even though all of these materials contain electrons. Thus for a more complete description, the effect of the periodic lattice of the crystal must be considered; from which the additional concepts of electron bands and effective mass are derived. Up until this point the electrons have been considered to be moving freely in a potential well having infinitely high sides, but with no other boundary conditions being required. Now a regular series of potential wells must be included within the potential well model, as shown in figure (19). As a result of this modification the description of the allowable electron wave-functions becomes a much more difficult problem. For example, it now becomes possible for electrons within the well, to be not only internally reflected from the walls of the well, but also by the nuclei in the crystal lattice. Due to the periodic nature of the lattice, and the quantum nature of the electrons; it is found that there are substantial regions in the energy spectrum of the electrons for which no solution of the electron wave-equation exist. These regions are termed the energy (or



Figure 19

Infinitely Deep Potential Well



Potential Including Crystal Structure

Schematic diagram showing an infinite potential well, and the same well with the crystal ion cores added, used to calculate the band structure of conducting materials

band) gaps, and are fundamental in determining the resistivities of solids.

For any material there will be a fixed number of energy bands dependent on the crystal structure of the material. At absolute zero these bands will be filled progressively, with the top of the last band defining the Fermi surface for that material. If electrons are to flow in the material as a result of an applied electrical potential gradient, then there must be empty states having a higher energy for them to be transferred into. This is due to the Pauli exclusion principle not allowing electrons to be scattered to a position within the Fermi surface, as two electrons are not allowed occupy the same quantum states. In a metal the top of the Fermi distribution occurs within an allowed band, and sufficient energy can be gained by an electron for it to easily move up into one of the empty states existing in the higher energy states in the band. If however, the top of the band and the Fermi surface coincide, then the only available free states into which an electron can move are in the next higher energy band. For an electron to obtain sufficient energy for such a transition to occur an enormous electric field would have to be applied, and hence such materials are insulators. Although simplistic, this argument works well for most substances, providing other effects, such as the broadening and overlapping of adjacent bands due to the electrons having extended wave-functions, are also considered.

In addition to the introduction of the concept of allowed electron bands within a solid comes the concept of an effective mass tensor. This concept is one result of the quantum partical nature of electrons. In one direction the effective mass of an electron is defined by the relation :-

$$m^* = \frac{h^2}{4 \pi^2 d^2 E/dk^2} \dots\dots\dots(8)$$

Where h is Plancks constant, E is the electrons energy and k is the k-vector of the electron. Thus the response of an electron travelling in the y-direction to a force (F<sub>x</sub>) applied in the x-direction would be :-

$$\frac{dV_y}{dt} = F_x \frac{4 \pi^2}{h^2} \frac{d^2 E}{dk_x dk_y} \dots\dots\dots(9)$$

For any combination of directions of force and direction of response 1/m<sup>\*</sup> becomes a tensor with components :-

$$\frac{1}{m^*} = \frac{4 \pi^2}{h^2} \frac{d^2 E}{dk_i dk_j} \dots\dots\dots(10)$$

where k<sub>i</sub> and k<sub>j</sub> are a pair of cartesian coordinates of k.

For the transition elements, such as Nickel and Iron, the band structure is very complex, especially the energy bands corresponding to d-electron states. In copper the 3d band is completely filled and there is one electron in the 4s band, and the material is thus a good conductor. For both

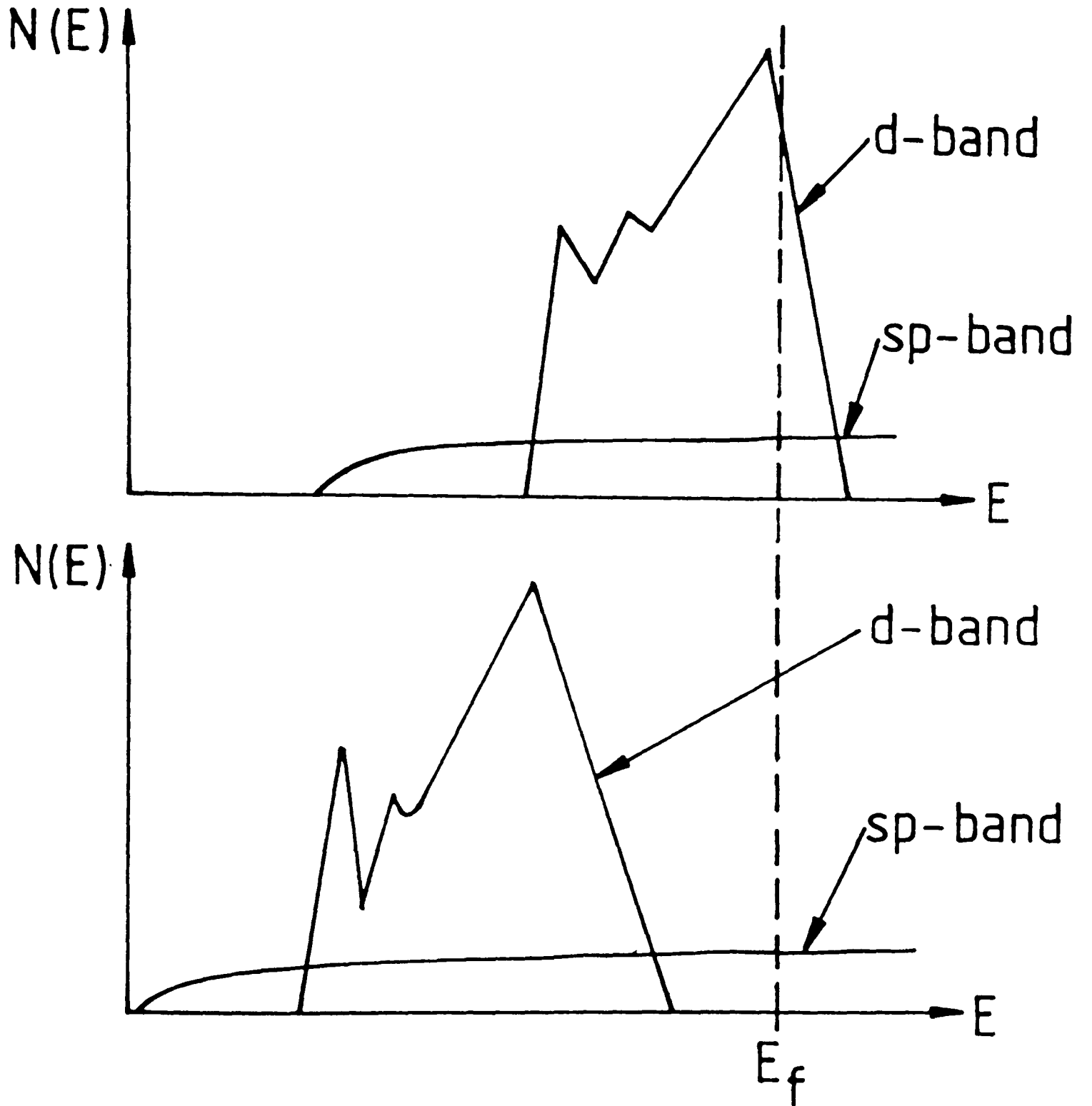
Nickel and Iron however, the 3d band which is capable of holding up to 10 electrons is not completely filled; and is additionally rather narrow resulting in electrons in this band having a large effective mass tensor which limits their mobility. Overlapping this band is a broad 4s band containing electrons having very different properties (Fermi velocity and effective mass) to those in the 3d band. It is assumed [6] that most of the current is carried by these, with the interband transitions needed for current to flow dominating the resistivity. This explains not only the relatively high resistivity of these materials, but also, if it is assumed that the d bands are split when they are magnetised with the majority spin bands now below the Fermi level; the decrease in resistivity upon ferromagnetic ordering.

Despite the success of the band theory in describing the more general electronic properties observed experimentally, such a description has still to be modified if it is to predict the ordinary and anisotropic magnetoresistance. If a spherical surface, and constant relaxation time are assumed, then it can be shown that no ordinary magnetoresistance effect can be derived [7]. The origin of the ordinary magnetoresistance effect can therefore only be understood by considering either two spherical overlapping bands each having different numbers of electrons, constant relaxation times and effective masses, or by assuming that the bands are non-spherical. However, it is still not possible to derive a theoretical description of the

observed anisotropic magnetoresistance without the introduction of some additional concepts to this modified theory. For instance, it has been assumed that the solutions to Shrodingers equation for the electrons moving in the potential due to the lattice are stationary states, which results in a theoretical infinite conductivity. To overcome this it is assumed that the electrons are scattered between states by a variety of processes such as lattice vibrations ( phonons ), impurities, and grain boundaries. Additionally it is postulated that a relativistic interaction is possible between the spin and the orbital motion of an electron which can, in certain cases, have a marked effect on the band structure of the material, and hence its electrical properties.

The calculation of the anisotropic magnetoresistance now proceeds using the Two-Band or two current model described in the previous paragraph, which specifically recognises that a distribution of relaxation times is possible over the Fermi surface. If the s-d scattering is indeed the predominant effect in the resistivity of these materials, then it seems reasonable to assume that an anisotropy in this scattering mechanism would result in the observed anisotropy in the magnetoresistance. At present the accepted mechanism for this anisotropy is the spin-orbit interaction, in which the d-orbit electrons have their spins coupled to their orbital motion. Due to the interaction of these d-orbit electrons with the internal magnetisation,

Figure 20



Graph showing the band-splitting of Ni due to spin-orbit coupling

the band structure of the material is now altered to that shown in figure (20). Those electrons having their spins parallel to the direction of the magnetisation ( spin up ), will form an s-band and a d-band, with the d-band having a high density of states at the Fermi level; whilst those having their spins aligned anti-parallel to the magnetisation ( spin down ) will form an equivalent band structure, but with the top of the d-band below the Fermi level. As the spin up electrons have the higher density of states at the Fermi level, there will be a greater probability of their being scattered than the spin down electrons ( assuming that spin direction is conserved in the scattering process ).

The final step in the mathematical description of the anisotropic magnetoresistance is somewhat involved, with two main schemes being used. In the earliest theory Smit [1] treated the spin-orbit interaction operator as a small perturbation, and considered its action only on the parallel spin states. By using first order perturbation theory, he found that electrons moving parallel to the direction of magnetisation are more easily trapped than those moving transverse to it; which accounts for the observed resistance anisotropy. In an improved analysis by Potter [8], in which both parallel and anti-parallel scattering processes are considered, it is shown that, if the anisotropy is due to spin up electron scattering, then the resistivity parallel to the magnetisation should be less than that transverse to it. This is in variance to Smit's theory, suggesting that the

anisotropy is due to the scattering of the spin-down electrons. In addition to the two theoretical descriptions given here, other work particularly that of Kondo [9], who assumed the effect to be due to the scattering of s electrons by the remaining orbital magnetic moment of the 3d electrons; should be mentioned as producing alternative viewpoints.

Although providing an insight into the dominant electron transport processes which result in the anisotropic magnetoresistance of ferromagnetic materials, calculations using these models can only provide order of magnitude results and for device applications the well known phenomenological equation (1) will suffice. The justification for this equation is found using symmetry arguments, similar to those used in the description of magnetostriction and is described by McGuire and Potter [3]. The difference in resistivity for the current flow parallel to the magnetisation direction, compared with the current flow perpendicular to that direction results in a tensor resistivity in Ohms law. The electric fields associated with the symmetric and antisymmetric parts of this tensor are associated with the magnetoresistance and Hall effects respectively. By analysing the magnetoresistivity tensor for a single crystal magnetised along one of its crystal axes the form of the resistivity along that axis can be found. To extend the theory to poly-crystalline samples the resistivity is integrated over a large number of randomly orientated crystallites by choosing a unit vector lying within a cone



about an arbitrary current direction. This has been done by Birss [10] for saturation magnetostriction producing the result given in equation (1).

#### 4.2) Device calculations applied to single sensors.

Given the expression in equation (1), Hunt [11] was the first to show that it was possible to rewrite this equation for thin film magnetoresistive elements as:-

$$P = P_0 + \Delta P \left( 1 - \frac{H_y^2}{H_0^2} \right) \dots \dots \dots (11),$$

where  $H_y$  is the total vertical field in the element, and  $H_0$  is the effective field acting to restrain the magnetisation along the element length.  $P$  is the measured resistivity,  $P_0$  the resistivity in the absence of an applied field, and  $\Delta P$  the anisotropic magnetoresistance change. To obtain such an expression the sensor configuration shown in figure (21) was adopted, and it was assumed that the sensor had an elliptical cross-section to make the de-magnetising field uniform whilst rendering the x-components of the field ineffective. Additionally an anisotropy field  $H_k$  was taken as being parallel to the current vector direction. By minimising the free energy of the system it can be shown that:-

$$-H_y \cos(\theta) + H_0 \sin(\theta) \cos(\theta) = 0$$

where  $H_0 = H_k + NM_s$ ,  $N$  being the ratio of the thickness to depth of the sensor, and  $M_s$  the spontaneous magnetisation moment. From this equation it can be seen that:-

Figure 24

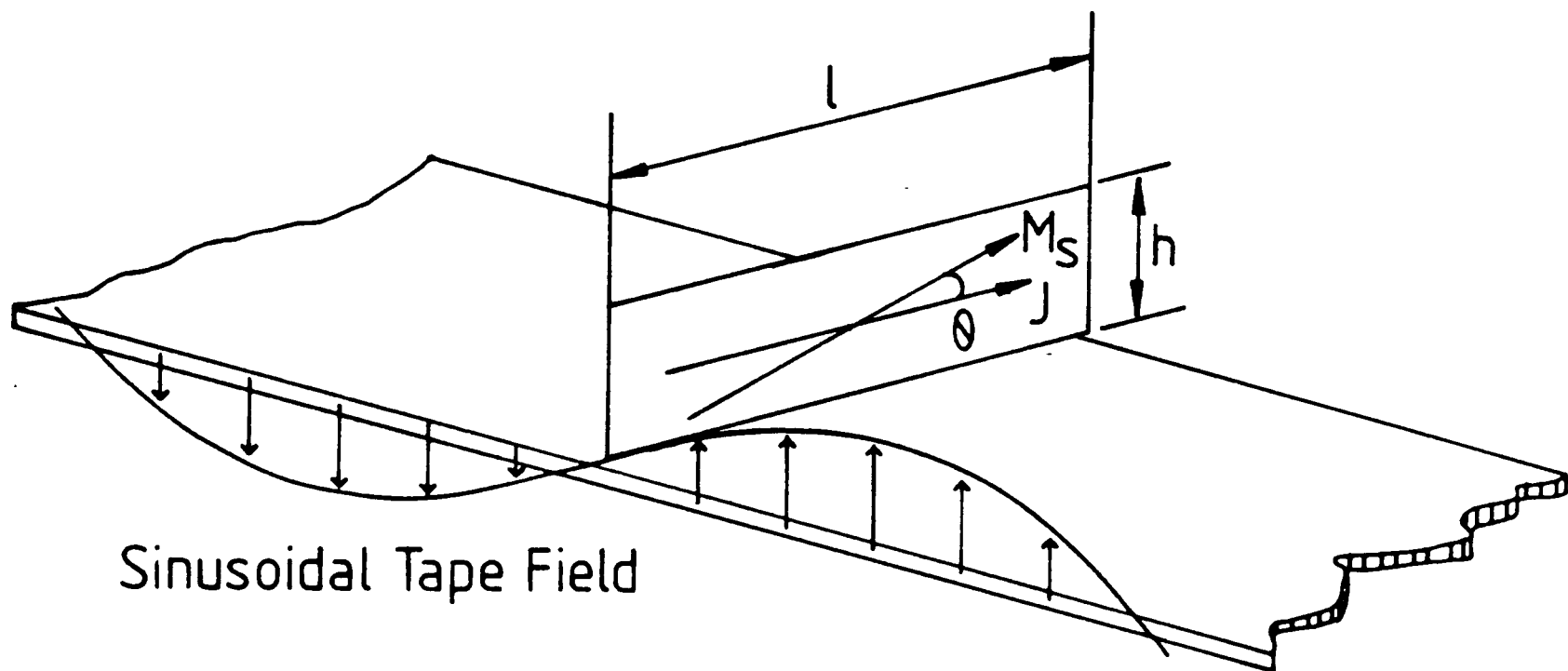


Diagram of the configuration used to calculate the performance of a single magnetoresistive element

$$\sin(\theta) = (H_y/H_o)$$

hence the variation in resistivity given in equation (11) is obtained.

To linearise the sensor output the vertical component of the field in the element ( $H_y$ ) must be composed of a tape field  $H_t$ , together with a bias field  $H_b$ . The resistivity then becomes:-

$$P = P_o + \Delta P \left( 1 - \frac{H_b^2}{H_o^2} - \frac{2H_b H_t}{H_o^2} - \frac{H_t^2}{H_o^2} \right) \quad (12)$$

This equation can be integrated over the device dimensions to obtain a signal voltage  $V$ .

$$V = 2I R_o \frac{\Delta P}{P} \frac{H_b}{H_o^2} \int \int H_t(y, z) \frac{dy}{W} \frac{dz}{L} \dots\dots\dots(13)$$

The constant and quadratic terms from equation (12) are ignored,  $R_o$  is the element bulk resistance,  $L$  and  $W$  are respectively the element length and width. By then allowing this equation to operate on the expression derived by Wallace [12] for the vertical component of the magnetic field above a sinusoidally recorded magnetic tape, the frequency response for a device having certain fixed dimensions is obtained:-

$$V = I R_o \frac{\Delta P}{P} \frac{4\pi M_r H_b}{H_o^2} e^{(-kd)} \frac{(-kt)}{(1 - e^{(-kt)})} \frac{(1 - e^{(-kh)})}{kh} \quad (14)$$

where  $M_r$  is the tape remnant magnetisation,  $d$  the head to tape separation,  $t$  the tape coating thickness and  $k$  the recorded wave vector ( $2\pi/\lambda$ ), where  $\lambda$  is recorded wavelength.

Although this analysis compared very favourably with experiments Hunt made on an unshielded permanent magnet biased sensor, a more rigorous analysis of the sensors performance taking into account anisotropy, shape, demagnetising, exchange, and bias field contributions, has been made by Anderson et. al. [13]. In this method an equation for the total torque density acting on  $M_s$  is obtained and solved using an iterative relaxation technique. First the equation for the demagnetising field is numerically solved for an initial angle  $\theta(x)$ . The torque is then calculated, and the numerical calculation to compute the angle iteratively relaxed according to a fixed formula until the torque reaches a negligible value. The final result for  $\theta(x)$  for which the torque is taken to be zero is then used to compute the resistance change given by the equation:-

$$\frac{R}{R_{\max}} = \frac{1}{W} \int_h^{h+w} \cos^2 \theta(x) dx \dots\dots\dots(15)$$

This equation follows from the phenomenological expression given in equation (1) and is solved using Simpsons rule.

The results predicted by this set of equations were then compared with results taken from experiments using a uniform

field excitation, and an isolated line charge transition to model the response to, and resolution in, an actual recording process. The uniform field experiments showed a very good agreement, and the isolated line charge experiments showed reasonably close agreement with the theoretical predictions. More recently these equations have been extended by Casselman and Hanka [14] to predict various design parameters used to improve the performance of magnetoresistive sensors.

Despite the fact that these results are not particularly suited to describing the reading of magnetic tape fields due to the decay of the tape field across the width of the sensor; they do emphasise the overly optimistic theoretical results produced by assuming a uniform demagnetising field, particularly for sensors having a thickness to width ratio as low as  $1 \times 10^{-4}$ . The more realistic picture of the demagnetising field within an the element described by these analyses, is produced by considering the effect of rotating the sensors magnetisation vector as a result of applying a linearising bias field. At a given angle to the current density, magnetic charges of opposite polarity are formed at the top and bottom of the element. These charges generate demagnetising fields that oppose the applied field; but due to their non-uniformity across the element width have the greatest effect on the bias angle at the sensors edges. Except in the case of a very high applied field, in which case the body of the film will be driven into saturation; the bias angle between the magnetisation direction, and current

vector direction close to the sensors edge tends to zero resulting in a "Dead-Zone" at the sensors edges.

Even though these more rigorous theoretical descriptions show that Hunts original equation describing the performance of a single unbiased, unshielded magnetoresistive sensor, contains some unrealistic assumptions, its ease in use, together with the good correlation it produces between experiment and theory make its use in describing practical devices valid to the present day.

#### 4.3) Theory for two-element devices.

Various models for two element magnetoresistive read heads have been proposed. These vary from the relatively simple, in which a non-magnetic bias conductor is deposited on top of the sensor [15]; to the more complex, in which the combination of an electrically insulated, centrally placed, non-magnetic, bias conductor and an anisotropy axis canted at an angle to the front edge of the sensors provide the bias field [16]. Two overall strategies have been developed to describe such heads depending on whether or not a shield structure has been used to improve the short wavelength resolution. In the first, due to flux leakage from the sensors to the shields a transmission line model is used to describe the magnetic inductions for the bias and signal fields in the element, whilst in the second the free energy of the various layers is minimised to provide the optimum

magnetisation rotation. For the device described in this thesis the minimisation model is most appropriate, but a brief description of the transmission line model is given.

The first use of a two-element differentially sensed sensor was given by Shelledy and Brock [17]. In this design the sensor was placed asymmetrically between the shields with a non-magnetic conductor adjacent to it, through which a portion of the sense current flowed. This current provided part of the bias field required, with the remainder being provided by the magnetic coupling between the sensor and the shield nearest to it. Following the work of Paton [18], and Thompson [19], two independent paths are chosen to describe the magnetic circuit, from which differential equations are derived to describe the fluxes and potentials in the structure. These are then solved to give the flux in the sensor. The fluxes at the media surface are calculated using a method similar to Potters [20]; and this together with the solution for the flux in the sensor and the standard magnetoresistive equation modified to apply to the differential structure, provides the analytical model of the head. This configuration has been further analysed more recently by O'Conner et. al. [21], providing a more accurate mathematical model.

Although of interest from the point of view of completeness this approach has not been adopted for elements without shields. O'Day proposed a design having a central

non-magnetic conductor with a magnetoresistive sensor on either side of it [22], but little theoretical description of such a structure has been found. The first practical analysis of this type of sensor was by Jeffers [16], who considered two elements which have their anisotropy axes canted at an angle to their lengths and are biased by a non-magnetic conductor between, and electrically insulated from them. An expression for the free energy of the two magnetic layers was derived and then minimised to provide the angles of rotation of the magnetisation vectors in each of the sensors. These can then be substituted in the standard equation for the differential detected signal voltage, and the Wallace equation for the tape field used to provide an equation for the dynamic head response. To overcome the "gap loss" factor introduced by the two elements being differentially sensed and separated spatially, the resultant dynamic performance equation is multiplied by an expression which takes account of the frequency dependence of this effect.

Using a method similar to this Van Ooyen et. al. [23] have described the response of a laminated NiFe/Mo/NiFe sandwich to uniform applied magnetic fields. The Anisotropy, Field and Demagnetising energies are calculated for the angles of magnetisation rotation in each of the two layers to give the total free energy of the system, which is then minimised. From these equations direct substitution of actual experimental values for the element thicknesses and separations gives the change in resistivity for this system



as a function of applied field. This theory provides a very good description of experimentally observed magnetoresistive changes in laminated elements, showing the increased sensitivity resulting from the decrease in the demagnetising fields due to the strong magnetostatic coupling between layers.

An extension of this theory has recently been given by Pohm et. al. [24], in which double layer magnetoresistive sensors are described. A one dimensional model is considered in which the drive field is assumed to originate from the field around a wide uniform current sheet. Equations are then derived which describe the rotation of the magnetisation moment in terms of the torque acting on it. Calculations of the angle of rotation of the magnetisation for extremely small sensors (typically 1-2 microns wide, 300 angstroms thick, with a 100 angstrom separation layer), show how important the inclusion of exchange terms is for this size of element. This model is particularly useful in the theoretical analysis of the multiple-layer head, in that it has allowed the demagnetising and average magnetoresistive responses of the coupled films to be calculated.

Although not directly related to the multiple-film self biased structure a head in which the bias is supplied by a soft magnetic layer adjacent to the sensor has recently been described using an analysis very similar to Van Ooyen. In this head based on a device described by Beaulieu and Nepala

[25], Jeffers et. al. [26] placed a second NiFe element on top of the sensor. This element has no current passing through it, and serves only to bias the sensor via its magnetostatic field, once it is magnetised by the field produced by the sense current in the detector. By making the separation between the NiFe layers zero, equations for the normalised energy density can be expressed in terms of the energy of the soft adjacent layer, the magnetoresistive sensor, and the coupling field. The field in the coupled element due to the sense current is taken to be that produced by an infinite current sheet as used by both Van Ooyen and Pohm. The energy was then minimised by solving these equations numerically for all cases except where the external applied field, and the easy axes of both NiFe elements are along the current direction; in which case an analytical solution is possible as shown by Van Ooyen.

#### 4.4) Analysis of the bias field produced by the sense current.

To obtain the average drive field in a sensor due to the current in an identical element adjacent to, but spatially and electrically separated from it a mathematical analysis of the problem has been carried out. In previous work [23,24,26] the field had been assumed to be the same as that produced by an infinite current sheet, thus neglecting edge effects in both elements. It was felt that with the sense current bias

Figure 22

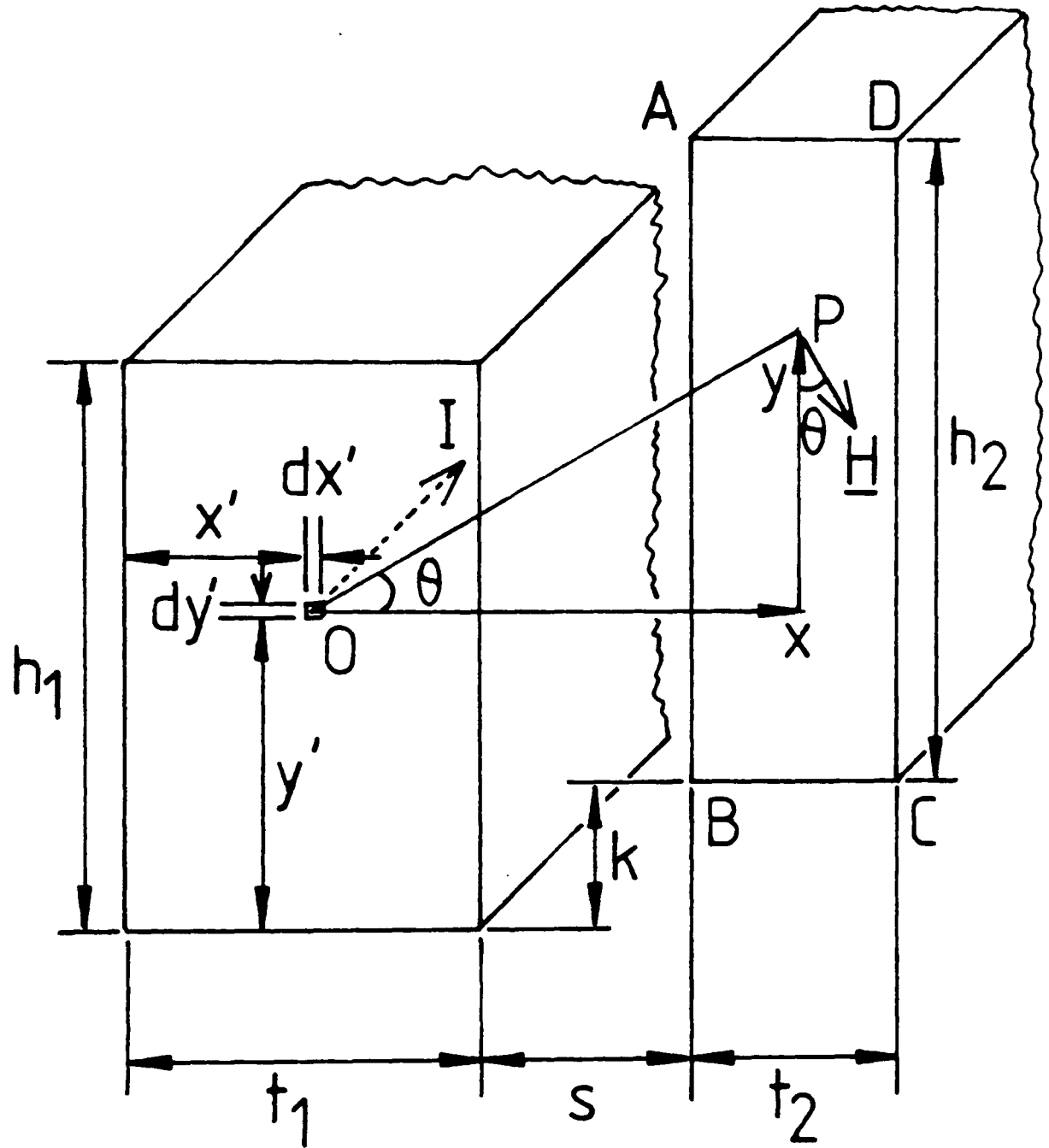


Diagram showing the geometry used to calculate the average field produced by an adjacent current carrying conductor

field playing such an important role in the dynamic performance of the head, unlike in various other bias methods in which the sense current simply scales the head output voltage; a more rigorous description was necessary. This produced an expression for the average field in one element which was dependent on the dimensions of that element and the current carrying element, their separation distance, and the current flowing to produce the field. The resulting theory together with certain predicted results produced by it was published in the paper shown in appendix (V).

A diagram of the configuration and symbols used is given in figure (22). Two realistic, simplifying assumptions were made about the system to aid the analysis.

1) The elements were infinite in length, thus overcoming end (as opposed to edge) effects. This is reasonable given the fact that the sensors are typically 5-10 times longer than they are wide, and 300 times longer than the separation between them.

2) The current is uniformly distributed throughout the current carrying element. Again reasonable considering the dimensions, together with the fact that both elements are R.F. sputtered from 99.99% pure targets onto a clean substrate surface.

Given an element of current  $dI$  flowing in conductor (1)

at point O, then from the Biot-Savat law the field at an arbitrary point P in conductor (2) is given by:-

$$H = \frac{dI}{2\pi(x^2 + y^2)^{1/2}} \dots\dots\dots(16)$$

and acts in a direction perpendicular to the line joining the two points. The vertical component of this field at P is:-

$$H_v = H \cos(\theta) \dots\dots\dots(17)$$

where (θ) is the angle between the field and the Y-axis. From the geometry given:-

$$\cos(\theta) = \frac{x}{(x^2 + y^2)^{1/2}} \dots\dots\dots(18)$$

By substituting equations (16) and (17) into (18) the vertical field at P is obtained:-

$$H_v = \frac{dI}{2\pi(x^2 + y^2)^{1/2}} \frac{x}{(x^2 + y^2)^{1/2}} \dots\dots\dots(19)$$

This equation can now be integrated over the cross-sectional areas of both elements to obtain the average field in conductor (2) due to all the current elements in conductor (1). Thus:-

$$H_{av} = \frac{dI}{2\pi} \frac{1}{t} \frac{1}{h} \int_{(-y')}^{(h-y')} \int_{(t+s-x')}^{(2t+s-x')} \frac{x}{(x^2 + y^2)} dx dy \quad (21)$$

This integral can be expanded to account for all

possible variations in geometry for the sensors and their positions relative to each other by re-defining the limits of integration:-

$$H = \frac{I}{a} \frac{2\pi t_1 h_1 t_2 h_2}{1 \ 1 \ 2 \ 2} \int_{x'=0}^t \int_{y'=0}^h \int_{x=(s+t_1-x')}^{(s+t_2-x'+t_2)} \int_{y=(k-y')}^{(k-y'+h_2)} \frac{x}{(x^2 + y^2)^2} dy dx dy' dx'$$

For the first case in which the elements have the same physical dimensions, and there is no y-separation between them the integration was performed analytically. The solution of the integration is extremely long; but produced accurate results when checked against measurements taken using a large scale experiment. However for the more involved case in which all possible variations in element width and separation are considered the simpler solution shown below was produced :-

$$H = \frac{I}{a} \frac{2\pi t_1 h_1 t_2 h_2}{1 \ 1 \ 2 \ 2} [ J(s_2, s_2+t_2, k_2+h_2, k_2+h_2) + J(s_1, s_1+t_1, k_1-h_1, k_1) - J(s_2, s_2+t_2, k_2-h_2, k_2) - J(s_1, s_1+t_1, k_1+h_1, k_1) ] \dots\dots\dots(20)$$

where

$$\begin{aligned}
 J(A, B, C, D) = & \frac{5}{6} (A-B)(D^2 - C^2) + \frac{1}{3} C^3 [\tan^{-1}(A/C) - \tan^{-1}(B/C)] \\
 & + \frac{1}{3} D^3 [\tan^{-1}(B/D) - \tan^{-1}(A/D)] + A^2 [C \tan^{-1}(C/A) - D \tan^{-1}(D/A)] \\
 & + B^2 [D \tan^{-1}(D/B) - C \tan^{-1}(C/B)] + \frac{1}{6} B (3D^2 - B^2) \ln(B^2 + D^2) \\
 & + \frac{1}{6} A (A^2 - 3D^2) \ln(A^2 + D^2) + \frac{1}{6} A (3C^2 - A^2) \ln(A^2 + C^2) \\
 & + \frac{1}{6} B (B^2 - 3C^2) \ln(B^2 + C^2).
 \end{aligned}$$

The result has been checked both by numerical integration and also by differentiation.

The experimental validity of the result was checked using a large scale experiment. A large conducting plate measuring 50 m.m. high by 0.025 m.m. thick and 300 m.m. long was supplied with a constant current of 40 amps. The vertical component of the resulting field in consecutive planes adjacent to the plate was measured using a Hall Probe the active area of which was 0.2 X 0.25 m.m. The probe was scanned across the conductor at a fixed separation with measurements being taken at regular intervals and the averaged to provide the average field for a given displacement of conductor. The results are given in figure (23) together with the theoretical predictions of the mathematical model. As can be seen in this figure good agreement is obtained between the theoretically predicted and

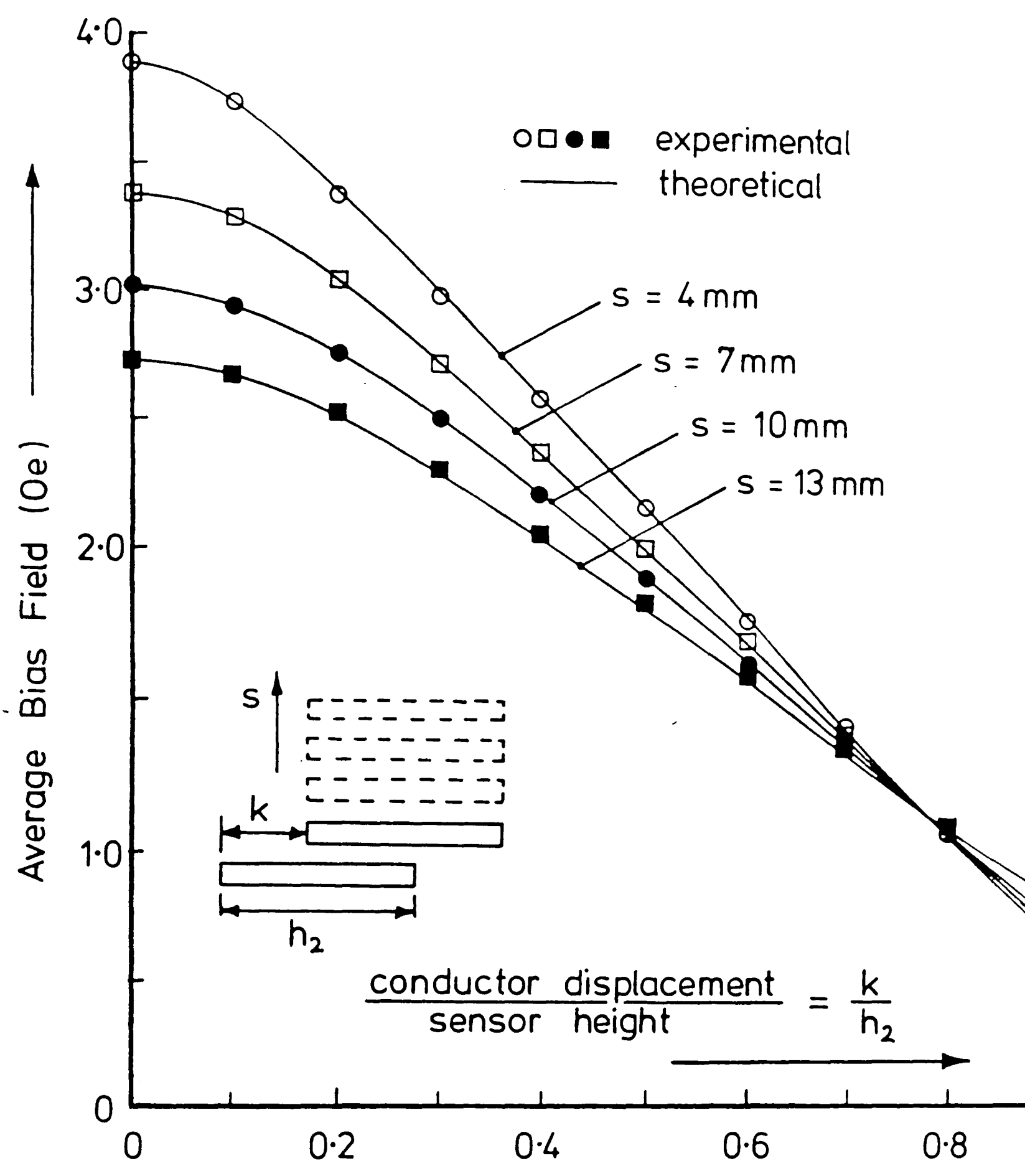


Figure 23

Graph of the theoretical, and experimentally measured, average bias field produced by the adjacent conductor carrying a current  $I$ .



experimentally measured fields. This is clearly demonstrated by both the prediction and observation of the unexpected cross-over point, at which the same average bias field is produced by a conductor width to offset separation ratio of 0.78; regardless of the separation distance between the sensor and conductor. Once experimental and mathematical validation of the theoretical result had been achieved, its use in predicting the effect of other variations in the design and manufacture of multiple-film sensors on the average bias field became possible.

In figures (24), (25) and (26) three possible variations have been considered. Firstly the average field variation due to the separation and thickness of the elements is considered. From this diagram it can be seen how, for realistic thicknesses of sensor, the average bias field diverges from that predicted using the infinite current sheet model. Secondly the result of sensor mismatch, due for instance to misalignment during photolithography, on the average field is evaluated. In this case it can be seen that horizontal variations in sensor alignment of less than 10% are tolerable. However in the final figure it can be seen how critical the etching of each of the elements in the structure becomes. The peak predicted average field occurs when the bias conductor is some 25% wider than the sensor which is impossible to achieve in the six-element multiple film configuration. For the more practical case in which the conductor and sensor are the same width, or in which the

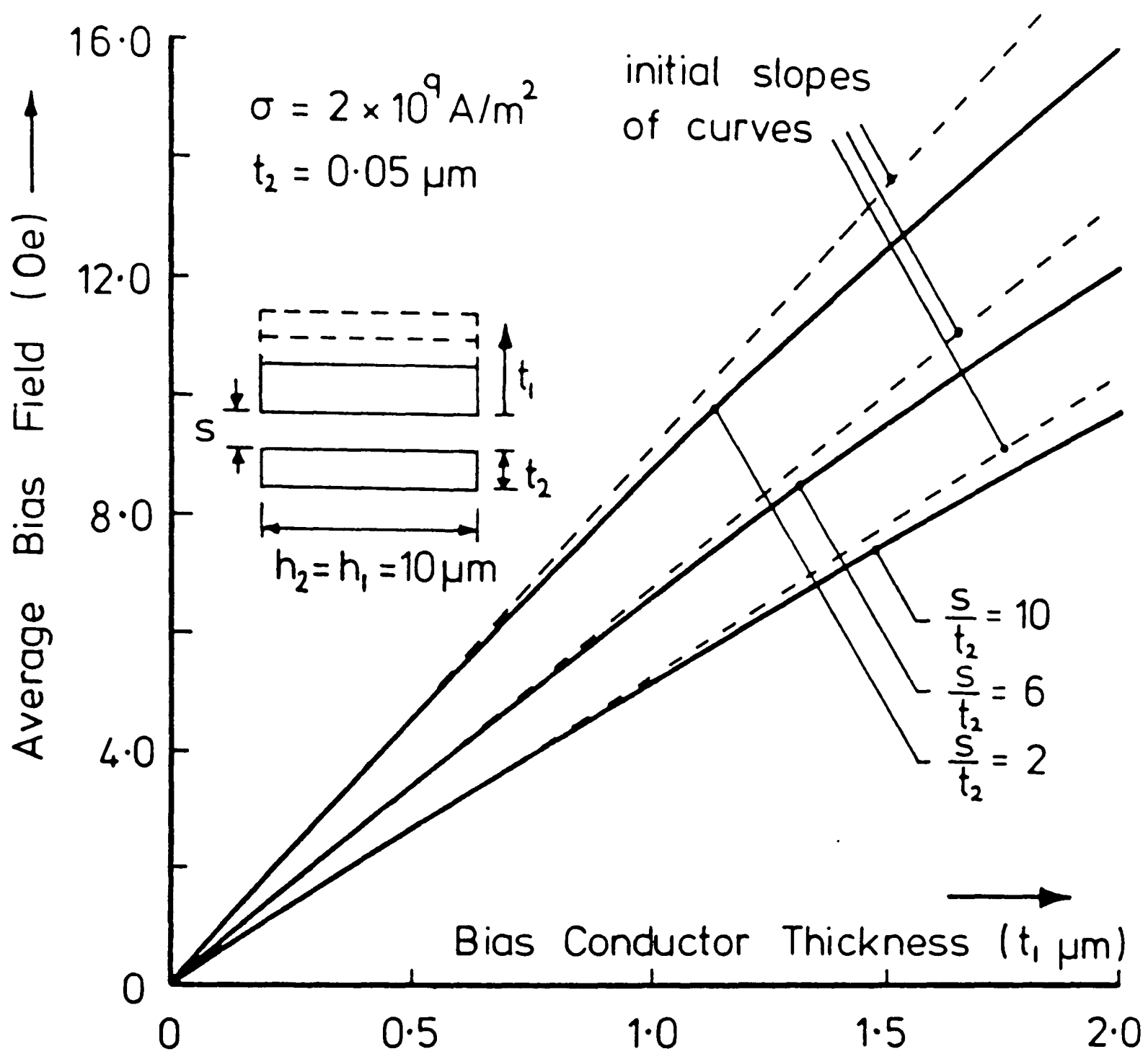


Figure 24

Graph showing the effect on the average bias field of variations in the element thicknesses

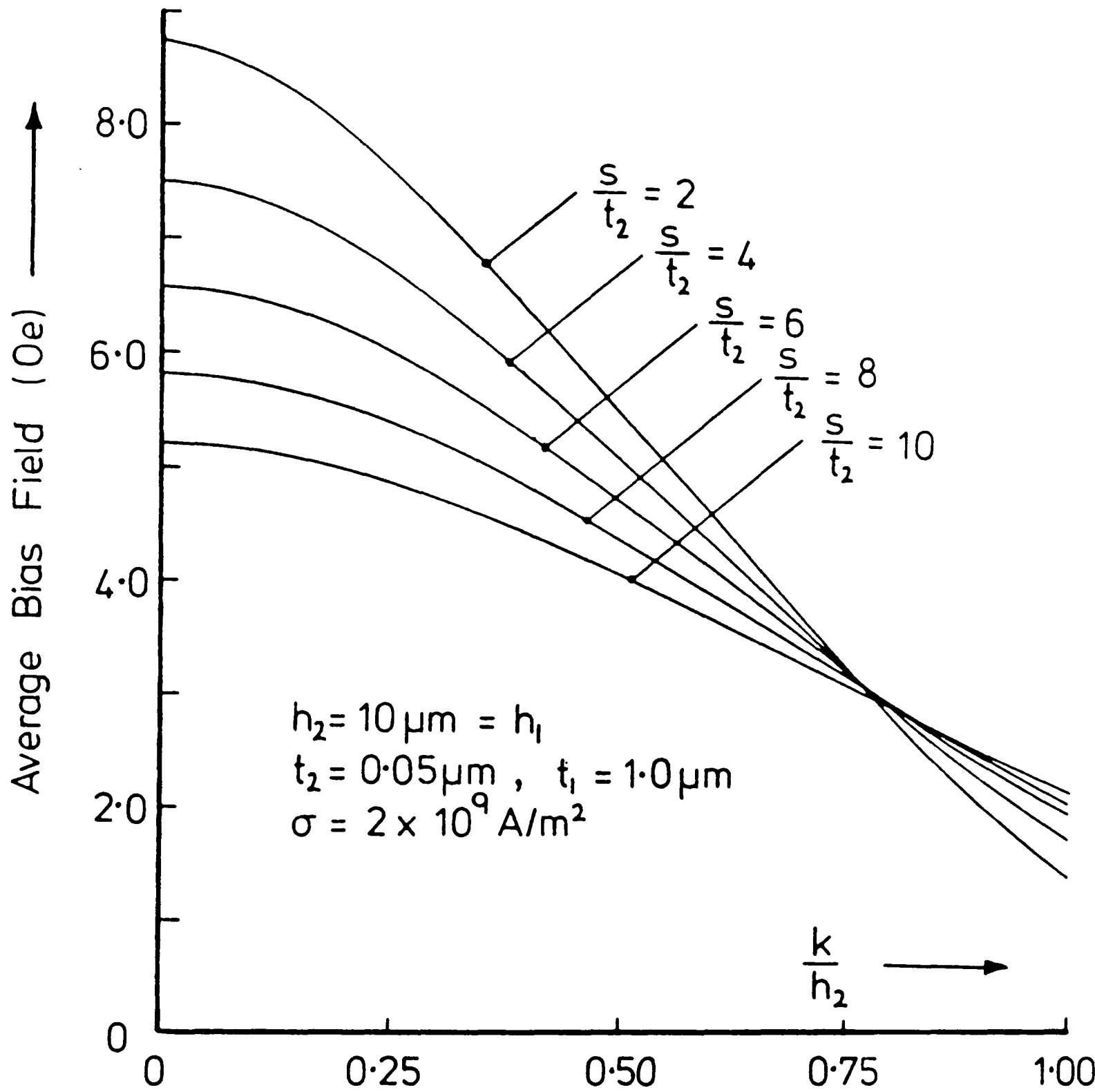


Figure 25

Graph showing the reduction in average bias field as a function of element offsets

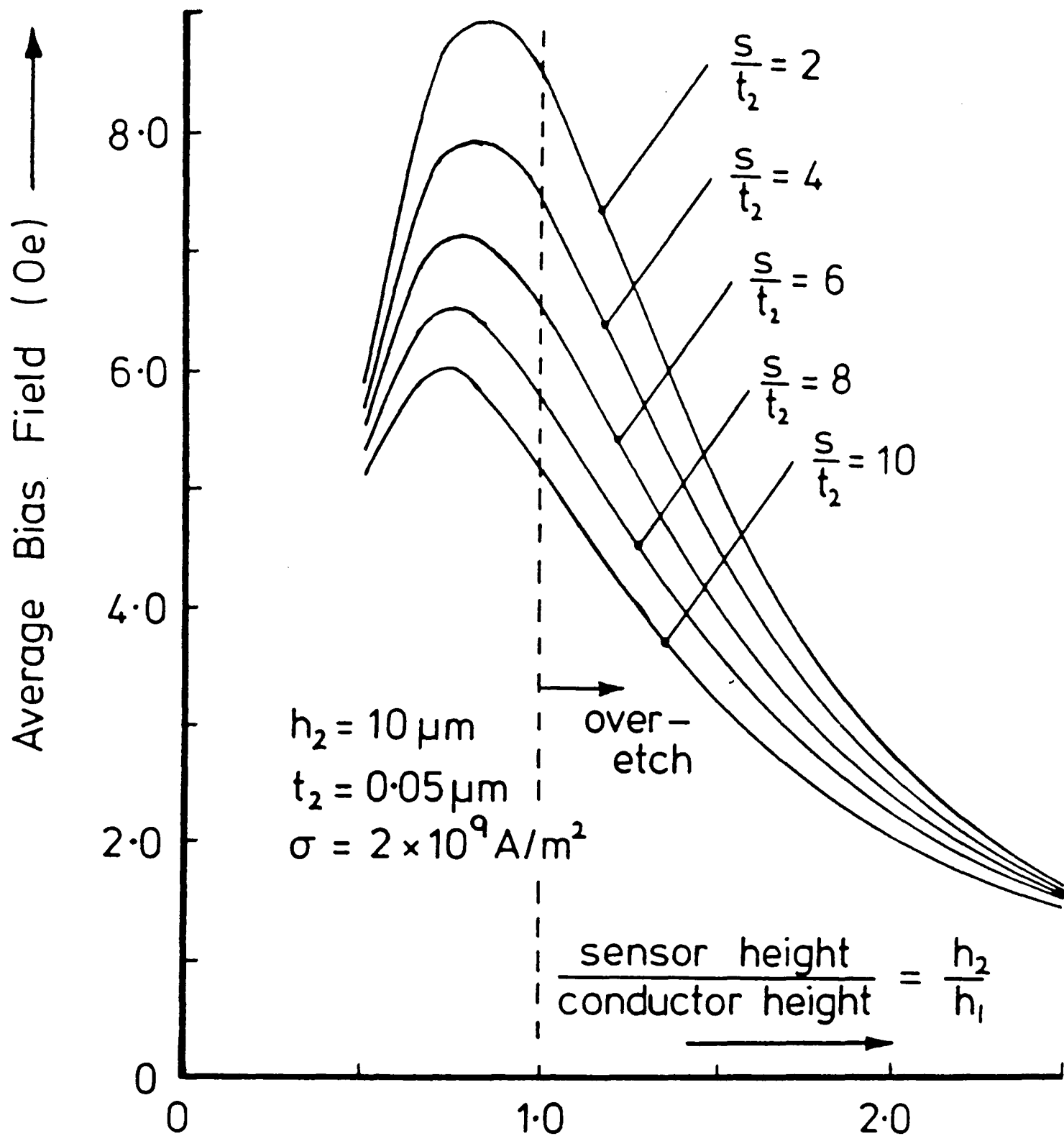


Figure 26

Graph showing how over etching of the bias conductor, can significantly reduce the sensor bias

conductor has been over-etched making it narrower than the sensor, a rapid loss in average bias field is predicted to occur, making accurate etching of the sense elements essential. For each of these figures the current density was kept constant, and typical element dimensions as used in practical devices were evaluated.

#### 4.5) Theory describing the response of the six-element, multiple-film device.

Although as has been described earlier in the text, there are several obvious advantages associated with the use of a multiple-film head in reading the information stored on standard audio frequency cassette tapes; the derivation of a theoretical expression for the performance of these devices proves to be rather difficult. Firstly, the use of the differential sensing mechanism for sensing the magnetoresistance of the two sets of three elements used in this head configuration; results in cancellation of the signal voltages as the recorded wavelength decreases. Secondly, as described in the previous section, assemblies of magnetoresistive elements can have radically different responses to externally applied fields from those of simple single element sensors. The solution to each of these problems is now described separately, with the complete solution given at the end of the section.

It has been shown that the quadratic component of the sensors magnetoresistive response gives rise to an undesirable second harmonic distortion [17]. By differentially sensing the voltage changes in the two magnetoresistive elements, this component can be eliminated, making the sensor output linear with respect to the signal. In order that differential sensing of the sensor array is possible, it has to be biased as shown in figure (27), with the two arms of the array having their magnetisation vectors rotated by the same amount, but in opposite directions. This is achieved by folding together two long magnetoresistive elements, and electrically inter-connecting them as described in Chapter Three.

As all of the sensors making up the array are fabricated in an identical fashion, the assumption is made that for equal current densities in each of the arms, both sets of elements are biased to the same degree. Although this is not strictly true, as the sensors on either side of the array have only a single neighbouring sensor to supply their bias fields; it is assumed to be reasonable due to the other coupling effects operating in the head. Thus, for an applied field acting on the whole head, the resistance of one arm of the array will be decreased, whilst that of the other arm will be increased. It is additionally assumed that by biasing each of the arms onto the most linear part of the response curve, the resistance changes in each arm will be equal. If a current constant is supplied to the sensors, then the

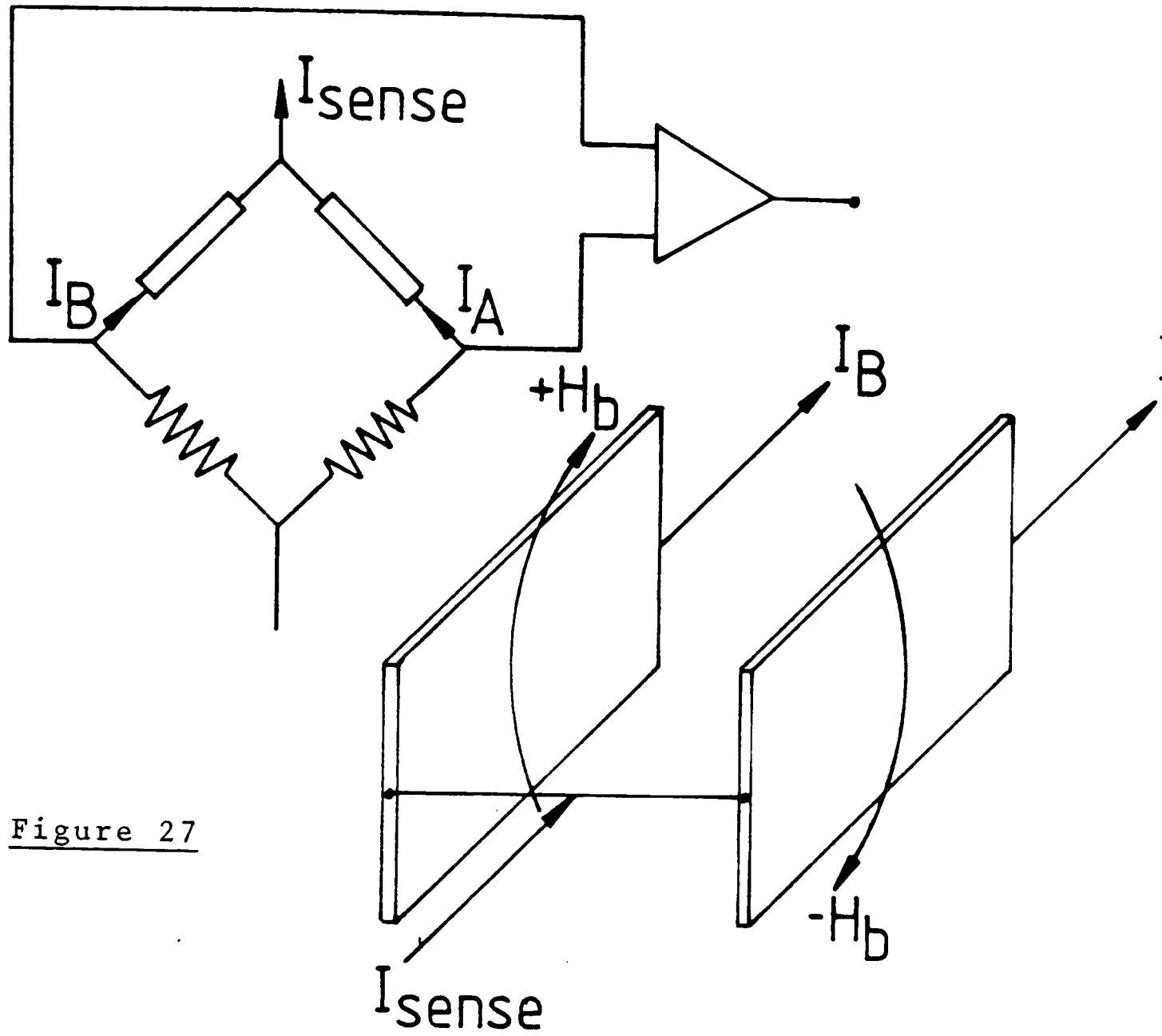
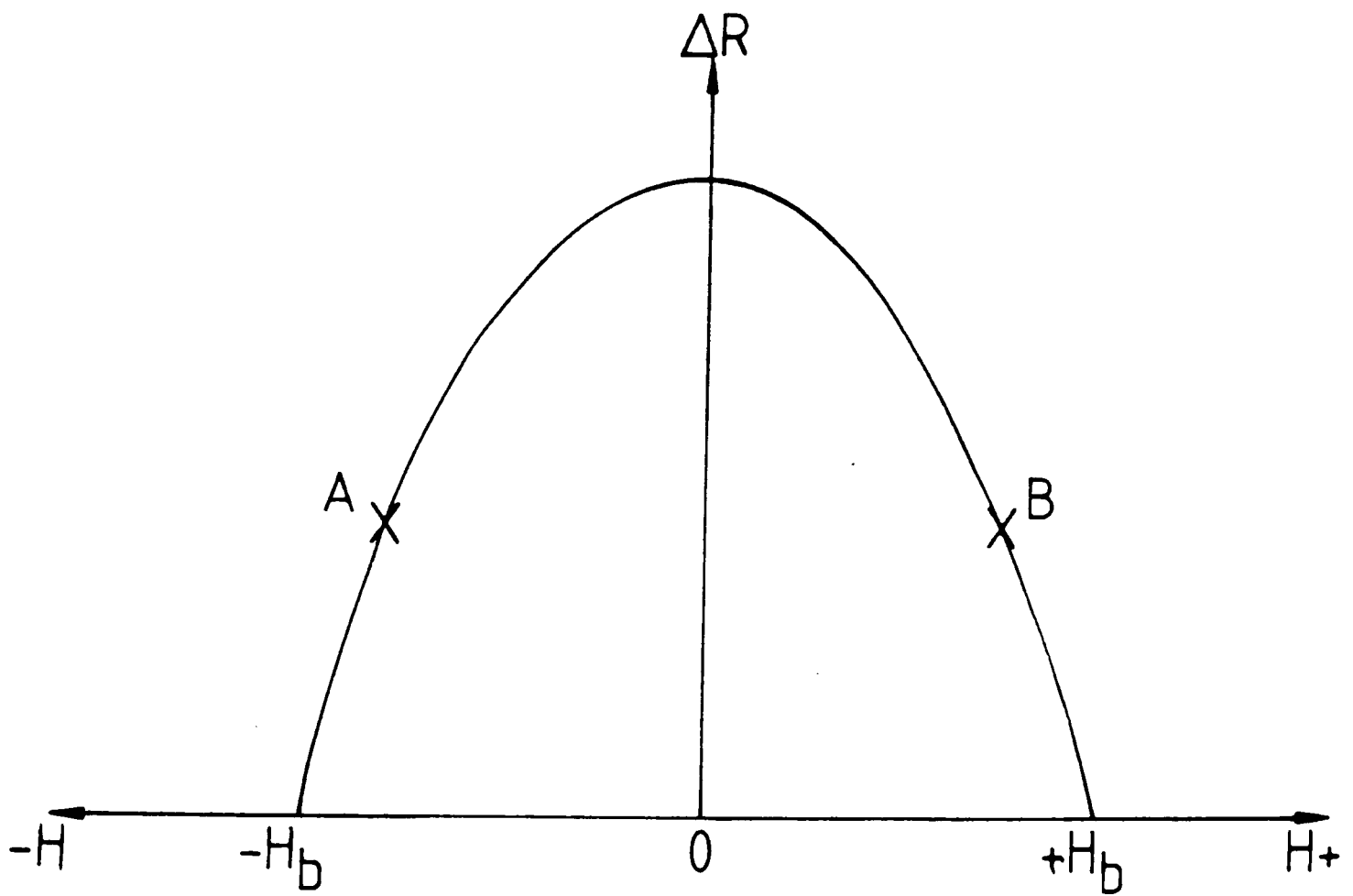


Figure 27



resulting voltage changes in the arms can be differentially sensed using a simple bridge network.

Although this method of obtaining a signal voltage works well for the case in which each of the elements in the array is acted upon by the same external field; a degree of signal cancellation due to the differential sensing mechanism will occur if the elements are sensing magnetic fields of differing magnitudes or directions. For instance, if the elements in one arm of the array sense a magnetic field which is equal in magnitude, but opposite in direction to that sensed by the sensors in the other arm of the array, then no signal voltage will occur. As each of the elements is physically separated from its neighbours by the insulation layer between them, this is exactly the case when the device is being used to read short recorded wavelengths. It is therefore important to establish the extent to which this effect limits the high frequency response of the head, and include the result in the theoretical description of the device.

In the analysis of this part of the problem, no allowance is made for the various frequency dependent losses associated with the magnetoresistive reading of information stored on magnetic tape. This allows a clearer assessment of the losses due solely to the cancellation effect to be made. It is therefore assumed that a single sensor would produce a maximum signal voltage of unity, which is frequency



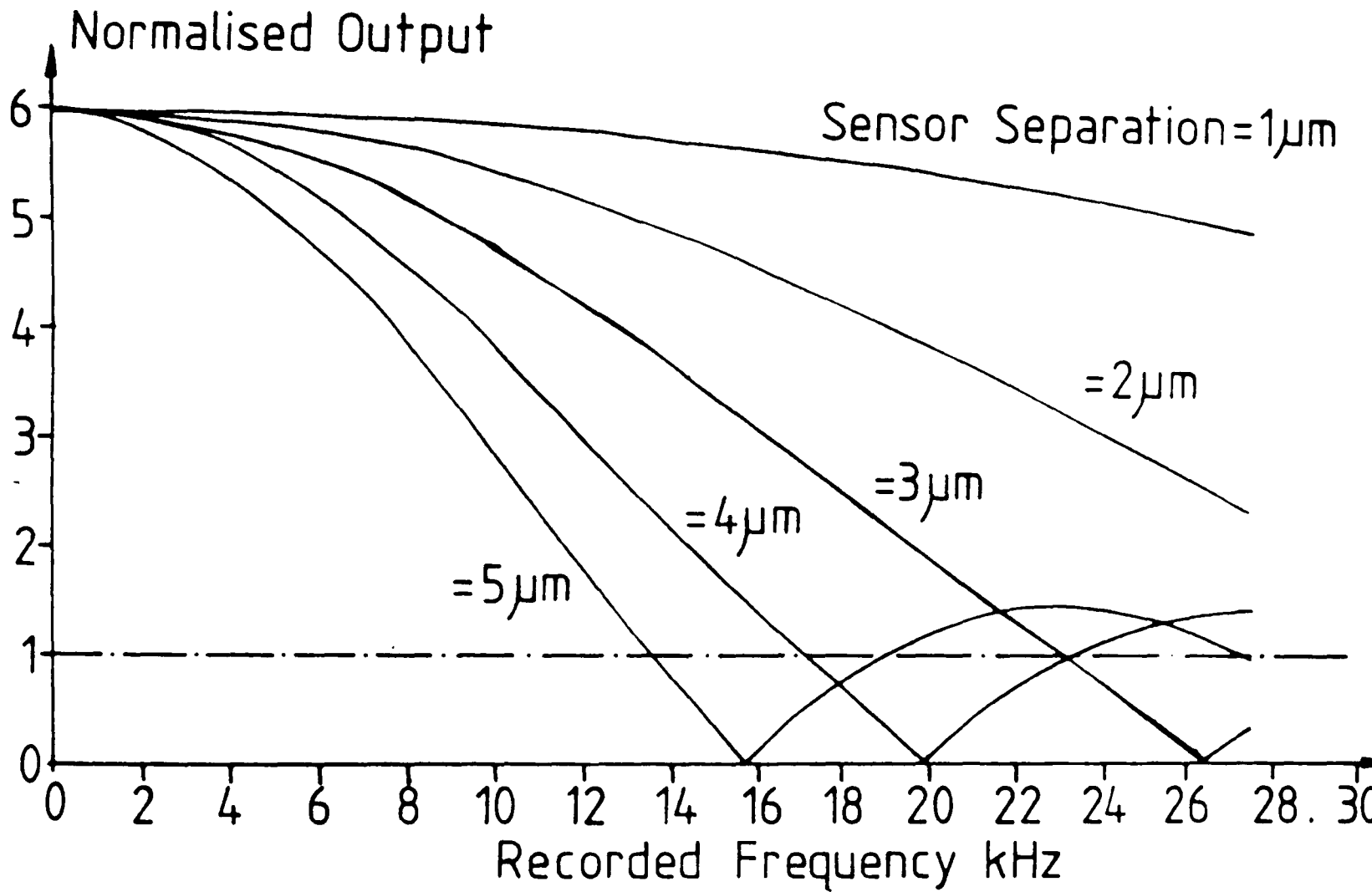
independent. Then, for a particular recorded wavelength (Y), the signal voltage produced by the sensors in the array separated by a fixed distance D is shown to be :-

$$V = \sum_{N=1}^6 \sin \left( \frac{2\pi}{S} \right) N + X \dots\dots\dots(21)$$

Where  $S = (Y/D)$ , and X is the distance between the first element in the array, and the tape field null, and the moment the voltage is measured. To obtain the maximum voltage that can be obtained from the head at a variety of recorded wavelengths and sensor separations, a computer programme was written. This programme calculated the maximum output for each particular frequency, by placing the first element in the array coincident with the field null on the tape, and performing the summation for each of the sensor voltages. X was then incremented in small steps across the full recorded wavelength, with the head signal voltage being recorded for each step. A variety of sensor separations were used to model the head response across a wide range of wavelengths, and the predicted results are shown in figure (28).

As can be seen from this diagram, the head performance at long wavelengths is significantly better than that of a single sensor. However, for realistic separation thicknesses, assuming the Silicon Dioxide layer between the sensors is to provide the necessary electrical insulation; the response to shorter recorded wavelengths is not as great an improvement. Despite these difficulties it is predicted by this model that

Figure 28



Graph of the theoretical, normalised six-element sensor peak outputs at different recorded frequencies for a variety of element separations.

the head will perform better than a single magnetoresistive sensor for recorded wavelengths in the audio range; provided that the insulation layers between the films can be kept to thicknesses of no more than 3-4 microns.

The extent to which the magnetostatic coupling between the sensors in the six-element head will affect its performance is a somewhat more complicated problem. Each of the sensors in one arm of the array are electrically and magnetically connected together. The two arms are then folded together as shown in figure (4), with the sense current flowing through each of the arms providing the bias field required by the opposite arm of the array to linearise its response. It can thus be seen that this structure is magnetically very complicated indeed, and to derive an expression for the tape-field response it is necessary to somewhat simplify the problem.

To do this it has been assumed that the structure can be unfolded, with the three sensors in each of the arms being treated as a single sensor separated by a fixed distance from a second identical sensor. The justification for this is that as all of the elements in one arm are magnetically connected at their ends; the coupling across the separation insulation between two sensors from the same arm, which are adjacent to each other in the sensor array; will have only a very limited affect on the magnetic behaviour of the total arm; and can therefore be ignored. However, the coupling

between the sensors making up opposite arms of the array remains; and must be included in the analysis of the structure. Thus the problem is reduced to one in which two long magnetoresistive elements are separated spatially from each other, but are magnetostatically coupled across this separation distance.

As a result of this assumption it becomes possible to describe the performance of the head using the equation:-

$$P^* = P_o + P_{max} \left[ 1 - \left( \frac{H_b}{H_o} \right)^2 \right] \dots\dots\dots(22)$$

Where  $P^*$  is the sum of the resistivities in each of the arms of the array,  $P_o$  is the isotropic part of the resistivity, and  $P_{max}$  is the magnetoresistive change.  $H_b$  is the bias field and  $H_o$  the field required to saturate the sensor. This equation is derived from Hunts original expression for the response of magnetoresistive elements to applied fields which is given in equation (11). It describes the field dependence of two magnetoresistive sensors which are biased in opposite directions, and are differentially sensed. It now becomes straight-forward to obtain an expression for the signal voltage, providing  $H_o$  and  $H_b$  can be evaluated for the multiple-film head.

A model has recently been derived which allows the angle between the magnetisation and the easy-axis to be

calculated for magnetoresistive elements separated by a non-magnetic, electrically insulating material [24]. This angle is shown to vary across the width of the elements, but can be calculated at a particular displacement (x) from the centre of the sensors using the equation :-

$$\theta(x) = \frac{H_t}{H_k} \left[ 1 - \frac{\cosh(Bx)}{\cosh(Bh)} \right] \dots\dots\dots(23)$$

where

$$B = \left( \frac{M H_k}{2\pi M^2 T S + 2A \left[ 1 - \frac{1}{\cosh(rT/2)} \right] + 2A} \right)^{1/2}$$

and

$$r = \left( \frac{4\pi M^2}{2A} \right)^{1/2}$$

In these equations M is the saturation magnetisation,  $H_k$  the anisotropy field, A the exchange constant, T the sensor thickness, S the separation between the sensors, and h the sensor half-height.  $H_t$  is the drive field and has been obtained in this analysis from the equation for the magnetic field at a point above an infinite current sheet.

Although this equation is specifically intended to provide the sensors magnetisation distribution across its width, it has proved to be very useful in the analysis of the multiple-film head, as it has allowed values for  $H_o$  and  $H_b$

to be obtained. To achieve this the equation has been integrated within the limits of the sensor height, to provide the average angle of the magnetisation across the sensor width :-

$$\theta_{\text{(average)}} = \frac{H_t}{H_k} \left[ 1 - \frac{\tanh(bh)}{Bh} \right] \dots\dots\dots (24)$$

The demagnetising field can then be calculated by assuming that when  $\theta=(\pi/2)$ , the sensor is magnetically saturated. Therefore the demagnetising field will simply be equal to the drive field when  $\theta$  is set to  $(\pi/2)$ . Additionally, the optimum bias field should occur when  $\theta=(\pi/4)$ , and the sensors are operating on the most linear part of the magnetoresistance response curve. The values for the bias field, and demagnetising field can thus be obtained by substituting for these values of  $(\theta)$  in equation (24), and solving for  $H_t$ . The dynamic tape-field response of the multiple-film head can then be calculated.

For two differentially sensed sensors it has been shown that [17]:-

$$e_1 - e_2 = IR \frac{P_{\text{max}}}{P} - 2 \frac{H_b}{H_o * H_o} H_{\text{signal}} \dots\dots\dots(25)$$

where  $e_1$  and  $e_2$  are the sensor voltages.  $I$  is the sense current, and  $R$  is the sum of the sensor resistances. The other terms in the equation are the same as those used in

equation (22). From the values for the bias field and saturation field obtained using (24), it can be shown that :-

$$\frac{H_b}{H_o * H_o} = \frac{(1 - (1/Bh)\tanh(Bh))}{\pi H_o k} = f(h) \dots\dots\dots(26)$$

By now letting equation (25) operate on the equation for the field above a sinusoidally recorded tape given by Wallace [12], in the same fashion as described by Hunt [11], an expression for the head output is obtained.

$$V = IR \frac{P_{max}}{P} 8\pi M_r (f(h)) e^{(-kd)} (1 - e^{(-kt)}) \frac{(1 - e^{-(kh)})}{kh}$$

The terms I, R,  $P_{max}$ , P, and h have been defined earlier in the text.  $4\pi M_r$  is the tape remnant flux density in Gauss, d is the head to tape separation, t the tape coating thickness, k is equal to  $(2\pi/Y)$ , where Y is the recorded wavelength; and  $(f(h))$  is the result derived from equation (26).

This equation, which defines the tape-field response of the multiple-film head has now to be connected to equation (21), which defines the losses associated with the differential sensing mechanism. To do this it is specifically recognised that equation (21) was derived for the case in which the head output was taken to be recorded wavelength independent. Thus, to obtain a complete expression for the head performance the equation for the tape-field performance has to be multiplied by equation (21). To do this the signal

voltage for a particular wavelength is calculated using the tape field equation. The reduction in the maximum signal obtainable is then found for this wavelength using equation (21), and the two are multiplied to produce a value for the theoretical head signal voltage. In this fashion an approximate analysis of the head performance has been completed.



REFERENCES CHAPTER FOUR  
-----

- 1) J. Smit Physica vol.XVI no.6 pp612 (1951)
- 2) H.C. van Elst Physica vol.25 pp708 (1959)
- 3) T.R. McGuire, R.I. Potter IEEE Tans. Mag. vol.MAG-11 no.4 pp1018 (1975)
- 4) P. Drude Annalen der Physik vol.1 pp566. and vol.3 pp369 (1900)
- 5) H.A. Lorentz "Collected papers, vol.8" Martin NijHoff The Hague (1935)
- 6) N.F. Mott Proc. Royal Soc. vol.A156 pp368 (1936)
- 7) R.H. Bube "Electronic Properties of Crystalline Solids" Acedemic Press (1974)
- 8) R.I. Potter Phys. Rev. B vol.1 no.6 pp2391 (1970)
- 9) J. Kondo Prog. Theoret. Physics (Kyoto) vol.27 pp772 (1962)
- 10) R.R. Birss "Symmetry and Magnetism" North-Holland Publishing Co. (1964)
- 11) R.P. Hunt IEEE Trans. Mag. vol.MAG-7 pp150 (1971)
- 12) R.L. Wallace Bell Systems Tech. Jnl. vol.30 pp1146 (1951)
- 13) R.L. Anderson, C.H. Bajorek, D.A. Thompson AIP Conf. Proc. 10 pp1445 (1973)
- 14) T.N. Casselman, S.A. Hanka IEEE Trans. Mag. vol.MAG-16 no.2 pp461 (1980)
- 15) G.W. Brock et. al. U.S. Patent No. 3,814,863
- 16) F. Jeffers IEEE Trans. Mag. vol.MAG-15 pp1628 (1979)
- 17) F.B. Shelledy, G.W. Brock IEEE Trans. Mag. vol.MAG-11 pp1206 (1975)
- 18) A. Paton J. Appl. Phys. vol.42 no.13 pp5868 (1971)
- 19) D.A. Thompson IEEE Trans Mag vol.MAG-11 no.4 (1975)
- 20) R.I. Potter Phys. Rev. B vol.10 pp4626 (1974)
- 21) D.J. O'Conner, F.B. Shelledy, D.E. Heim IEEE Trans. M vol.MAG-21 no.5 pp1560 (1985)

- 22) R.L. O'Day et.al. U.S. Patent No. 3,814,863
- 23) J.A.C. van Ooyen, W.F. Druyvestyn, L. Postma J. Appl. P  
vol.53 no.3 pp2596 (1984)
- 24) A.V. Pohm, C.S. Comstock, L. Peary IEEE Trans. Mag. vol.MAG  
no.5 pp863 (1984)
- 25) T.D. Beaulieu, D.A. Nepla U.S. Patent 3,86,751
- 26) F.Jeffers IEEE Trans. Mag. vol. MAG-21 no.5 pp1563 (1985)

CHAPTER FIVE

-----

" Experimental results "

## 5.0) Experimental results.

### 5.1) Experimental methods used to evaluate the heads performance

To evaluate the performance of the finished heads a variety of tests were performed on devices ranging from a simple two-element configuration, to the most complicated six-element multiple-film heads. In order to test the biasing capability of the structure a simple electro-magnet supplied from a mains transformer was used. This arrangement was capable of providing fields of more than sufficient in magnitude to magnetically saturate the sensors. The use of this system to examine the biasing characteristics of the heads, as opposed to testing them directly using standard cassette tapes, means that distortion of the results due to the the losses associated with the sensing of the tape signal can be discounted. By comparing the amplitude of the magnetoresistive signals waveform at the fundamental (50 Hz) frequency with that of the second harmonic, the extent to which the biasing arrangement is operating correctly can also be determined.

An additional advantage associated with this evaluation method is the fact that the sensors have only to be wire bonded to the flexible lead-out pattern to test them.

This overcomes the need to fully assemble the heads complete with cover slip and ceramic side cheeks, package them, and then lap the front face to provide the required tape to element separation. Thus the maximum percentage magnetoresistive change of the sensors can be quickly and easily evaluated by measuring the sensor resistance and the constant current supplied to it; and then magnetically saturating the device with the electro-magnet and measuring the resulting magnetoresistive signal voltage. This allows defective heads to be rejected without having to needlessly fully assemble them, which is a very laborious process.

To test the response of the finished devices to variations in wavelength recorded on magnetic tape, standard cassette tapes and tape transport mechanisms were used. The tapes used were B.A.S.F. standard Audio cassette tapes type 4.75 (Fe), which are recorded to D.I.N standard 45513/6. They have a reference signal section of wavelength 142.64 microns recorded on them at a standard flux density of 250 nWb/m, after which there are two additional sections which are recorded at the same wavelength and also a wavelength of 4.75 microns, but 20 dB below the reference level. These provide both head alignment and tone reference levels for testing standard inductive heads. Following these sections there are a variety of other wavelengths recorded on the tape ranging from 1,509 microns to 6.75 microns, these are also recorded at the reduced level. Therefore the use of these standard tapes allows the head performance at a variety of

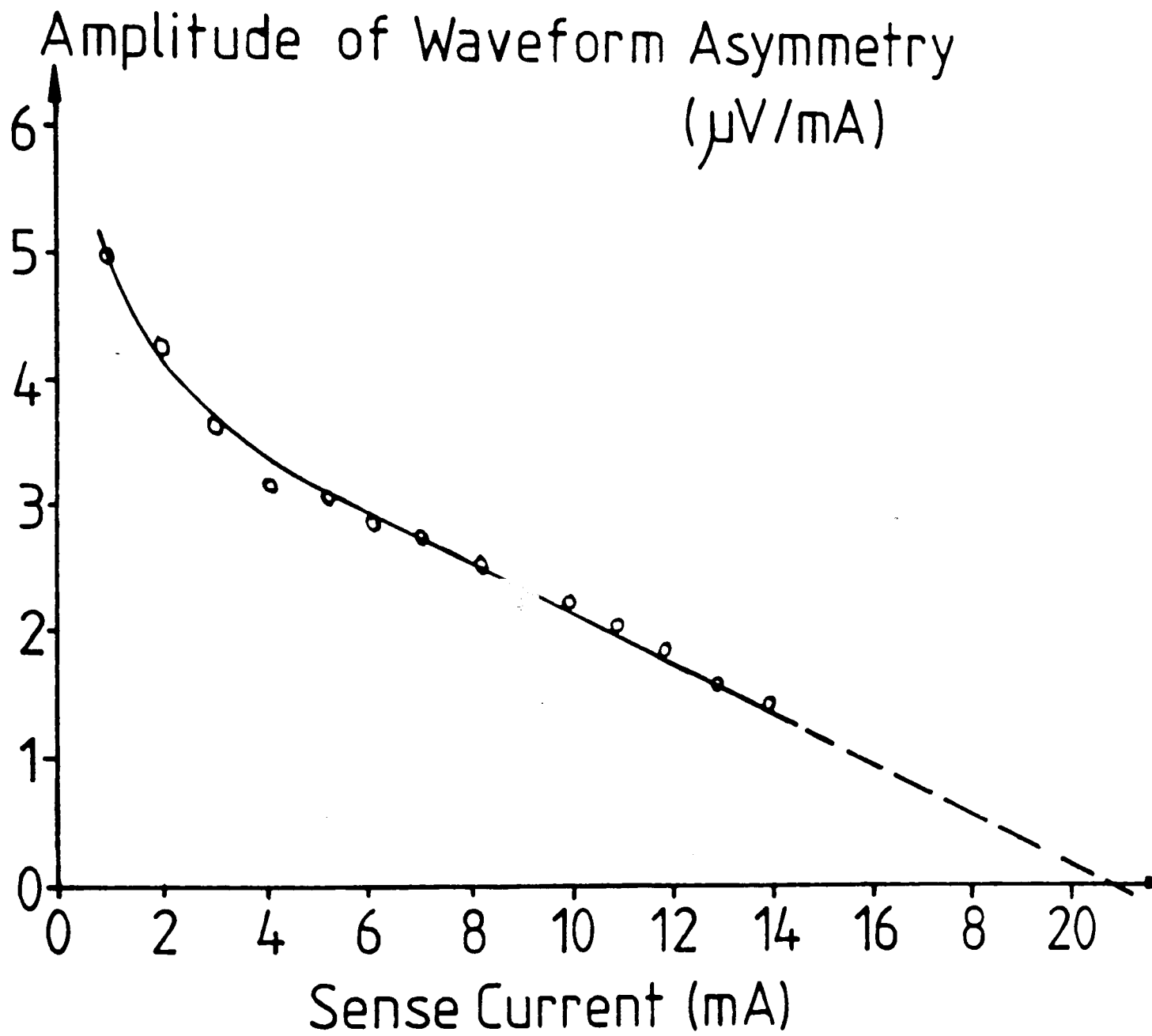
wavelengths to be evaluated accurately using the specification for the tape supplied by the manufacturer.

The tape transport mechanism used to test the heads with the standard tape consisted of a basic chassis containing the drive motor, and its controls, but little else. To enable the heads azimuth to be adjusted they were first mounted onto a positioning plate which had the same dimensions as that which would have held the conventional inductive head in place. This was then attached to the mechanism using the pre-drilled holes in the chassis, with two long screws and return springs. To alter the angle of the sensors relative to the tape, these screws could be tightened, or released as required. As the standard tape is recorded across the full width of the tape, no additional vertical adjustment was included in the head alignment mechanism. However, it was found that by tightening or releasing both of the retaining screws by the same amount, it was possible to align the sensor with one of the tracks recorded on a standard music cassette relatively easily.

#### 5.2) Results from two-element device.

Due to the complicated nature of the multiple-film head, and the difficulties encountered in its fabrication; a substrate containing simple two-element self biased structures was fabricated first to aid the understanding of the fabrication processes. The sensors which are

Figure 29



Graph showing the Amplitude of the second harmonic component produced by the two-element sensor, as the sense current used is increased

manufactured using this reduced scheme are very similar to devices which have been described previously [1], in most respects; but have the same sensor and conductor configurations, as the multiple-film six-element structure. They require the same type of film deposition and photolithographic processing as the more complicated multiple-film device, but fewer steps are needed to complete them. A head was constructed, as described in chapter three, from one of the sets of sensors on this substrate and used to evaluate the success of the fabrication process and biasing scheme.

When tested in the uniform field provided by the electro-magnet it was found that this configuration biased well with very little distortion for a wide range of sense currents and applied fields. To obtain a value for the optimum current required to correctly bias the device, the sense current was increased in steps, and at each point the asymmetry in the waveform measured. A graph of the results is given in figure (29). By extrapolation from the readings taken to the point at which the asymmetry would have zero amplitude, and hence the sensor performance would be at its most linear; the optimum sensor current was found to be 21 (mA). The result could only be obtained by this method, due to the difficulty in measuring the waveform asymmetry as the sense current was increased and the waveform tended towards a pure sine wave.



Using the measured sensor dimensions, the value extrapolated for the optimum sense current, and the measured sensor separation; the optimum bias field provided by the sense current for this device was calculated to be 4.95 Oe, using the theoretical expression derived in section 4.4, and given in equation (20). This value was then compared directly with the value for the optimum bias field obtained using equation (24) which was derived in section 4.5. By substituting the value of  $\theta = (\pi/4)$ , together with the sensors measured dimensions, and separation the bias field obtained using this equation was found to be 5.35 Oe. The correlation between these results implies that the use of equation (26) to obtain the values for the sensors bias and demagnetising fields is justified. Additionally, the ability to linearise the output using the sense current indicated that the biasing scheme worked as intended.

### 5.3) Results taken from the six-element head.

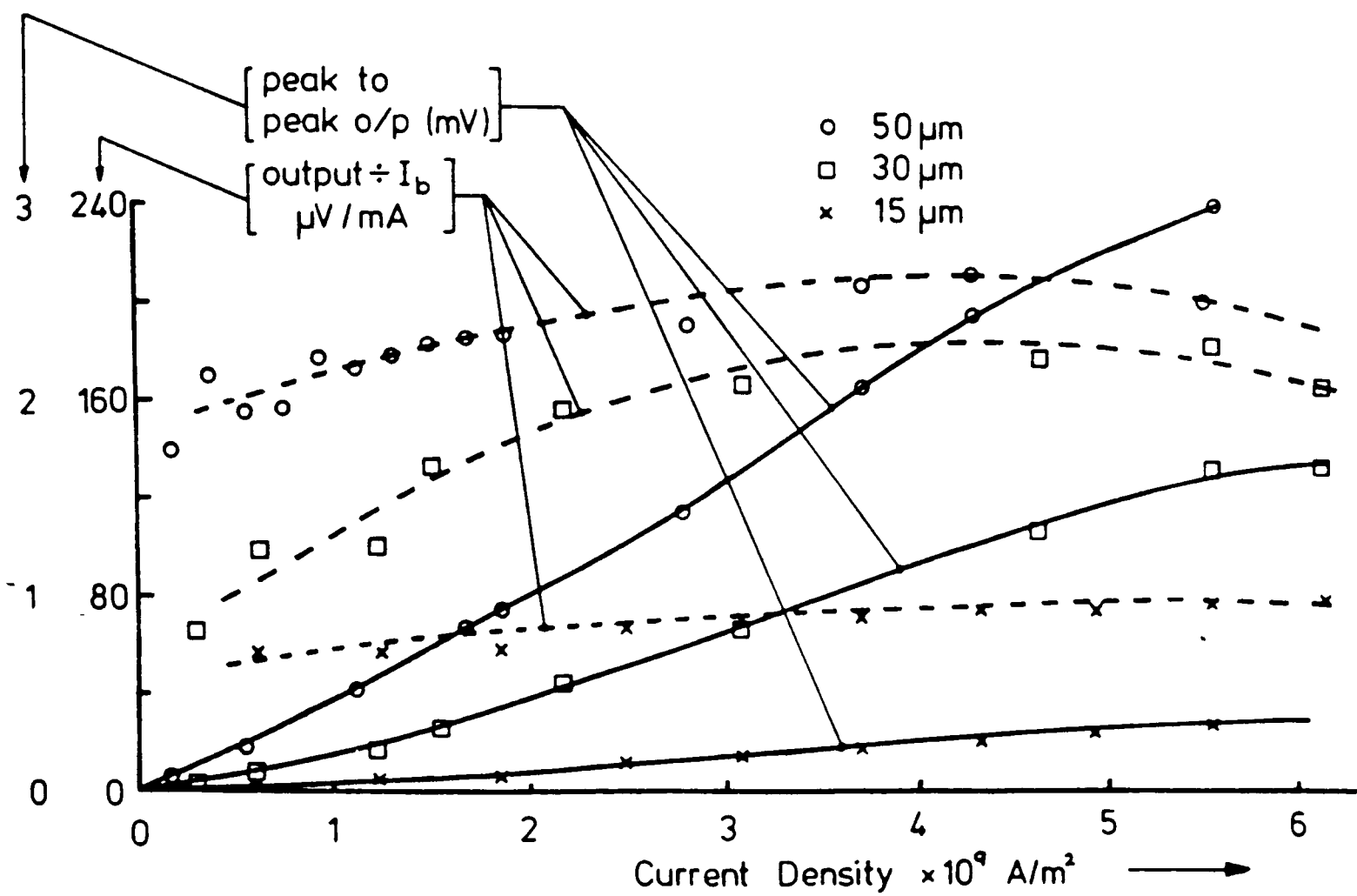
A six-element multiple-film was then fabricated and tested. Due to the increased number of layers used in this sensor compared with the two-element device ( fifteen as opposed to five ), this proved to be a very arduous task indeed. Eventually however, a substrate was successfully completed, from which several sets of sensors were made into full working replay heads. These were tested using both the uniform field supplied by the electro-magnet, and the standard cassette test tapes. As each of the devices

completed was from the same substrate, no variation in the head performance as a function of sensor separation or thickness could be investigated. It was however possible to examine the effect variation of the widths of the elements had on the devices sensitivity to uniform applied fields, and tape signal fields.

Three heads were manufactured, having sensor widths of 15, 30, and 50 microns respectively. The thickness of each of the sensors in the array was measured during the substrate fabrication, and found to be 540 Angstroms; with the separation between them due to the thickness of the insulation layer being measured as 4400 Angstroms. The value for the anisotropy field for this thickness of material was found to be 6 Oe, and the percentage anisotropic magnetoresistive change 2%. Additionally, the measured decrease in the sensor resistances for each of the heads was consistent with the increase in element width for all of the devices completed.

When tested in the uniform field all of these devices showed negligible distortion of the output waveform for a wide range of sensor currents, and applied fields. Indeed no investigation of the type performed using the two-element structure could be carried out, due to the high degree of signal linearity of the heads, even at very small sensor currents. However the linearity of the current scaling factor could be checked using this apparatus; with the assumption

Figure 30

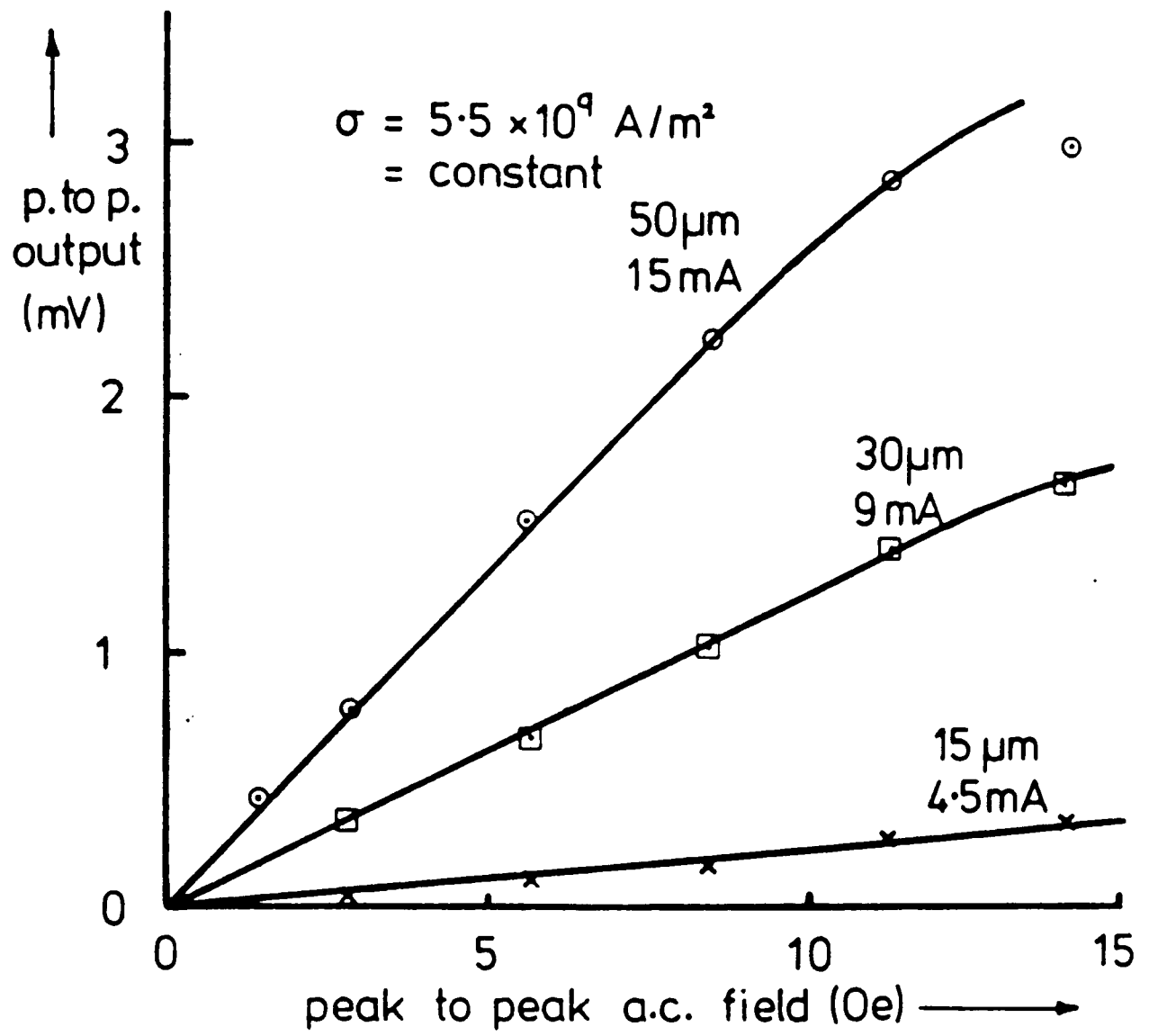


Graph showing the variation in output of the six-element device, as the sense current density is increased

that non-linear bias effects would result in distortions in the response of the sensors for varying current densities. In figure (30) the results of this investigation are plotted graphically, with the current density being used in preference to the sensor current, in order to normalise the signal output voltages for the various widths of sensor. As can be seen from these results the sensor sensitivity appears to be a function of the element width, with increased sensitivity as the width is increased.

To evaluate any distortion due to non-linear biasing not apparent from these results, the peak-to-peak output of the different sensors was divided by the sense current used to take each reading and plotted against the current density. In this fashion it was hoped that a more realistic appraisal of the relative head performances could be obtained. These results are also shown in figure (30), and would appear to demonstrate a non-linearity in the biasing of the wider elements; in addition to their improved sensitivity. This improvement in sensitivity to uniform fields of the wider sensors is consistent with the theoretical analysis given in section 4.5, if the demagnetising field averaged across the sensor width is compared with the demagnetising field calculated at the centre of the sensor. Using equation (24), these values have been calculated for the device widths measured and provided earlier in the text; they are given in Oersteds:-

Figure 31



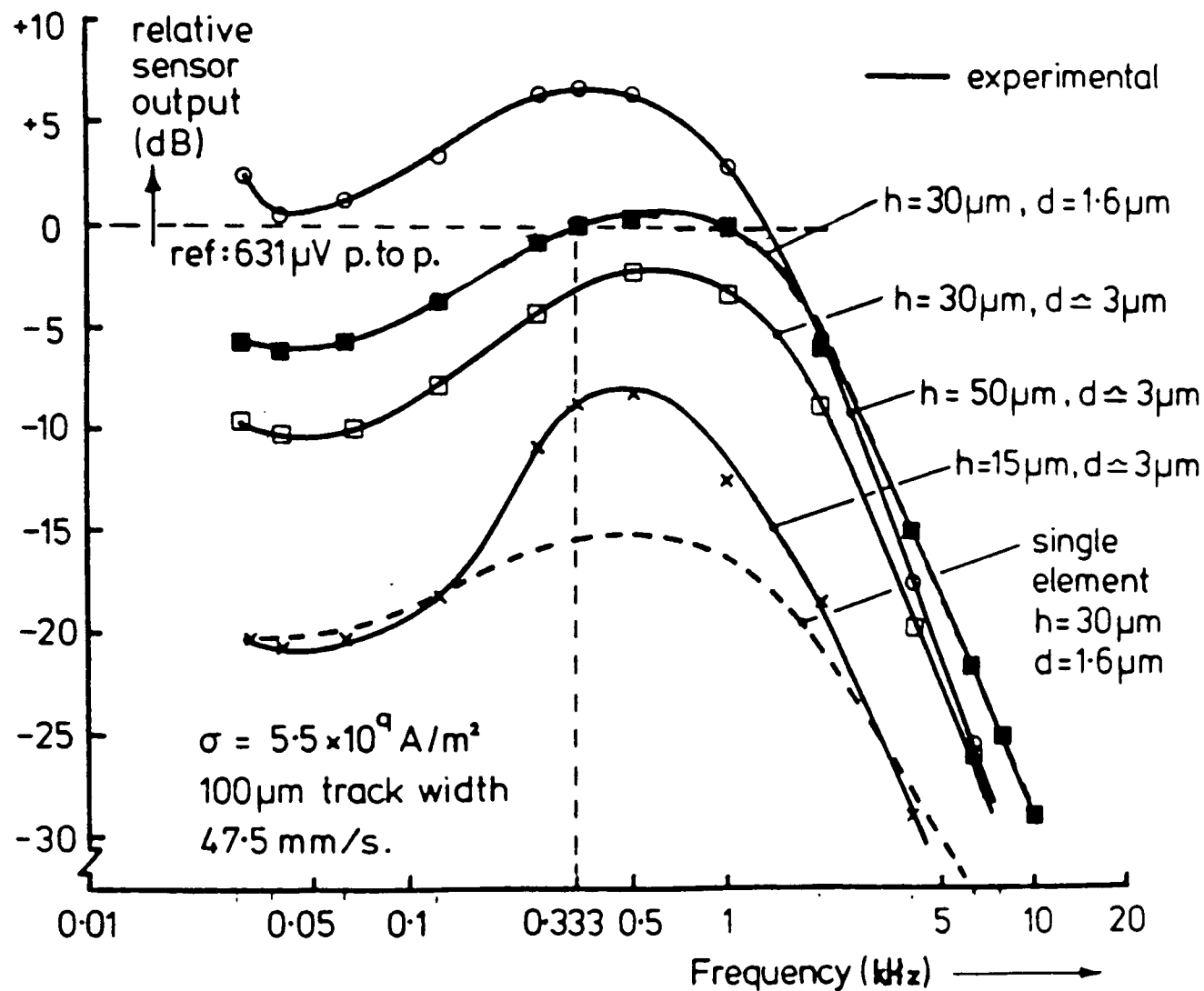
Graph showing the output linearity of the six-element device for a fixed sense current density, as the applied field is varied

Sensor Width (microns)	H (centre) o	H (average) o
15	15.51	22.40
30	10.28	13.75
50	9.52	11.62

The values obtained show that the ratio of the demagnetising field calculated for the centre of the sensor to that averaged over the sensors width, is 0.69 for the 15 micron sensor, 0.75 for the 30 micron sensor; and 0.82 for the 50 micron sensor. This ratio is directly related to a sensors sensitivity to applied fields, in that for an ideal film the magnetisation across the full width of the sensor would rotate coherently. In a real magnetoresistive element however, the large demagnetising fields found at the elements edges, reduce its sensitivity to applied fields. Thus the smaller this ratio becomes, due to the increasing effect of the demagnetising fields at the sensors edges, the less sensitive the element. Hence this theoretical result would appear to explain the reduction in sensitivity as the sensor width is decreased.

Figure (31) shows graphically the results taken when the field was varied from 0 to 15 Oe. The current density was kept constant for all readings, and the field values were obtained using a calibrated Hall probe. As can be seen from this graph the predicted increase in drive field required to saturate the sensors, as their widths are decreased is observed. However readings were not taken up to the field

Figure 32



Dynamic results taken from the six-element sensor, using a standard cassette tape

values required to fully saturate the heads, and hence an exact correlation with the theory is not possible.

The dynamic performance of the heads was then tested using the standard cassette mechanism. For all tests the current density was held constant at  $5.5 \text{ A/m}^2$ , in order to produce a realistic comparison between the output signals produced by sensors of different widths. A complete set of results was produced for an estimated sensor to tape spacing (D) of 3 microns for all three heads. This distance was evaluated by examining the front edge of the finished head using an optical microscope. By tilting the head towards the objective lense of the microscope, the sensors could be easily seen through the substrate and cover-slip sandwich. As the element width is known from the photolithographic measurements, the distance of the un-lapped substrate remaining could be estimated, thus providing the tape-to-sensor separation.

From the results taken at this separation distance it was found that the 50 micron wide sensor performed better than either the 30 or 15 micron wide sensors, producing a larger output across the full range of recorded wavelengths available. Due to the theoretically predicted loss of short wavelength reponse, with increased separation distance, it was decided to continue the lapping process for one of the heads in an attempt to improve its performance. The limiting factor in this procedure had been found from previous



experiments to be the thin layer of glue between the substrate and chip. Even using the smallest glue-layer possible to hold the glass pieces together; particles from the lapping compound could still become embedded in the glue, fatally damaging the sensor array. Thus the lapping process continued in small stages, with the head having its dynamic performance and tape-to-sensor distance remeasured at every stage. Eventually the head failed, with the last complete set of results being obtained at an estimated separation of 1.6 microns.

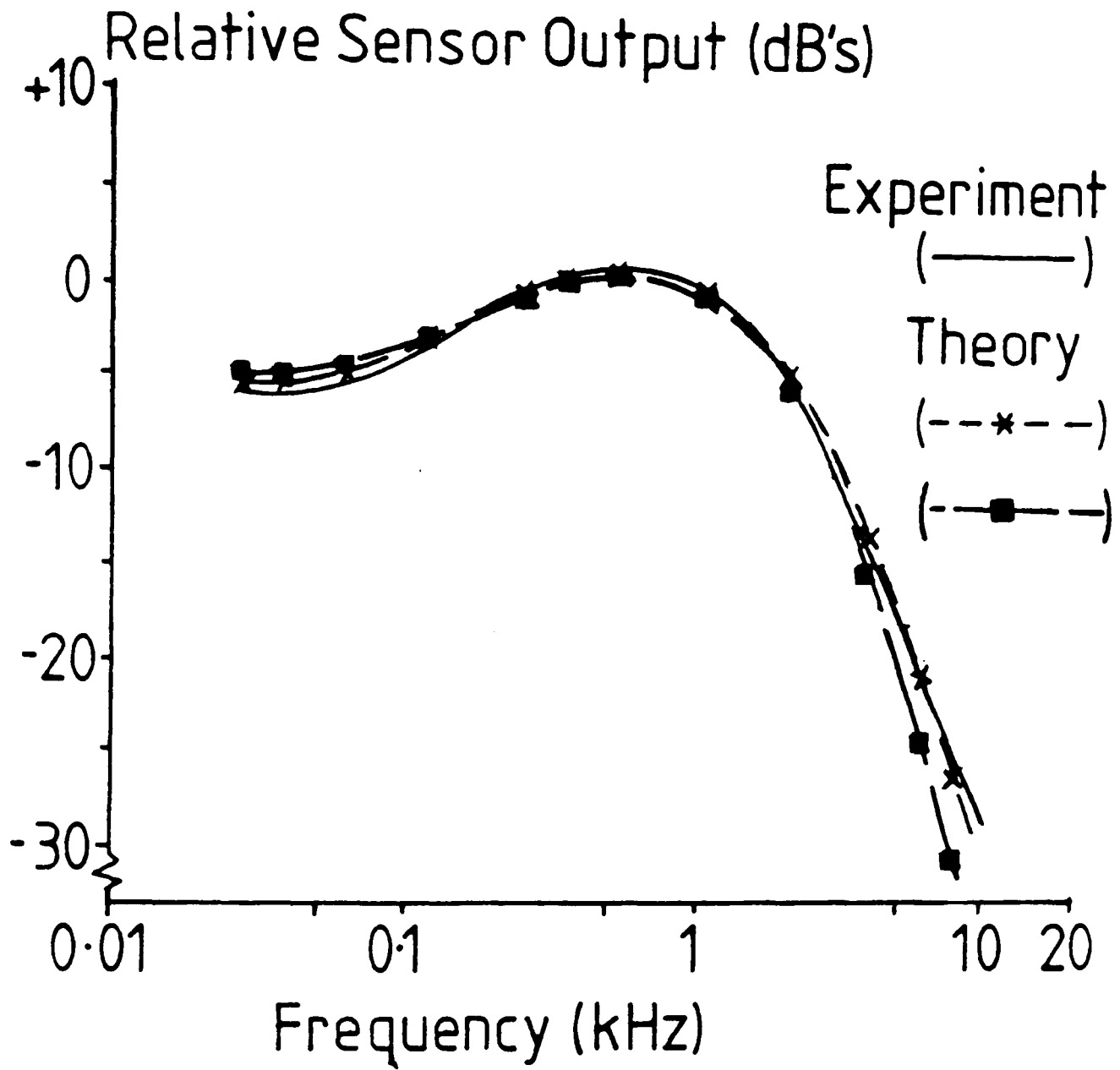
The complete set of results, for each of the heads at the initial separation distance; in addition to those obtained from the head lapped to provide the reduced sensor-to-tape spacing are shown graphically in figure (32). The sensor outputs are plotted using the output of the 30 micron wide sensor lapped to the reduced separation distance and reading a wavelength of 142.64 microns as reference. This figure clearly demonstrates the improvement in the head performance possible by reducing the separation between the sensors and the tape. Also shown in the figure are results produced using the previously described theoretical output from a single element due to Hunt [2]. The dimensions used in the calculations are the same as the reference elements, and an output is predicted which is typically some 15 dB's below that produced by the experimental head. This indicates that the increased signal voltages available from the multiple-film configuration, for which these heads were

designed and fabricated; can be realised in practice.

An attempt was then made to fit the head output predicted using the expression derived in section 4.5 to the results measured using the experimental head with the reduced tape-to-sensor separation. The result of this exercise is shown graphically in figure (33), with the relative sensor outputs plotted, using the same reference level as used in figure (32). The data on the tape field is taken from the information provided by the manufacturer, and for the magnetic properties of the sensors the values are taken to be an anisotropy constant of 6 Oe, a saturation magnetisation of  $10^4$  Gauss and an exchange constant of  $10^{-6}$  erg/cm. The dimensions for the insulation thickness, sensor height, and tape to sensor separation, are 4400 Angstroms, 30 microns, and 1.6 microns respectively. These results are plotted on the graph using the squares, and as can be seen from the figure the fit to the experimental results is not good.

It was therefore postulated that as even small variations in any of the distances used can have a marked effect on the relative performance of the head, particularly at short recorded wavelengths; a better fit to the experimental data might be possible using slightly different values. Additionally, if an improved fit were possible using lengths that were not too dissimilar to those measured, an insight into the relative importance of each length and its measurement accuracy might be also obtained. Such a fit was

Figure 33



Experimental results fitted to the theoretical model for the multiple film head

indeed possible for an insulation thickness of 3000 Angstroms, a tape to sensor distance of 1.4 microns, and a sensor height of 28 microns. These results are plotted as the crosses in figure (33).

The use of these values may be justified for the sensor to tape spacing; as this is only estimated as described previously, and the sensor width; due to a combination of reduced sensitivity at the sensor edges resulting from demagnetising effects, and over-etching during the device fabrication. However, the value for the separation between the sensors is measured using a stylus instrument during the fabrication of the device. The improvement in the fit of the theoretical results to the experimental data obtained using the reduced insulation thickness would thus appear to imply that the decrease in the head output at short wavelengths due to the cancellation effect described in section 4.5, plays a lesser part in the performance of the device than accounted for in the theoretical description.

#### REFERENCES CHAPTER FIVE

- 
- 1) G.W. Brock et. al. U.S. Patent No. 3,814,863
  - 2) R.P. Hunt IEEE Trans. Mag. vol.MAG-7 pp150 (1971)

CHAPTER SIX

-----

" Discussion "

## 6.0) Discussion.

In the introduction to this thesis the benefits of using the anisotropic magnetoresistance effect observed in thin ferromagnetic films to read information stored on magnetic tapes was discussed. It was pointed out that sensors utilising the effect have certain advantages over conventional inductive replay heads, not the least of these being the ability to fabricate, using standard photolithographic processes, extremely small sensing elements. As these elements are capable of producing comparatively good signal to noise ratios, due to their outputs being scaled by the sense current; the trackwidth recorded on the tape can be decreased. Thus it becomes possible to improve significantly the storage capacity of existing tape formats without altering the width of the tape or its transport mechanism in any way.

Although the access time of compact cassettes is prohibitively long for them to be used competitively in either personal or business computers; for the storage of speech or music they remain ideal. Thus the ability to increase the number of tracks available on a particular width of tape, whilst maintaining the quality of the signal on playback make this method of information retrieval very attractive. To this end the aim of the research presented in this thesis was to design, optimise, fabricate and evaluate

the performance of a magnetoresistive replay head having a novel sensor configuration. The design of the head was such that it would offer an increase in output over existing magnetoresistive heads, particularly when reading recorded wavelengths in the audio range.

To achieve this goal, experiments have been performed to determine the preparation conditions required to provide thin films of NiFe in which the percentage magnetoresistive change is maximised. These experiments have involved the design and construction of two pieces of apparatus, which enable various galvano-magnetic properties of the films deposited to be measured. As a result of the data produced, a method of film production has been derived which allows the routine deposition of films having large anisotropic magnetoresistances. Such films can then be patterned into sensors using similar photolithographic techniques to those commonly used in the manufacture of micro-chips. By optimising the mask design necessary to produce the sensor configuration required, it has been possible to provide a range of heads on a single substrate, each consisting of an array of sixteen sensors.

Several heads having a variety of sensor widths have been fabricated and tested. From the results of tests performed using these heads it was concluded that the configuration chosen does indeed offer an improvement in output over previously described magnetoresistive heads.

However, when the experimental results are compared with the theoretical description of the head which has been derived, several points emerge. The first of these is that the anticipated losses due to signal cancellation within the head do not appear to have as great an effect as postulated. To overcome this problem it would be necessary to extend the theory describing the cancellation effect to incorporate the thicknesses of the elements making up the sensor array. In addition to this, the output of these novel heads appears to be extremely linear even for very small sense currents. Although the theoretical expression for the head performance specifically includes the magnetostatic coupling between the elements in the calculation of the sensors demagnetising field, some simplifying assumptions have been made in its derivation. Thus it is anticipated that more research would also be necessary to completely describe the interaction in order to explain the heads linearity.



APPENDIX I

```

10 PRINT "PLEASE TYPE IN THE FOLLOWING INFORMATION ....."
20 PRINT
30 PRINT
40 P=4*(ATN(1))
50 PRINT "LENGTH OF FIRST Y-DIMENSION"
60 INPUT YA
70 PRINT "LENGTH OF FIRST X-DIMENSION"
80 INPUT XA
90 PRINT "OVERALL LENGTH OF PATTERN"
100 INPUT Y
110 PRINT "FIRST CONDUCTOR WIDTH"
120 INPUT C
130 PRINT "FIRST GAP WIDTH"
140 INPUT G
150 X=(20*C)+(19*G)+(G/2)
160 Y1=SQR(X)*SQR(X+IA)
170 S=Y1/X
180 A1=ATN(S)
190 A1=A1*(180/P)
200 T=Y1/(X+XA)
210 A2=ATN(T)
220 A2=A2*(180/P)
230 PRINT
240 PRINT
250 PRINT
260 R0=14E-8
270 T1=2.0E-7
280 G1=C*S
290 G2=G*S
300 G3=(X+XA)*C/X
310 G4=(X+XA)*G/X
320 PRINT "VALUE OF Y1 =";TAB(13);Y1
330 PRINT
340 PRINT "ANGLE ALPHA =";TAB(13);A1
350 PRINT
360 PRINT "ANGLE BETA =";TAB(12);A2
370 PRINT
380 PRINT "TOTAL TRACK WIDTH =";TAB(19);(X*2)
390 PRINT
400 PRINT "HALF TRACK WIDTH (X) =";TAB(22);X
410 PRINT
420 PRINT " CNDR(1)          GAP(1)"
430 PRINT C,G
440 PRINT " CNDR(2)          GAP(2)          CNDR(3)          GAP(3)"
450 PRINT G1,G2,G3,G4
460 PRINT
470 PRINT " RESTNCE";TAB(11);"Y1";TAB(21);"X1";TAB(31);"Y2";TAB(41);
;TAB(51);"X2";TAB(61);"Y4"
480 FOR J=1 TO 20 STEP 1
490 YB=(Y-YA-(C*S))
500 XB=(XA+C-G3)
510 C3=(YA+(C*S))
520 C2=(Y-YA)
530 B=YA
540 B1=XA
550 B2=C2
560 B3=YB
570 B4=XB
580 B5=C3

```

```

610 N2=INT(C2)
620 N3=INT(YB)
630 N4=INT(XB)
640 N5=INT(C3)
650 F=YA-N
660 F1=XA-N1
670 F2=C2-N2
680 F3=YB-N3
690 F4=XB-N4
700 F5=C3-N5
710 IF F>0.5 GOTO 890 ELSE 770
720 IF F1>0.5 GOTO 910 ELSE 790
730 IF F2>0.5 GOTO 930 ELSE 810
740 IF F3>0.5 GOTO 950 ELSE 830
750 IF F4>0.5 GOTO 970 ELSE 850
760 IF F5>0.5 GOTO 990 ELSE 870
770 YA=INT(YA)
780 GOTO 720
790 XA=INT(XA)
800 GOTO 730
810 C2=INT(C2)
820 GOTO 740
830 YB=INT(YB)
840 GOTO 750
850 XB=INT(XB)
860 GOTO 760
870 C3=INT(C3)
880 GOTO 1010
890 YA=1+N
900 GOTO 720
910 XA=1+N1
920 GOTO 730
930 C2=1+N2
940 GOTO 740
950 YB=1+N3
960 GOTO 750
970 XB=1+N4
980 GOTO 760
990 C3=1+N5
1000 GOTO 1010
1010 R1=(R0/T1)*((YA*1.0E-6)/(C*1.0E-6))
1020 R2=(R0/T1)*(((XA+C)*1.0E-6)/((C*S)*1.0E-6))
1030 R3=(R0/T1)*(((Y-YA-(C*S))*1.0E-6)/(G3*1.0E-6))
1040 R=R1+R2+R3
1050 PRINT R;TAB(10);YA;TAB(20);XA;TAB(30);C2;TAB(40);YB;TAB(50);X1
60);C3
1060 YA=B
1070 XA=B1
1080 C2=B2
1090 YB=B3
1100 XB=B4
1110 C3=B5
1120 YA=(YA+(C*S)+(G*S))
1130 XA=(XA+(C+G)-(G3+G4))
1140 NEXT J
1150 END

```

>READY

APPENDIX II

## CONDUCTOR PATTERN OPTIMISATION IN THIN-FILM HEADS

D.J. Mapps and M.L. Watson

Plymouth Polytechnic England

As areal packing densities rise (1) there is a tendency for decreasing track-width, especially for high-capacity digital storage. This can easily be achieved by thin-film heads but when track width falls, problems can arise if the impedance contribution of the lead-out conductor pattern is significant when compared with the impedance of the sensor element (2).

### Resistance Equalisation

Figure 1 shows part-diagrams of a lead-out pattern for a 16-track M-R sensed digital audio cassette head. The M-R sensors have a resistance of about  $20\Omega$  and lead-out resistances of about  $15\Omega$ . Lead out resistances must be equalised so that all tracks produce equal outputs. Figure 1(b) shows part of a single lead-out conductor in the array of figure 1(a). The total resistance of any conductor in the array ABCD is

$$R = \frac{\rho}{t} \left[ \frac{y_1 - x \frac{\tan \beta}{\tan \alpha}}{w} + \frac{x \left( \frac{\tan \beta}{\tan \alpha} \right) - x}{w \tan \alpha} + \frac{x \tan \beta}{w} \right] \quad (1)$$

$x_1$  and  $x_2$  are fixed by the cassette tape width and the standard compact cassette head package dimensions but  $y_1$  is variable.

Substituting values for  $\tan \alpha$  and  $\tan \beta$  in equation (1) and differentiating for a minimum with respect to  $x$  gives

$$y_1^2 = x_1 x_2 \quad (2)$$

as the critical condition for equal resistances in all conductors. Also, since  $\tan \alpha \tan \beta = 1$  for this condition,  $\beta$  and  $\alpha$  must be  $>$  and  $<$   $45^\circ$  respectively.

## Capacitance and Inductance

Lead-out capacitance and inductance are important at high repetition frequencies. The implications of equalising resistances as defined by equation (2) means that capacitances and inductances will vary. For fields obeying Laplace's equation, capacitances and inductances are unaltered if dimensional proportionality is maintained as implied in figure 1(a). The maximum per-unit error in these quantities in the region ABCD is therefore easily evaluated as  $= \tan \beta - \tan \alpha$ . The magnitudes of capacitance and inductance per unit conductor length are calculated by an iteration method and shown in figure 2.

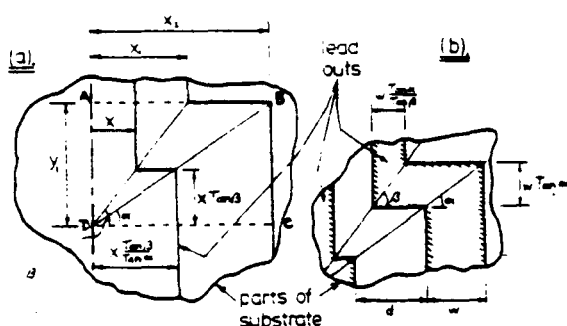


Fig.1. Conductor pattern design for a 16-track compact cassette thin-film head.

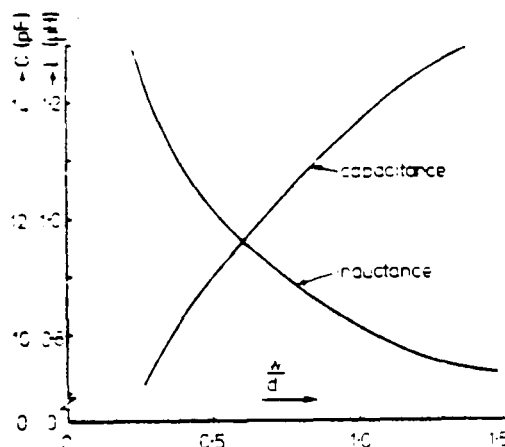


Fig.2. Conductor capacitance and inductance as a function of mark/space ratio  $\frac{w}{d}$ .

### References

1. G.V.Kelly et.al. I.E.E.E.Trans.Mag.17, No.6, November 1981
2. W.Metzdorf et.al. Paper17.2. 1981 Intermag Conf.Grenoble.

Category 11

Dr. D.J. Mapps  
 Dept. Electrical & Electronic  
 Engineering,  
 Plymouth Polytechnic  
 Plymouth, England.  
 (0752) 21312.

APPENDIX III





```

0120
00109:NEUG ST1;
00110:POLY(5)S,0,0:130,90,-10,-2,-110,2,-10,-90;
00111:ENDG;
00112:NEUG ST2;
00113:POLY(5)S,0,0:130,90,-10,-62,-110,10,110,20,-110;
00114:      10,110,20,-110,2,-10,-90;
00115:ENDG;
00116:NEUG ST3;
00117:POLY(5)S,0,0:130,90,-10,-52,-110,10,110,20,-110;
00118:      10,110,10,-110,2,-10,-90;
00119:ENDG;
00120:NEUG SACT;
00121:DITTO GROUP ST1,90,-90;
00122:      720,-90;
00123:      1350,-90;
00124:      2400,-90;
00125:      3030,-90;
00126:DITTO GROUP ST2,300,-90;
00127:      930,-90;
00128:      1770,-90;
00129:      2190,-90;
00130:      2820,-90;
00131:DITTO GROUP ST3,510,-90;
00132:      1140,-90;
00133:      1560,-90;
00134:      1980,-90;
00135:      2610,-90;
00136:ENDG;
00137:NEUG K3A;
00138:POLY(3)S,0,0:310,180,-50,-40,40,-90,125,40;
00139:      -40,-40,-125,90,40,40,-50,-180;
00140:ENDG;
00141:NEUG K3B;
00142:POLY(3)S,0,0:310,180,-50,-40,40,-100,-125,40;
00143:      -40,-40,-125,100,40,40,-50,-180;
00144:ENDG;
00145:NEUG K3C;
00146:POLY(3)S,0,0:310,180,-50,-40,40,-110,-125,40;
00147:      40,-40,-125,110,40,40,50,-180;
00148:ENDG;
00149:NEUG K3D;
00150:POLY(3)S,0,0:310,180,-50,-40,40,115,-125;
00151:      40,40,-40,-125,115,40,40,50,-180;
00152:ENDG;
00153:NEUG K3E;
00154:POLY(3)S,0,0:310,180,50,40,40,-120,125,40;
00155:      40,-40,-125,120,40,40,-50,180;
00156:ENDG;
00157:NEUG K3F;
00158:POLY(3)S,0,0:310,180,-50,40,40,-125,125,40,-40;
00159:      -40,-125,125,40,40,-50,-180;
00160:ENDG;
00161:NEUG T1A;
00162:GROUP K3A,0,0,XX,X,8,420;
00163:ENDG;
00164:NEUG T1B;
00165:GROUP K3B,0,0,XX,X,8,420;
00166:ENDG;
00167:NEUG T1C;
00168:GROUP K3C,0,0,XX,X,8,420;
00169:ENDG;
00170:NEUG T1D;
00171:GROUP K3D,0,0,XX,X,8,420;

```

```

00172:ENDG;
00173:NEUG T1E;
00174:GROUP K3E,0,0,XX,X,8,420;
00175:ENDG;
00176:NEUG T1F;
00177:GROUP K3F,0,0,XX,X,8,420;
00178:ENDG;
00179:
00180:NEUG M1;
00181:POLY(5)S,0,0:100,25,-10,-10,80,10,-10,-25;
00182:ENDG;
00183:NEUG M2;
00184:POLY(5)S,0,0:100,30,10,-10,-80,10,-10,30;
00185:ENDG;
00186:NEUG M3;
00187:POLY(5)S,0,0:100,35,10,-10,-80,10,-10,-35;
00188:ENDG;
00189:NEUG M4;
00190:POLY(5)S,0,0:100,40,10,-10,-80,10,10,-40;
00191:ENDG;
00192:NEUG M5;
00193:POLY(5)S,0,0:100,50,-10,-10,-80,10,10,-50;
00194:ENDG;
00195:NEUG M6;
00196:POLY(5)S,0,0:100,60,-10,-10,-80,10,-10,-60;
00197:ENDG;
00198:NEUG SM1;
00199:GROUP M1,0,0,XX,X,16,210;
00200:ENDG;
00201:NEUG SM2;
00202:
00203:GROUP M2,0,0,XX,X,16,210;
00204:ENDG;
00205:NEUG SM3;
00206:GROUP M3,0,0,XX,X,16,210;
00207:ENDG;
00208:NEUG SM4;
00209:GROUP M4,0,0,XX,X,16,210;
00210:ENDG;
00211:NEUG SM5;
00212:GROUP M5,0,0,XX,X,16,210;
00213:ENDG;
00214:NEUG SM6;
00215:GROUP M6,0,0,XX,X,16,210;
00216:ENDG;
00217:NEUG S1;
00218:RECT(1)-2,-2:104,132;
00219:ENDG;
00220:NEUG BS1;
00221:GROUP S1,0,0,XX,X,16,210;
00222:ENDG;
00223:NEUG S2;
00224:POLY(2)S,-4,-4:108,136,-30,-60,-48,50,48,10;
00225:      -78,-136;
00226:ENDG;
00227:NEUG BS2;
00228:GROUP S2,0,0,XX,X,16,210;

```

00228:GROUP S2,0,0,XX,X,16,210;  
 00229:ENDG;  
 00230:NEUG S3;  
 00231:POLY(4)S,-2,-2:104,62,80,140,-24,-202;  
 00232:POLY(4)S,208,-2:104,202,-24,-140,-80,-62;  
 00233:ENDG;  
 00234:NEUG BS3;  
 00235:GROUP S3,0,0,XX,X,8,420;  
 00236:ENDG;  
 00237:NEUG T1;  
 00238:POLY(6)S,0,15:10,165,-9,170,-28,-198,27,-137;  
 00239:POLY(6)S,20,145:65,205,-28,-175,-37,-30;  
 00240:POLY(6)S,90,15:10,35,40,-30,30,30,40,-35,10,65,  
 00241:51,270,-28,-270,-51,-65;  
 00242:POLY(6)S,225,145:65,30,-37,175,-28,-205;  
 00243:POLY(6)S,300,15:10,137,27,198,-28,-170,-9,-165;  
 00244:ENDG;  
 00245:NEUG TS1;  
 00246:GROUP T1,0,0,XX,X,8,420;  
 00247:ENDG;  
 00248:NEUG T2;  
 00249:POLY(6)S,0,20:10,160,-9,170,-28,-198,27,-132;  
 00250:POLY(6)S,20,145:65,205,-28,-175,-37,-30;  
 00251:POLY(6)S,90,20:10,35,40,-30,30,30,40,-35,10,  
 00252:65,-51,265,-28,-265,-51,-65;  
 00253:POLY(6)S,225,145:65,30,-37,175,-28,-205;  
 00254:POLY(6)S,300,20:10,132,27,198,-28,-170,-9,-160;  
 00255:ENDG;  
 00256:NEUG TS2;  
 00257:GROUP T2,0,0,XX,X,8,420;  
 00258:ENDG;  
 00259:NEUG T3;  
 00260:POLY(6)S,0,25:10,155,-9,170,-28,-198,27,-127;  
 00261:POLY(6)S,20,145:65,205,-28,-175,-37,-30;  
 00262:POLY(6)S,90,25:10,35,40,-30,30,30,40,-35,10,65,  
 00263:51,260,-28,-260,-51,-65;  
 00264:POLY(6)S,225,145:65,30,-37,175,-28,-205;  
 00265:POLY(6)S,300,25:10,127,27,198,-28,-170,-9,-155;  
 00266:ENDG;  
 00267:NEUG TS3;  
 00268:GROUP T3,0,0,XX,X,8,420;  
 00269:ENDG;  
 00270:NEUG T4;  
 00271:POLY(6)S,0,30:10,150,-9,170,-28,-198,27,-122;  
 00272:POLY(6)S,20,145:65,205,-28,-175,-37,-30;  
 00273:POLY(6)S,90,30:10,35,40,-30,30,30,40,-35,10,65,  
 00274:51,255,-28,-255,-51,-65;  
 00275:POLY(6)S,225,145:65,30,-37,175,-28,-205;  
 00276:POLY(6)S,300,30:10,122,27,198,-28,-170,-9,-150;  
 00277:ENDG;  
 00278:NEUG TS4;  
 00279:GROUP T4,0,0,XX,X,8,420;  
 00280:ENDG;  
 00281:NEUG T5;  
 00282:POLY(6)S,0,40:10,140,-9,170,-28,-198,27,-112;  
 00283:POLY(6)S,20,145:65,205,-28,-175,-37,-30;  
 00284:POLY(6)S,90,40:10,35,40,-30,30,30,40,-35,10,65,  
 00285:51,245,-28,-245,-51,-65;  
 00286:POLY(6)S,225,145:65,30,-37,175,-28,-205;  
 00287:POLY(6)S,300,40:10,112,27,198,-28,-170,-9,-140;  
 00288:ENDG;  
 00289:NEUG TS5;  
 00290:GROUP T5,0,0,XX,X,8,420;

00291:ENDG;  
 00292:NEUG T6;  
 00293:POLY(6)S,0,50:10,130,-9,170,-28,-198,27,-102;  
 00294:POLY(6)S,20,145:65,205,-28,-175,-37,-30;  
 00295:POLY(6)S,90,50:10,35,40,-30,30,30,40,-35,10,  
 00296:65,-51,275,-28,-275,-51,-65;  
 00297:POLY(6)S,225,145:65,30,-37,175,-28,-205;  
 00298:POLY(6)S,300,50:10,102,27,198,-28,-170,-9,-130;  
 00299:ENDG;  
 00300:NEUG TS6;  
 00301:GROUP T6,0,0,XX,X,8,420;  
 00302:ENDG;  
 00303:NEUG K2A;  
 00304:POLY(10)S,-40,0:35,5,-25,255,31,90,-28,-80,-13,-270;  
 00305:POLY(10)S,-15,10:10,180,90,160,-28,-150,-72,-190;  
 00306:POLY(10)S,315,10:10,190,-72,150,-28,-160,90,-180;  
 00307:POLY(10)S,315,0:35,270,-13,80,-28,-90,31,-255,-25,-5;  
 00308:ENDG;  
 00309:NEUG K2AT;  
 00310:GROUP K2A,0,0,XX,X,8,420;  
 00311:ENDG;  
 00312:NEUG K2B;  
 00313:POLY(10)S,-40,0:35,8,-25,252,31,90,-28,-80,-13,-270;  
 00314:POLY(10)S,-15,13:10,177,90,160,-28,-150,-72,-187;  
 00315:POLY(10)S,315,13:10,187,-72,150,-28,-160,90,-177;  
 00316:POLY(10)S,315,0:35,270,-13,80,-28,-90,31,-252,-25,-8;  
 00317:ENDG;  
 00318:NEUG K2BT;  
 00319:GROUP K2B,0,0,XX,X,8,420;  
 00320:ENDG;  
 00321:NEUG K2C;  
 00322:POLY(10)S,-40,0:35,10,-25,250,31,90,-28,-80,-13,-270;  
 00323:POLY(10)S,-15,15:10,175,90,160,-28,-150,-72,-185;  
 00324:POLY(10)S,315,15:10,185,-72,150,-28,-160,90,-175;  
 00325:POLY(10)S,315,0:35,270,-13,80,-28,-90,31,-250,-25,-10;  
 00326:ENDG;  
 00327:NEUG K2CT;  
 00328:GROUP K2C,0,0,XX,X,8,420;  
 00329:ENDG;  
 00330:NEUG K2E;  
 00331:POLY(10)S,-40,0:35,13,-25,247,31,90,-28,-80,-13,-270;  
 00332:POLY(10)S,-15,18:10,172,90,160,-28,-150,-72,-182;  
 00333:POLY(10)S,315,18:10,182,-72,150,-28,-160,90,-172;  
 00334:POLY(10)S,315,0:35,270,-13,80,-28,-90,31,-247,-25,-13;  
 00335:ENDG;  
 00336:NEUG K2DT;  
 00337:GROUP K2D,0,0,XX,X,8,420;  
 00338:ENDG;  
 00339:NEUG K2E;  
 00340:POLY(10)S,-40,0:35,18,-25,242,31,90,-28,-80,-13,-270;  
 00341:POLY(10)S,-15,23:10,167,90,160,-28,-150,-72,-177;  
 00342:POLY(10)S,315,23:10,177,-72,150,-28,-160,90,-167;  
 00343:POLY(10)S,315,0:35,270,-13,80,-28,-90,31,-242,-25,-18;  
 00344:ENDG;  
 00345:NEUG K2ET;  
 00346:GROUP K2E,0,0,XX,X,8,420;  
 00347:ENDG;

P60  
00346:GROUP K2F,0,0,XX,X,8,420;  
00347:ENDG;  
00348:NEUG K2F;  
00349:POLY(10)S,-40,0:35,23,-25,237,31,90,-28,-80,-13,-270;  
00350:POLY(10)S,-15,28:10,162,90,160,-28,-150,-72,-172;  
00351:POLY(10)S,315,28:10,172,72,150,-28,-160,90,162;  
00352:POLY(10)S,315,0:35,270,-13,80,-28,90,31,-237,-25,-23;  
00353:ENDG;  
00354:NEUG K2T;  
00355:GROUP K2F,0,0,XX,X,8,420;  
00356:ENDG;  
00357:NEUG K2;  
00358:POLY(10)S,105,0:10,90,80,90,10,100,-36,250,-28,-250,-36,-100;  
00359:ENDG;  
00360:NEUG K2T;  
00361:GROUP K2,0,0,XX,X,8,420;  
00362:ENDG;  
00363:NEUG SACD;  
00364:DITTO GROUP SD1,90,-90;  
00365:720,-90;  
00366:1350,-90;  
00367:2400,-90;  
00368:3030,-90;  
00369:DITTO GROUP SD2,300,-90;  
00370:930,-90;  
00371:1770,-90;  
00372:2190,-90;  
00373:2820,-90;  
00374:DITTO GROUP SD3,510,-90;  
00375:1140,-90;  
00376:1560,-90;  
00377:1980,-90;  
00378:2610,-90;  
00379:ENDG;  
00380:NEUG DB1;  
00381:POLY(2)S,15,10:15,-10,115,5,-15,10,-115,-5;  
00382:ENDG;  
00383:NEUG DB2;  
00384:POLY(2)S,-15,13:15,-13,115,8,-15,13,-115,-8;  
00385:ENDG;  
00386:NEUG DB3;  
00387:POLY(2)S,-15,15:15,-15,115,10,-15,15,-115,-10;  
00388:ENDG;  
00389:NEUG DB4;  
00390:POLY(2)S,-15,18:15,-18,115,13,-15,18,-115,-13;  
00391:ENDG;  
00392:NEUG DB5;  
00393:POLY(2)S,-15,23:15,-23,115,18,-15,23,-115,-18;  
00394:ENDG;  
00395:NEUG DB6;  
00396:POLY(2)S,-15,28:15,-28,115,23,-15,28,-115,-23;  
00397:ENDG;  
00398:NEUG TDB1;  
00399:GROUP DB1,0,0,XX,X,16,210;  
00400:ENDG;  
00401:NEUG TDB2;  
00402:GROUP DB2,0,0,XX,X,16,210;  
00403:ENDG;  
00404:NEUG TDB3;  
00405:GROUP DB3,0,0,XX,X,16,210;  
\$

120  
 00405:GROUP DB3,0,0,XX,X,16,210;  
 00406:ENDG;  
 00407:NEUG TDB4;  
 00408:GROUP DB4,0,0,XX,X,16,210;  
 00409:ENDG;  
 00410:NEUG TDB5;  
 00411:GROUP DB5,0,0,XX,X,16,210;  
 00412:ENDG;  
 00413:NEUG TDB6;  
 00414:GROUP DB6,0,0,XX,X,16,210;  
 00415:ENDG;  
 00416:NEUG DA1;  
 00417:POLY(1,7)S,-15,0:115,10,15,5,115,-10,-15,-5;  
 00418:ENDG;  
 00419:NEUG DA2;  
 00420:POLY(1,7)S,-15,0:115,13,15,8,-115,-13,-15,-8;  
 00421:ENDG;  
 00422:NEUG DA3;  
 00423:POLY(1,7)S,-15,0:115,15,15,10,-115,-15,-15,-10;  
 00424:ENDG;  
 00425:NEUG DA4;  
 00426:POLY(1,7)S,-15,0:115,18,15,13,-115,-18,-15,-13;  
 00427:ENDG;  
 00428:NEUG DA5;  
 00429:POLY(1,7)S,-15,0:115,23,15,18,115,23,-15,18;  
 00430:ENDG;  
 00431:NEUG DA6;  
 00432:POLY(1,7)S,-15,0:115,28,15,23,-115,28,-15,-23;  
 00433:ENDG;  
 00434:NEUG TDA1;  
 00435:GROUP DA1,0,0,XX,X,16,210;  
 00436:ENDG;  
 00437:NEUG TDA2;  
 00438:GROUP DA2,0,0,XX,X,16,210;  
 00439:ENDG;  
 00440:NEUG TDA3;  
 00441:GROUP DA3,0,0,XX,X,16,210;  
 00442:ENDG;  
 00443:NEUG TDA4;  
 00444:GROUP DA4,0,0,XX,X,16,210;  
 00445:ENDG;  
 00446:NEUG TDA5;  
 00447:GROUP DA5,0,0,XX,X,16,210;  
 00448:ENDG;  
 00449:NEUG TDA6;  
 00450:GROUP DA6,0,0,XX,X,16,210;  
 00451:ENDG;  
 00452:NEUG IA7;  
 00453:POLY(3)S,-22,-7:144,29,-5,-12,-15,5,15,7,-139,  
 00454:17,20,-5,-15,5,5,12;  
 00455:ENDG;  
 00456:NEUG IAB;  
 00457:POLY(6)S,-22,-7:144,29,-144,-17,20,-5,-15,5,  
 00458:-5,-12;  
 00459:ENDG;  
 00460:NEUG IA9;  
 00461:POLY(8)S,-22,-7:144,5,-20,7,15,-7,5,24,-144,  
 00462:-29;  
 00463:ENDG;  
 00464:NEUG IA10;  
 00465:POLY(9)S,-22,-7:144,29,-5,-12,-15,5,15,7,-139,  
 00466:-29;  
 00467:ENDG;

00468:NEUG IA11;  
 00469:POLY(5)S,-22,-7:144,29,-139,-5,15,7,-15,12,-5,  
 00470:-29;  
 00471:ENDG;  
 00472:NEUG IB7;  
 00473:POLY(3)S,-22,-7:144,35,-5,-15,-15,8,15,7,-139,  
 00474:-20,20,-8,-15,8,-5,-15;  
 00475:ENDG;  
 00476:NEUG IBB;  
 00477:POLY(6)S,-22,-7:144,35,-144,-20,20,-8,-15,8,-5,  
 00478:-15;  
 00479:ENDG;  
 00480:NEUG IB9;  
 00481:POLY(8)S,-22,-7:144,5,-20,10,15,-10,5,30,-144,  
 00482:-35;  
 00483:ENDG;  
 00484:NEUG IB10;  
 00485:POLY(9)S,-22,-7:144,35,-5,-15,-15,8,15,7,-139,  
 00486:-35;  
 00487:ENDG;  
 00488:NEUG IB11;  
 00489:POLY(5)S,-22,-7:144,35,139,5,15,-10,15,15,-5,  
 00490:-35;  
 00491:ENDG;  
 00492:NEUG IC7;  
 00493:POLY(3)S,-22,-7:144,39,5,-17,15,10,15,7,139,  
 00494:-22,20,-10,-15,10,-5,-17;  
 00495:ENDG;  
 00496:NEUG IC8;  
 00497:POLY(6)S,-22,-7:144,39,-144,-22,20,-10,-15,10,-5,  
 00498:-17;  
 00499:ENDG;  
 00500:NEUG IC9;  
 00501:POLY(8)S,-22,-7:144,5,-20,12,15,-12,5,34,-144,  
 00502:-39;  
 00503:ENDG;  
 00504:NEUG IC10;  
 00505:POLY(9)S,-22,-7:144,39,-5,-17,-15,10,15,7,-139,  
 00506:-39;  
 00507:ENDG;  
 00508:NEUG IC11;  
 00509:POLY(5)S,-22,-7:144,39,139,5,15,-12,-15,17,-5,  
 00510:-39;  
 00511:ENDG;  
 00512:NEUG ID7;  
 00513:POLY(3)S,-22,-7:144,45,-5,-20,-15,13,15,7,-139,  
 00514:25,20,-13,-15,13,-5,-20;  
 00515:ENDG;  
 00516:NEUG ID8;  
 00517:POLY(6)S,-22,-7:144,45,144,25,20,-13,-15,13,  
 00518:-5,-20;  
 00519:ENDG;  
 00520:NEUG ID9;  
 00521:POLY(8)S,-22,-7:144,5,-20,15,15,-15,5,40,-144,  
 00522:-45;  
 00523:ENDG;  
 00524:NEUG ID10;  
 8

120  
00643:RECT(1)-910,30:40,40;  
00644:RECT(2)-840,30:40,40;  
00645:RECT(3)-770,30:40,40;  
00646:RECT(5)-630,30:40,40;  
00647:RECT(6)-560,30:40,40;  
00648:RECT(1)3420,30:40,40;  
00649:RECT(2)3490,30:40,40;  
00650:RECT(3)3560,30:40,40;  
00651:RECT(4)3630,30:40,40;  
00652:RECT(5)3700,30:40,40;  
00653:RECT(6)3770,30:40,40;  
00654:RECT(1)3855,7400:40,40;  
00655:RECT(2)1005,7400:40,40;  
00656:RECT(3)1155,7400:40,40;  
00657:RECT(4)-700,30:40,40;  
00658:RECT(4)1305,7400:40,40;  
00659:RECT(5)1455,7400:40,40;  
00660:RECT(6)1605,7400:40,40;  
00661:ENDG;  
00662:NEUG SQR530;  
00663:DITTO GROUP R1,-210,40030;  
00664: -280,40030;  
00665: -350,40030;  
00666: -420,40030;  
00667: 4120,40030;  
00668: 4050,40030;  
00669: 3980,40030;  
00670: 3910,40030;  
00671: 2355,47400;  
00672: 2205,47400;  
00673: 2055,47400;  
00674: 1905,47400;  
00675:ENDG;  
00676:NEUG SQR524;  
00677:DITTO GROUP R1, 210,30030;  
00678: -280,30030;  
00679: 4120,30030;  
00680: 4050,30030;  
00681: 2355,37400;  
00682: 2205,37400;  
00683:ENDG;  
00684:NEUG SQR518;  
00685:DITTO GROUP R1, 210,20030;  
00686: -420,20030;  
00687: 4120,20030;  
00688: 3910,20030;  
00689: 2355,27400;  
00690: 1905,27400;  
00691:ENDG;  
00692:NEUG SQR512;  
00693:DITTO GROUP R1,-280,10030;  
00694: -350,10030;  
00695: 4050,10030;  
00696: 3980,10030;  
00697: 2205,17400;  
00698: 2055,17400;  
00699:ENDG;  
00700:NEUG SQR56;  
00701:DITTO GROUP R1, 350,30;  
00702: -420,30;  
00703: 3980,30;  
00704: 3910,30;  
00705: 2055,7400;

00706: 1905,7400;  
00707:ENDG;  
00708:NEUG SQR55;  
00709:DITTO GROUP R1,7650,30;  
00710: 7510,30;  
00711: 11980,30;  
00712: 11840,30;  
00713: 10055,7400;  
00714: 9755,7400;  
00715:ENDG;  
00716:NEUG SQR511;  
00717:DITTO GROUP R1,7720,10030;  
00718: 7580,10030;  
00719: 7510,10030;  
00720: 11910,10030;  
00721: 12050,10030;  
00722: 11840,10030;  
00723: 10205,17400;  
00724: 9905,17400;  
00725: 9755,17400;  
00726:ENDG;  
00727:NEUG SQR517;  
00728:DITTO GROUP R1,7790,20030;  
00729: 7510,20030;  
00730: 12120,20030;  
00731: 11840,20030;  
00732: 10355,27400;  
00733: 9755,27400;  
00734:ENDG;  
00735:NEUG SQR523;  
00736:DITTO GROUP R1,7790,30030;  
00737: 7650,30030;  
00738: 7580,30030;  
00739: 7510,30030;  
00740: 12120,30030;  
00741: 11980,30030;  
00742: 11910,30030;  
00743: 11840,30030;  
00744: 10355,37400;  
00745: 10055,37400;  
00746: 9905,37400;  
00747: 9755,37400;  
00748:ENDG;  
00749:NEUG SQR529;  
00750:DITTO GROUP R1,7790,40030;  
00751: 7720,40030;  
00752: 7650,40030;  
00753: 7510,40030;  
00754: 12120,40030;  
00755: 12050,40030;  
00756: 11980,40030;  
00757: 11840,40030;  
00758: 10355,47400;  
00759: 10205,47400;  
00760: 10055,47400;  
00761: 9755,47400;  
00762:ENDG;  
8

```

120
00524:NEUG ID10;
00525:POLY(9)S,-22,-7:144,45,-5,-20,-15,13,15,7,-139,
00526:                -45;
00527:ENDG;
00528:NEUG ID11;
00529:POLY(5)S,-22,-7:144,45,-139,-5,15,-10,-15,15,-5,
00530:                -45;
00531:ENDG;
00532:NEUG IE7;
00533:POLY(3)S,-22,-7:144,55,-5,-25,-15,18,15,7,-139,
00534:                -30,20,-18,-15,18,-5,-25;
00535:ENDG;
00536:NEUG IE8;
00537:POLY(6)S,-22,-7:144,55,-144,30,20,-18,-15,18,
00538:                -5,-25;
00539:ENDG;
00540:NEUG IE9;
00541:POLY(8)S,-22,-7:144,5,20,20,15,-20,5,50,-144,
00542:                55;
00543:ENDG;
00544:NEUG IF10;
00545:POLY(9)S,-22,-7:144,55,-5,-25,-15,18,15,7,-139,
00546:                -55;
00547:ENDG;
00548:NEUG IE11;
00549:POLY(5)S,-22,-7:144,55,-139,-5,15,-20,-15,25,
00550:                -5,-55;
00551:ENDG;
00552:NEUG IF7;
00553:POLY(3)S,-22,-7:144,65,-5,-30,-15,23,15,7,-139,-35,
00554:                20,-23,-15,23,-5,-30;
00555:ENDG;
00556:NEUG IF8;
00557:POLY(6)S,-22,-7:144,65,-144,-35,20,-23,-15,23,-5,
00558:                -30;
00559:ENDG;
00560:NEUG IF9;
00561:POLY(8)S,-22,-7:144,5,-20,25,15,-25,5,60,-144,
00562:                -65;
00563:ENDG;
00564:NEUG IF10;
00565:POLY(9)S,-22,-7:144,65,-5,-30,-15,23,15,7,-139,
00566:                65;
00567:ENDG;
00568:NEUG IF11;
00569:POLY(5)S,-22,-7:144,65,-139,-5,15,-25,-15,30,-5,
00570:                -65;
00571:ENDG;
00572:NEUG TA7;
00573:GROUP IA7,0,0,XX,X,16,210;
00574:GROUP IA8,0,0,XX,X,16,210;
00575:GROUP IA9,0,0,XX,X,16,210;
00576:GROUP IA10,0,0,XX,X,16,210;
00577:GROUP IA11,0,0,XX,X,16,210;
00578:ENDG;
00579:NEUG TB7;
00580:GROUP IB7,0,0,XX,X,16,210;
00581:GROUP IB8,0,0,XX,X,16,210;
00582:GROUP IB9,0,0,XX,X,16,210;
00583:GROUP IB10,0,0,XX,X,16,210;
00584:GROUP IB11,0,0,XX,X,16,210;
00585:ENDG;
00586:NEUG TC7;

```

```

00587:GROUP IC7,0,0,XX,X,16,210;
00588:GROUP IC8,0,0,XX,X,16,210;
00589:GROUP IC9,0,0,XX,X,16,210;
00590:GROUP IC10,0,0,XX,X,16,210;
00591:GROUP IC11,0,0,XX,X,16,210;
00592:ENDG;
00593:NEUG TD7;
00594:GROUP ID7,0,0,XX,X,16,210;
00595:GROUP ID8,0,0,XX,X,16,210;
00596:GROUP ID9,0,0,XX,X,16,210;
00597:GROUP ID10,0,0,XX,X,16,210;
00598:GROUP ID11,0,0,XX,X,16,210;
00599:ENDG;
00600:NEUG TE7;
00601:GROUP IE7,0,0,XX,X,16,210;
00602:GROUP IE8,0,0,XX,X,16,210;
00603:GROUP IE9,0,0,XX,X,16,210;
00604:GROUP IE10,0,0,XX,X,16,210;
00605:GROUP IE11,0,0,XX,X,16,210;
00606:ENDG;
00607:NEUG TF7;
00608:GROUP IF7,0,0,XX,X,16,210;
00609:GROUP IF8,0,0,XX,X,16,210;
00610:GROUP IF9,0,0,XX,X,16,210;
00611:GROUP IF10,0,0,XX,X,16,210;
00612:GROUP IF11,0,0,XX,X,16,210;
00613:ENDG;
00614:NEUG C1;
00615:POLY(5)S,-930,10:780,80,-10,-70,-60,60,60,10,
00616:                -70,-70,-60,60,60,10,-70,-70,-60,
00617:                60,60,10,-70,-70,-60,60,60,10,70,
00618:                -70,60,60,60,10,-70,-70,60,60,
00619:                60,10,-70,-70,-60,60,60,10,70,
00620:                -70,-60,60,60,10,-70,-70,60,
00621:                60,60,10,70,70,-60,60,60,10,
00622:                -70,-70,-60,60,60,10,-70,80;
00623:POLY(5)S,3400,10:780,80,-10,-70,-60,60,60,10,
00624:                -70,-70,-60,60,60,10,-70,70,
00625:                -60,60,60,10,-70,-70,-60,60,60,
00626:                10,-70,-70,-60,60,60,10,-70,-70,
00627:                -60,60,60,10,-70,-70,-60,60,60,
00628:                10,-70,-70,-60,60,60,10,-70,
00629:                -70,-60,60,60,10,-70,-70,-60,
00630:                60,60,10,-70,-70,-60,60,60,10,
00631:                -70,-80;
00632:POLY(5)L,-1475,-530:300,0,-150,500,150,500,-300,
00633:                0,150,-500,-150,-500;
00634:POLY(5)L,4725,-530:300,0,-150,500,150,500,150,
00635:                500,-300,0,150,-500,-150,-500;
00636:POLY(5)L,705,7400:40,30,-40,30,0,-60;
00637:POLY(5)L,2505,7400:40,-30,0,60,-40,-30;
00638:ENDG;
00639:NEUG R1;
00640:RECT(5)0,0:40,40;
00641:ENDG;
00642:NEUG R2;
00643:RECT(1)-910,30:40,40;

```

120  
 00762:ENDG;  
 00763:NEUG SORS28;  
 00764:DITTO GROUP R1, 15790, 40030;  
 00765: 15720, 40030;  
 00766: 15650, 40030;  
 00767: 20120, 40030;  
 00768: 20050, 40030;  
 00769: 19980, 40030;  
 00770: 18355, 47400;  
 00771: 18205, 47400;  
 00772: 18055, 47400;  
 00773:ENDG;  
 00774:NEUG SORS22;  
 00775:DITTO GROUP R1, 15790, 30030;  
 00776: 15650, 30030;  
 00777: 15580, 30030;  
 00778: 20120, 30030;  
 00779: 19980, 30030;  
 00780: 19910, 30030;  
 00781: 18355, 37400;  
 00782: 18055, 37400;  
 00783: 17905, 37400;  
 00784:ENDG;  
 00785:NEUG SORS16;  
 00786:DITTO GROUP R1, 15790, 20030;  
 00787: 20120, 20030;  
 00788: 18755, 27400;  
 00789:ENDG;  
 00790:NEUG SORS10;  
 00791:DITTO GROUP R1, 15720, 10030;  
 00792: 15580, 10030;  
 00793: 20050, 10030;  
 00794: 19910, 10030;  
 00795: 18205, 17400;  
 00796: 17905, 17400;  
 00797:ENDG;  
 00798:NEUG SORS4;  
 00799:DITTO GROUP R1, 15650, 30;  
 00800: 19980, 30;  
 00801: 18055, 7400;  
 00802:ENDG;  
 00803:NEUG SORS3;  
 00804:DITTO GROUP R1, 23510, 30;  
 00805: 23580, 30;  
 00806: 27840, 30;  
 00807: 27910, 30;  
 00808: 25755, 7400;  
 00809: 25905, 7400;  
 00810:ENDG;  
 00811:NEUG SORS9;  
 00812:DITTO GROUP R1, 23510, 10030;  
 00813: 23720, 10030;  
 00814: 27840, 10030;  
 00815: 28050, 10030;  
 00816: 25755, 17400;  
 00817: 26205, 17400;  
 00818:ENDG;  
 00819:NEUG SORS15;  
 00820:DITTO GROUP R1, 23510, 20030;  
 00821: 23580, 20030;  
 00822: 23650, 20030;  
 00823: 23720, 20030;  
 00824: 27840, 20030;

00825: 27910, 20030;  
 00826: 27980, 20030;  
 00827: 28050, 20030;  
 00828: 25755, 27400;  
 00829: 25905, 27400;  
 00830: 26055, 27400;  
 00831: 26205, 27400;  
 00832:ENDG;  
 00833:NEUG SORS21;  
 00834:DITTO GROUP R1, 23510, 30030;  
 00835: 23650, 30030;  
 00836: 27790, 30030;  
 00837: 27840, 30030;  
 00838: 27980, 30030;  
 00839: 28120, 30030;  
 00840: 25755, 37400;  
 00841: 26055, 37400;  
 00842: 26355, 37400;  
 00843:ENDG;  
 00844:NEUG SORS27;  
 00845:DITTO GROUP R1, 23510, 40030;  
 00846: 23580, 40030;  
 00847: 23720, 40030;  
 00848: 23790, 40030;  
 00849: 27840, 40030;  
 00850: 27910, 40030;  
 00851: 28050, 40030;  
 00852: 28120, 40030;  
 00853: 25755, 47400;  
 00854: 25905, 47400;  
 00855: 26205, 47400;  
 00856: 26355, 47400;  
 00857:ENDG;  
 00858:NEUG SORS26;  
 00859:DITTO GROUP R1, 31790, 40030;  
 00860: 31720, 40030;  
 00861: 31580, 40030;  
 00862: 36120, 40030;  
 00863: 36050, 40030;  
 00864: 35910, 40030;  
 00865: 34355, 47400;  
 00866: 34205, 47400;  
 00867: 33005, 47400;  
 00868:ENDG;  
 00869:NEUG SORS20;  
 00870:DITTO GROUP R1, 31790, 30030;  
 00871: 31650, 30030;  
 00872: 36120, 30030;  
 00873: 35980, 30030;  
 00874: 34355, 37400;  
 00875: 34055, 37400;  
 00876:ENDG;  
 00877:NEUG SORS14;  
 00878:DITTO GROUP R1, 31720, 20030;  
 00879: 31650, 20030;  
 00880: 31580, 20030;  
 00881: 36050, 20030;

20  
00881: 36050,20030;  
00882: 35980,20030;  
00883: 35910,20030;  
00884: 34205,27400;  
00885: 34055,27400;  
00886: 33905,27400;  
00887:ENDG;  
00888:NEUG SQRS8;  
00889:DITTO GROUP R1,31720,10030;  
00890: 36050,10030;  
00891: 34205,17400;  
00892:ENDG;  
00893:NEUG SQRS2;  
00894:DITTO GROUP R1,31580,30;  
00895: 35910,30;  
00896: 33905,7400;  
00897:ENDG;  
00898:NEUG SQRS1;  
00899:DITTO GROUP R1,39510,30;  
00900: 43840,30;  
00901: 41755,7400;  
00902:ENDG;  
00903:NEUG SQRS7;  
00904:DITTO GROUP R1,39510,10030;  
00905: 39580,10030;  
00906: 39650,10030;  
00907: 43840,10030;  
00908: 43910,10030;  
00909: 43980,10030;  
00910: 41755,17400;  
00911: 41905,17400;  
00912: 42055,17400;  
00913:ENDG;  
00914:NEUG SQRS13;  
00915: DITTO GROUP R1,39510,20030;  
00916: 39650,20030;  
00917: 39720,20030;  
00918: 43840,20030;  
00919: 43980,20030;  
00920: 44050,20030;  
00921: 41755,27400;  
00922: 42055,27400;  
00923: 42205,27400;  
00924:ENDG;  
00925:NEUG SQRS19;  
00926: DITTO GROUP R1,39510,30030;  
00927: 39580,30030;  
00928: 39790,30030;  
00929: 43840,30030;  
00930: 43910,30030;  
00931: 44120,30030;  
00932: 41755,37400;  
00933: 41905,37400;  
00934: 42055,37400;  
00935:ENDG;  
00936:NEUG SQRS25;  
00937: DITTO GROUP R1,39510,40030;  
00938: 39720,40030;  
00939: 39790,40030;  
00940: 43840,40030;  
00941: 44050,40030;  
00942: 44120,40030;  
00943: 44120,40030;

00944: 41755,47400;  
00945: 42205,47400;  
00946: 42355,47400;  
00947:ENDG;  
00948:NEUG REG;  
00949:POLY(1)S,0,0:32,32,5,-27,-22,22,22,5,-27,-32;  
00950:POLY(6)S,-48,0:32,32,-5,-27,-22,22,22,5,-27,-32;  
00951:RECT(2)6,6:20,20;  
00952:RECT(11)-42,6:20,20;  
00953:POLY(2)S,0,52:32,32,-5,-27,-22,22,22,5,-27,-32;  
00954:POLY(2)S,-48,52:32,32,-5,-27,-22,22,22,5,-27,-32;  
00955:RECT(3)6,58:20,20;  
00956:RECT(5)-42,58:20,20;  
00957:POLY(7)S,0,104:32,32,-5,-27,-22,22,22,5,-27,-32;  
00958:RECT(4)6,110:20,20;  
00959:POLY(4)S,0,156:32,32,-5,-27,-22,22,22,5,-27,-32;  
00960:RECT(5)6,162:20,20;  
00961:POLY(5)S,0,208:32,32,-5,-27,-22,22,22,5,-27,-32;  
00962:RECT(6)6,214:20,20;  
00963:POLY(6)S,0,260:32,32,-5,-27,-22,22,22,5,-27,-32;  
00964:RECT(7)6,266:20,20;  
00965:POLY(7)S,0,312:32,32,-5,-27,-22,22,22,5,-27,-32;  
00966:RECT(8)6,318:20,20;  
00967:POLY(8)S,0,364:32,32,-5,-27,-22,22,22,5,-27,-32;  
00968:RECT(9)6,370:20,20;  
00969:POLY(9)S,0,416:32,32,-5,-27,-22,22,22,5,-27,-32;  
00970:RECT(10)6,422:20,20;  
00971:POLY(10)S,0,468:32,32,-5,-27,-22,22,22,5,-27,-32;  
00972:RECT(11)6,474:20,20;  
00973:POLY(3)S,-48,104:32,32,5,-27,22,22,22,5,27,32;  
00974:RECT(5)-42,110:20,20;  
00975:ENDG;  
00976:NEUG D15;  
00977:GROUP K1,0,0;  
00978:GROUP SACD,0,0;  
00979:GROUP TDA1,0,0;  
00980:GROUP TDB1,0,0;  
00981:GROUP TA7,0,0;  
00982:GROUP K2T,0,0;  
00983:GROUP K2AT,0,0;  
00984:GROUP C1,0,0;  
00985:GROUP R2,0,0;  
00986:ENDG;  
00987:NEUG D20;  
00988:GROUP K1,0,0;  
00989:GROUP SACD,0,0;  
00990:GROUP K2T,0,0;  
00991:GROUP K2BT,0,0;  
00992:GROUP C1,0,0;  
00993:GROUP R2,0,0;  
00994:GROUP TDA2,0,0;  
00995:GROUP TDB2,0,0;  
00996:GROUP TB7,0,0;  
00997:ENDG;  
00998:NEUG D25;  
00999:GROUP K1,0,0;  
01000:GROUP SACD,0,0;  
5




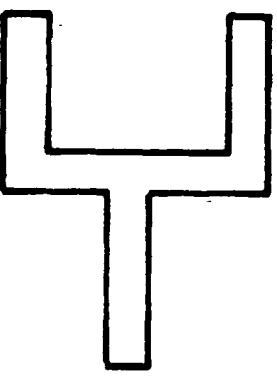

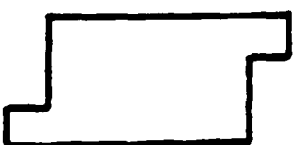
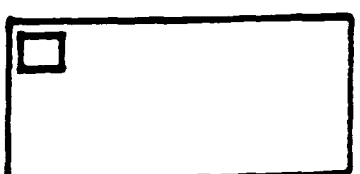
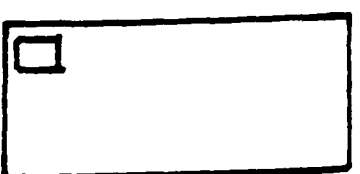







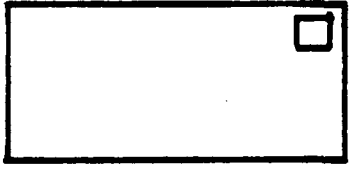

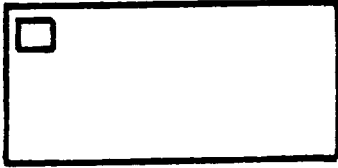
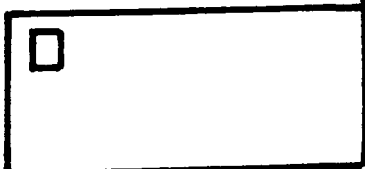

120  
01000:GROUP SACD,0,0;  
01001:GROUP TDA3,0,0;  
01002:GROUP TDB3,0,0;  
01003:GROUP TC7,0,0;  
01004:GROUP K2T,0,0;  
01005:GROUP K2CT,0,0;  
01006:GROUP C1,0,0;  
01007:GROUP R2,0,0;  
01008:ENDG;  
01009:NEUG D30;  
01010:GROUP K1,0,0;  
01011:GROUP SACD,0,0;  
01012:GROUP TDA4,0,0;  
01013:GROUP TDB4,0,0;  
01014:GROUP TD7,0,0;  
01015:GROUP K2T,0,0;  
01016:GROUP K2DT,0,0;  
01017:GROUP C1,0,0;  
01018:GROUP R2,0,0;  
01019:ENDG;  
01020:NEUG D40;  
01021:GROUP K1,0,0;  
01022:GROUP SACD,0,0;  
01023:GROUP TDA5,0,0;  
01024:GROUP TDB5,0,0;  
01025:GROUP TE7,0,0;  
01026:GROUP K2T,0,0;  
01027:GROUP K2ET,0,0;  
01028:GROUP C1,0,0;  
01029:GROUP R2,0,0;  
01030:ENDG;  
01031:NEUG D50;  
01032:GROUP K1,0,0;  
01033:GROUP SACD,0,0;  
01034:GROUP TDA6,0,0;  
01035:GROUP TDB6,0,0;  
01036:GROUP TE7,0,0;  
01037:GROUP K2T,0,0;  
01038:GROUP K2ET,0,0;  
01039:GROUP C1,0,0;  
01040:GROUP R2,0,0;  
01041:ENDG;  
01042:NEUG REG1;  
01043:GROUP REG,-2391,0,XX,2,2,2000,Y,2,5000;  
01044:ENDG;  
01045:NEUG T15;  
01046:GROUP K1,0,0;  
01047:GROUP TS1,0,0;  
01048:GROUP SACT,0,0;  
01049:GROUP T1A,0,0;  
01050:GROUP SM1,0,0;  
01051:GROUP BS1,0,0;  
01052:GROUP BS2,0,0;  
01053:GROUP R2,0,0;  
01054:GROUP BS3,0,0;  
01055:GROUP C1,0,0;  
01056:ENDG;  
01057:NEUG T20;  
01058:GROUP K1,0,0;  
01059:GROUP TS2,0,0;  
01060:GROUP SACT,0,0;  
01061:GROUP T1B,0,0;  
01062:GROUP SA2,0,0;

01063:GROUP BS1,0,0;  
01064:GROUP BS2,0,0;  
01065:GROUP R2,0,0;  
01066:GROUP BS3,0,0;  
01067:GROUP C1,0,0;  
01068:ENDG;  
01069:NEUG T25;  
01070:GROUP K1,0,0;  
01071:GROUP TS3,0,0;  
01072:GROUP SACT,0,0;  
01073:GROUP T1C,0,0;  
01074:GROUP SM3,0,0;  
01075:GROUP BS1,0,0;  
01076:GROUP BS2,0,0;  
01077:GROUP R2,0,0;  
01078:GROUP BS3,0,0;  
01079:GROUP C1,0,0;  
01080:ENDG;  
01081:NEUG T30;  
01082:GROUP K1,0,0;  
01083:GROUP TS4,0,0;  
01084:GROUP SACT,0,0;  
01085:GROUP T1D,0,0;  
01086:GROUP SM4,0,0;  
01087:GROUP BS1,0,0;  
01088:GROUP BS2,0,0;  
01089:GROUP R2,0,0;  
01090:GROUP BS3,0,0;  
01091:GROUP C1,0,0;  
01092:ENDG;  
01093:NEUG T40;  
01094:GROUP K1,0,0;  
01095:GROUP TS5,0,0;  
01096:GROUP SACT,0,0;  
01097:GROUP T1E,0,0;  
01098:GROUP SM5,0,0;  
01099:GROUP BS1,0,0;  
01100:GROUP BS2,0,0;  
01101:GROUP R2,0,0;  
01102:GROUP BS3,0,0;  
01103:GROUP C1,0,0;  
01104:ENDG;  
01105:NEUG T50;  
01106:GROUP K1,0,0;  
01107:GROUP TS6,0,0;  
01108:GROUP SACT,0,0;  
01109:GROUP T1F,0,0;  
01110:GROUP SM6,0,0;  
01111:GROUP BS1,0,0;  
01112:GROUP BS2,0,0;  
01113:GROUP R2,0,0;  
01114:GROUP BS3,0,0;  
01115:GROUP C1,0,0;  
01116:ENDG;  
01117:GROUP REG1,0,0;  
01118:GROUP SQRS1,0,0;  
01119:GROUP SQRS2,0,0;  
8

APPENDIX IV

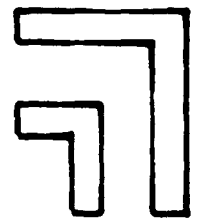
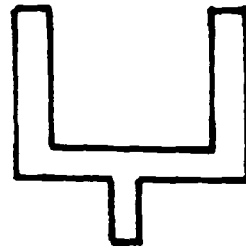
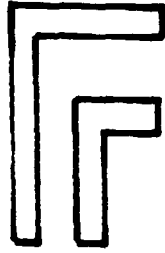
Fabrication Details 6 - Element Head

1. Sputter Ni Fe
2. Etch Ni Fe  Mask One
3. Sputter Si O<sub>2</sub> + Ni Fe
4. Etch Ni Fe  Mask Two
5. Etch Si O<sub>2</sub>  Mask Three
6. Sputter Cr + Au
7. Etch Cr + Au  Mask Twelve
8. Sputter Si O<sub>2</sub>
9. Etch Si O<sub>2</sub>  Mask Five
10. Sputter Ni Fe
11. Etch Ni Fe  Mask Two
12. Etch Si O<sub>2</sub>  Mask Six
13. Sputter Si O<sub>2</sub>
14. Etch Si O<sub>2</sub>  Mask Six
15. Sputter Ni Fe

- 16. Etch Ni Fe  Mask Seven
- 17. Etch Si O<sub>2</sub>  Mask Eight
- 18. Sputter Si O<sub>2</sub>
- 19. Etch Si O<sub>2</sub>  Mask Nine
- 20. Sputter Ni Fe
- 21. Etch Ni Fe  Mask Seven
- 22. Etch Si O<sub>2</sub>  Mask Eight
- 23. Sputter Si O<sub>2</sub>
- 24. Etch Si O<sub>2</sub>  Mask Eight
- 25. Sputter Ni Fe
- 26. Etch Ni Fe  Mask Two
- 27. Etch Si O<sub>2</sub>  Mask Six
- 28. Sputter Si O<sub>2</sub>
- 29. Etch Si O<sub>2</sub>  Mask Six
- 30. Etch Si O<sub>2</sub>  Mask Five

31. Sputter Cr + Au

32. Etch Cr + Au



33. Sputter Thick Cr + Au

Mask Ten

34. Etch Cr + Au - Mask 11 (see section 3.2 ii)

APPENDIX V

# Asymmetric biasing fields from mismatched current-carrying overlay conductors on magnetoresistive replay sensors

D. J. Mapps, M. L. Watson, and D. T. Wilton  
 Plymouth Polytechnic, Drake Circus, Plymouth, Devon, PL48AA, United Kingdom

Magnetoresistive thin-film sensors used in magnetic recording applications are often linearized using a transverse biasing field. For single-domain behavior the biasing field is computed as the average planar value throughout the volume of the sensor element. This paper shows how the correct bias field can be calculated in the general case for a nonmagnetic current-carrying overlay bias conductor not having the same dimensions as the sensor and not symmetrically positioned. This allows the effect of mismatching, for example due to faulty fabrication, to be predicted. The theoretical expressions are confirmed by experiment using a Hall probe. Various graphs are presented which show how the theory can be used in practical cases with typical sensor and conductor dimensions.

## INTRODUCTION

Magnetoresistive thin films are frequently used for reading information on magnetic tape. The tape fields rotate the magnetic vector in a sensor film and modulate its resistance. In the original paper by Hunt<sup>1</sup> the effect on the magnetization in the sensor was deduced by averaging the tape field over the film dimensions and this gave good agreement with experiment assuming the film to behave as a single magnetic domain. More recent work has confirmed this model as long as the single domain behavior is present<sup>2</sup> and present-day films, typically 500 Å thick have outputs which are accurately predicted by the average field method.

A sinusoidally recorded tape will produce a low-amplitude, double-frequency modulation in the resistance of an unbiased sensor film. This is adequate for some high-field digital applications but for low-field digital or analogue applications it is convenient to use a linearizing dc biasing field from a current-carrying overlay bias film.

Bias films have typically the same planar dimensions as the Permalloy sensor films but of varying thickness. This makes the average bias field amplitude fairly reproducible at a given bias current but in some cases, where large numbers of devices are deposited on the same substrate, optical alignment deviations, or photomask imperfections can cause some of the overlay bias films to be mismatched with

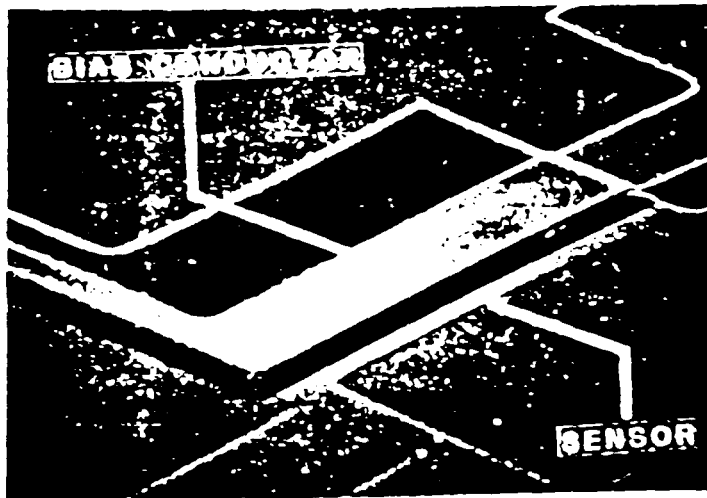


FIG 1 Photograph of a mismatched sensor and overlay bias conductor

the sensor films underneath as shown in the photograph of Fig. 1. This causes the eventual bias current to produce in the sensor film an average field of the wrong magnitude for correct biasing leading to reduced outputs with increased harmonic distortion. A mathematical analysis of this asymmetric effect has not been reported so it is the purpose of this paper to present such an analysis. This allows early decisions to be made, i.e., at the substrate or wafer stage, about the acceptance or rejection of individual chip sensors as well as providing a useful tool in thin-film structure design

## THEORY

The problem is one of deducing the average magnetic field parallel to the surfaces of the rectangular-sectioned sensor film due to a uniform current flowing in another rectangular-sectioned conductor film nearby. If the conductor film is considered as an array of current filaments as shown in Fig. 2, then because the distances  $dx'$ ,  $dy'$  are small compared with the conductor length, they can be considered infinitely long for the purposes of calculation of magnetic field. Ampère's circuital law can be used for a circular path around each filament  $dx'dy'$  to evaluate the field.

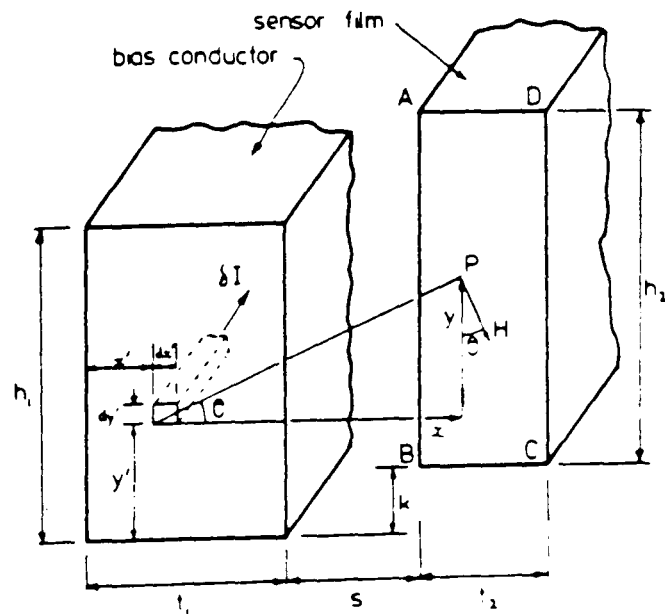


FIG 2 Diagram of a section through a sensor and overlay conductor showing a filamental current  $\delta I$  and the variables used in the theoretical derivation

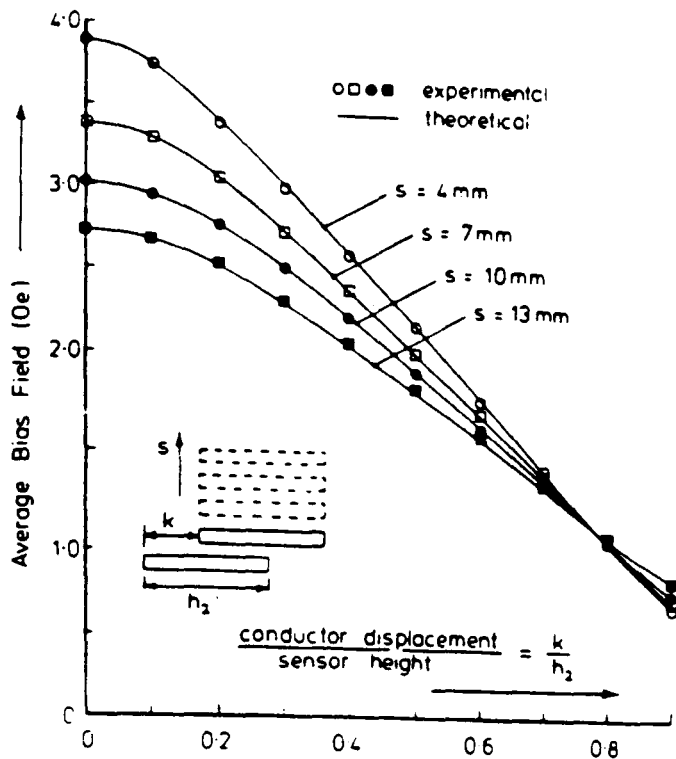


FIG. 3. The theoretical average sensor bias field predicted from Eq (7) compared with experimental results using a Hall probe

In Fig. 2, consider the field at  $P$  due to the filament  $dx'dy'$ . Ampère's law gives

$$\oint H dl = NI, \quad (1)$$

where  $H$  is constant for a circular path of length  $2\pi r$ ,  $N = 1$ , and filament current =  $\delta I$ . Hence

$$H \oint dl = \delta I \quad \therefore H = \frac{\delta I}{2\pi r} \quad (2)$$

This field is tangential to the circular path so the component parallel to the vertical surfaces  $AB$  and  $DC$  of the film is given by

$$\delta H_x = \frac{\delta I}{2\pi r} \cos \theta = \frac{x\delta I}{2\pi(x^2 + y^2)} \quad (3)$$

The average value of  $\delta H_x$  in the  $x$  direction due to the filament  $dx'dy'$  is

$$H_x = \frac{I}{2\pi t_1 h_1 t_2 h_2} \int_{x=0}^{t_1} \int_{y=0}^{h_1} \int_{x=s-t_1-x}^{s+t_1-x-t_1} \int_{y=k-y}^{h_1-y-k} \left( \frac{x}{x^2 + y^2} \right) dy dx dy' dx' \quad (6)$$

The solution of Eq. (6) is too lengthy to be given here but the result can be summarized as

$$H_x = \frac{I}{4\pi t_1 h_1 t_2 h_2} [J(s+t_2, s+t_2+t_1, k+h_2-h_1, k+h_2) + J(s, s-t_1, k-h_1, k) - J(s+t_2, s+t_2+t_1, k-h_1, k) - J(s, s+t_1, k+h_2-h_1, k+h_2)],$$

where

$$J(A, B, C, D) = \frac{5}{6} (A-B)(D^2 - C^2) + \frac{1}{3} C^3 \left[ \tan^{-1} \left( \frac{A}{C} \right) - \tan^{-1} \left( \frac{B}{C} \right) \right] - \frac{1}{3} D^3 \left[ \tan^{-1} \left( \frac{B}{D} \right) - \tan^{-1} \left( \frac{A}{D} \right) \right] + A^2 \left[ C \tan^{-1} \left( \frac{C}{A} \right) - D \tan^{-1} \left( \frac{D}{A} \right) \right] + B^2 \left[ D \tan^{-1} \left( \frac{D}{B} \right) - C \tan^{-1} \left( \frac{C}{B} \right) \right] + \frac{1}{6} B (3D^2 - B^2) \ln(B^2 + D^2) + \frac{1}{6} A (A^2 - 3D^2) \ln(A^2 - D^2) + \frac{1}{6} A (3C^2 - A^2) \ln(A^2 + C^2) + \frac{1}{6} B (B^2 - 3C^2) \ln(B^2 + C^2) \quad (7)$$

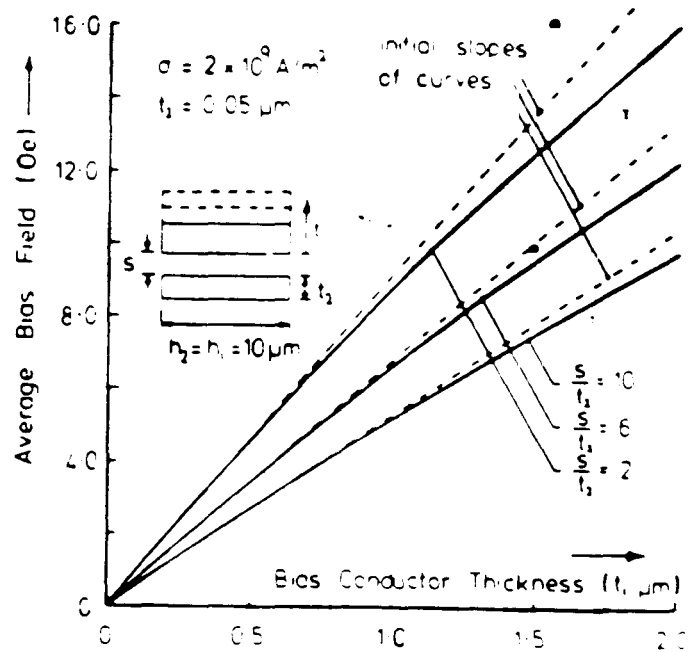


FIG. 4. Showing how the thickness of a bias conductor affects average sensor bias fields at variable separation distances and constant current density

$$\frac{1}{AD} \int \delta H_x dx = \frac{1}{t_2} \int_{x=s-t_1-x}^{s+t_1-x-t_1} \left( \frac{x\delta I}{2\pi(x^2 + y^2)} \right) dx \quad (4)$$

The average value of  $\delta H_x$  all over  $ABCD$  due to the filament  $dx'dy'$  is

$$\frac{\delta I}{2\pi t_2 h_2} \int_{x=0}^{t_1} \int_{y=0}^{h_1} \left( \frac{x}{x^2 + y^2} \right) dx dy \quad (5)$$

Substituting for current  $\delta I = I/t_1 h_1 dx'dy'$  and integrating the function of Eq. (5) over the area of the bias element essentially sums the effects of all the filaments  $dx'dy'$  of the total current  $I$ . Hence, the average vertical field in the sense element due to a current  $I$  in the rectangular sectioned bias element is given by



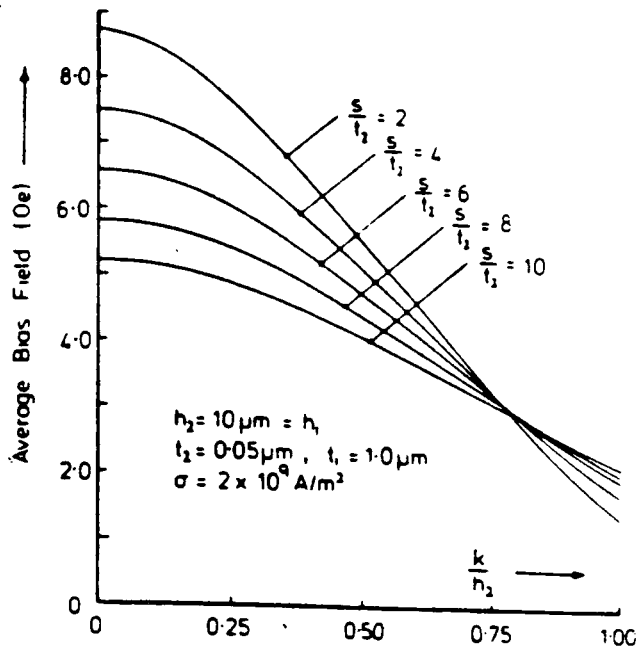


FIG. 5. Sensor bias field roll-off as a function of conductor offset

The accuracy of result (7) as a mathematical derivation was confirmed by differentiation and also by using a numerical integration on computer.

#### EXPERIMENTAL VERIFICATION

To test the validity of this method of evaluating the average bias field, an experiment was devised using a thick, wide, current-carrying copper plate and a Hall probe. The probe was arranged so that it always measured the vertical field component. The probe was scanned across the plate for a distance equal to the relative width of the sensor and the field values averaged. This produced results directly compatible with the mathematical predictions for the dimensions used. The plate measured 50 mm high by 0.25 mm thick, making it roughly to the scale of a typical thin-film conductor. Hall probe dimensions were  $0.2 \times 0.25$  mm. The comparison between theory and experiment for a plate current of 40 A is shown in Fig. 3 where the maximum differences were well within experimental error. Figure 3 also shows an interesting crossover where the average vertical bias field from an offset conductor spaced away from the magnetic thin-film can actually be greater than the bias field from the same conductor placed nearer the plane of the sensor surface. The crossover in Fig. 3 is confirmed in theory and practice.

#### EFFECT OF ASYMMETRY ON THE BIAS FIELD

A series of graphs has been plotted to show how the dimensional variables relate to each other and to the average biasing field for typical magnetoresistive sensor and bias conductors. The current density  $\sigma$  is held constant at  $2 \times 10^9$  A/m<sup>2</sup> throughout. The graphs are shown in Figs. 4, 5, and 6. Figure 4 shows how increasing the thickness of a centralized bias conductor can increase the bias field. Note that as the thick bias conductor approaches the sensor, so the deviation from the dashed initial slope line increases showing that the

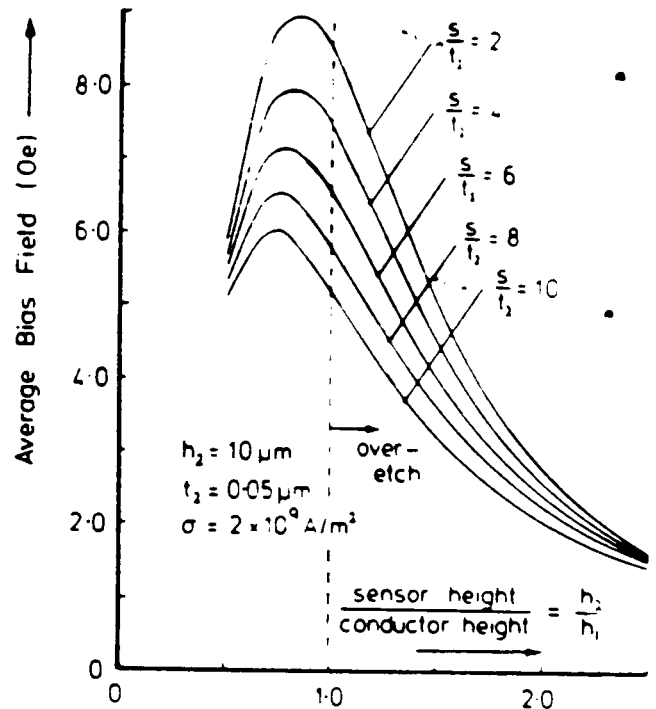


FIG. 6. Showing how overetching of a nominally equal height bias conductor can lead to a significant reduction in sensor bias field

bias field will be reduced from that expected by an infinitely thin conductor. Figure 5 is similar to Fig. 3 but this time with typical film dimensions. The crossover of the characteristics shows that the bias field is independent of separation at the critical point when a mismatch of about 80% occurs. A mismatch of 10% is seen to be tolerable for most practical cases when the bias conductor and sensor film are of equal height. The sensor is less tolerant of mismatch as the separation decreases.

Figure 6 shows that overetching of the bias conductor during the microfabrication process has a severe effect on the bias field, especially if the bias conductor and sense element are close together. A typical conductor/sensor pair would be separated by about  $0.3 \mu\text{m}$  so the  $s/t_2 = 6$  case is the one which might normally apply.

#### CONCLUSIONS

- (1) A complete analysis has been carried out for predicting the average in-plane bias field for rectangular sectioned thin-film bias conductors on rectangular-sectioned thin-film magnetoresistive sensors
- (2) The analysis is completely general so it allows the prediction of bias field for any film dimensions in a symmetrical or asymmetrical arrangement.
- (3) Hall probe experiments have confirmed the accuracy of the theoretical predictions within experimental error

<sup>1</sup>F. J. Jeffers and H. Karsh, IEEE Trans. Magn. MAG-20, 703 (1984)  
<sup>2</sup>R. P. Hunt, IEEE Trans. Magn. MAG-7, 150 (1971)  
<sup>3</sup>F. J. Jeffers, IEEE Trans. Magn. MAG-15, 1628F (1979)